Novel robotic mechanisms for upper-limb rehabilitation and assessment.

by

Stephen Joseph Ball

A thesis submitted to the Department of
Electrical and Computer Engineering
in conformity with the requirements for
the degree of Doctor of Philosophy

Queen's University
Kingston, Ontario, Canada
August 2008

Copyright © Stephen Joseph Ball, 2008

Abstract

Robotic rehabilitation and assessment of the human upper-limb following stroke is currently limited in part by the inability of robots to replicate natural motion. In particular, motion of the shoulder girdle is usually neglected, despite the fact that the shoulder girdle is necessary to stabilize and orient the upper-limb during activities of daily living. Without direct control of the shoulder girdle, it is not possible to monitor or prevent a patient from making compensatory movements, which inhibits functional recovery, nor is there a means to properly regain strength and coordination. The more the robot is able to realistically mimic upper-limb motion, the more able the robot will be to assist with true functional movement training, which gives the patient the best chance of motor recovery. To address this issue, a new adjustable robotic exoskeleton called MEDARM is proposed for rehabilitation and assessment of the shoulder complex. MEDARM provides independent control of six degrees of freedom of the upper-limb: two at the sternoclavicular joint, three at the glenohumeral joint and one at the elbow.

A key design feature of the new robot is an innovative curved track mechanism actuated by a cable-drive transmission system. To facilitate a performance evaluation of this new mechanism, a planar version of MEDARM was designed. A full prototype of this planar robot was constructed and several fundamental metrics, including friction, inertia, and compliance, were used to test its mechanical performance. Additionally, the functionality of the robot was examined using preliminary data recorded during a standard reaching task, and by implementing some basic rehabilitation algorithms. This thesis describes the design of MEDARM and its planar counterpart in detail and the performance evaluation of the prototype is presented.

Acknowledgments

I would like to thank my supervisor, Stephen Scott, for giving me the opportunity to work on this project. His guidance, encouragement and enthusiasm has been an immense support throughout my research. I am also very grateful for the advice and guidance provided by my co-supervisor, Keyvan Hashtrudi-Zaad.

My sincere gratitude goes out to the BKIN boys for their help and encouragement. Specifically, I would like to thank Ian Brown for so willingly sharing his insight and knowledge of robot design, which continually steered me in the right direction. Also, I would like to thank Luke Harris for doing an extraordinary job of machining all of my custom parts, even though all my drawings were metric.

Thanks to the rest of the L.I.M.B. Lab for their interest and support throughout my time here. In particular, I would like to thank Kim Moore for her dedication to making sure I always had everything I needed.

I am grateful to my family and friends for their continual love and support. Finally, I wish to give a very special thanks to my wife Angela for her company, her laughs and her unconditional love.

Contents

Abstract i

Acknowledgments ii

Table of Contents iii

List of Tables vi

List of Figures vii

Nomenclature ix

Chapter 1: Introduction **1**

1.1 Motivation 1

1.2 Research Contributions 2

1.3 Outline 3

Chapter 2: Literature Review **5**

2.1 Human Upper-Limb Mechanics 5

2.1.1 The Joints 5

2.1.2 Kinematic Modeling of the Upper-Limb 9

2.1.3 Upper-Limb Anthropometry 11

2.2 Upper-Limb Stroke Rehabilitation 12

2.2.1 Assessment 12

2.2.2 Therapy 14

2.2.3 Existing Devices for the Upper-Limb 21

Chapter 3: Technical Background **25**

3.1 Cable-Driven Robot Mechanics 25
3.1.1 Relating Joint Angles and Cable Displacements 27
3.1.2 Relating Joint Torques and Cable Forces 31
3.2 Cable Routing Structure Selection 34
3.3 Four-Bar Linkage Mechanics 38
3.3.1 Kinematic Analysis 39
3.3.2 Force Analysis 43

Chapter 4: MEDARM **45**

4.1 MEDARM Design Objectives 45
4.1.1 Therapeutic Functionality Objectives 46
4.1.2 Robot-User Interface Objectives 48
4.1.3 Technical Objectives 50
4.2 MEDARM Design Overview 51
4.3 MEDARM Mechanical Design 54
4.3.1 Shoulder Girdle Mechanism 54
4.3.2 Glenohumeral Joint Axis Orientation 57
4.3.3 Joint Design 67
4.3.4 User Attachment and Alignment 70
4.4 MEDARM Actuation System 73
4.4.1 Cable-Drive System 74
4.4.2 Shoulder Girdle Drive System 78
4.4.3 Dynamic Model and Simulation 81
4.4.4 Motor Details 84
4.5 Estimated Cost 85

Chapter 5: Planar MEDARM **86**

5.1 Planar MEDARM Design Objectives 87

5.2 Planar MEDARM Design Overview 89
5.3 Planar MEDARM Mechanical Design 91
5.3.1 Mechanism Design 91
5.3.2 Joint Design 95
5.3.3 User Attachment and Alignment 96
5.4 Planar MEDARM Actuation System 97
5.4.1 Cable-Drive System 98
5.4.2 Electronics and Control 102
5.4.3 Dynamic Model and Simulation 104
5.5 Cost 108

Chapter 6: Planar MEDARM Evaluation **109**

6.1 Planar MEDARM Performance Evaluation 109
6.1.1 Measured Parameters 109
6.1.2 Systems Tested 114
6.1.3 Results 116
6.1.4 Suggested Upgrades and Improvements 121
6.2 Cost Comparison 126
6.3 Rehabilitation Applications 127
6.3.1 Resistive Exercise 127
6.3.2 Assistive Trajectory Tracking 130

Chapter 7: Conclusions and Future Work **136**

7.1 Project Overview 136
7.2 Future Directions 138
7.3 Final Words 140

Bibliography **141**

List of Tables

2.1 Anthropometric height and mass measurements 11

2.2 Human upper-limb segment length and mass properties 12

2.3 Existing end-effector rehabilitation robots 22

2.4 Existing exoskeleton rehabilitation robots 23

2.5 Existing hybrid rehabilitation robots 24

4.1 Summary of MEDARM design objectives 47

4.2 Comparison of the possible cable routing structures for 4DOF system 76

4.3 Maximum torque output for each joint 84

4.4 Estimated parts cost for MEDARM 85

5.1 Comparison of the possible cable routing structures for 3DOF system 99

5.2 Parts cost for Planar MEDARM 108

6.1 Cost comparison of Planar MEDARM and KINARM 126

List of Figures

2.1 Skeletal structure of the human upper-limb 6

2.2 Upper-limb motion terminology 7

2.3 Upper-limb kinematic models 10

3.1 Cable routing scheme for a simple 2DOF manipulator 29

3.2 Pulley pair types 29

3.3 Rectifying operator diagrams 32

3.4 Torque resolver implementation schematic 34

3.5 Schematic of a Grashof four-bar linkage 38

3.6 A vector schematic of a four-bar linkage 40

3.7 Free body diagram for a four-bar linkage 44

4.1 Complete view of MEDARM 52

4.2 Individual DOF in MEDARM 53

4.3 Shoulder girdle mechanism 55

4.4 Virtual four-bar linkage mechanism 56

4.5 Glenohumeral joint axis orientation 58

4.6 Spherical joint frame definition 61

4.7 Reduction of possible parameter combinations 64

4.8 3D workspace manipulability and distribution 66

4.9 Exploded view of joint 4 67

4.10 Section view of joint 4 68

4.11 Drive pulley design 69

4.12 Shoulder girdle adjustment 71
4.13 Arm cuff adjustments 72
4.14 Cable layout for the shoulder/elbow mechanism 75
4.15 Shoulder girdle cable routing 79
4.16 Sample simulation results 83

5.1 The KINARM robotic assessment system 87
5.2 Planar MEDARM CAD drawings 89
5.3 Planar MEDARM virtual display system 90
5.4 Mechanism design logic 92
5.5 Planar MEDARM compared with KINARM 94
5.6 Virtual four-bar linkage mechanism 94
5.7 User attachment and adjustment 97
5.8 Cable routing scheme 98
5.9 Electronic and motion control system schematic 103
5.10 Simulated dynamic manipulability 107

6.1 Photographs of Planar MEDARM 110
6.2 Reaching task layout 114
6.3 Alternate 3DOF cable routing scheme 115
6.4 2DOF cable routing scheme 116
6.5 Friction, inertia and compliance test results 118
6.6 Reaching experiment results 120
6.7 Joint-based resistive load results 128
6.8 End-point resistive load results 130
6.9 Assistive trajectory algorithm 131
6.10 Assistive trajectory algorithm segment 133
6.11 Assistive trajectory algorithm results 134

Nomenclature

Acronyms

CAD	Computer Aided Design
CIMT	Constraint Induced Movement Therapy
DOF	Degrees of Freedom
F-M	Fugl-Meyer Assessment Score
FIM	Functional Independence Measure
KINARM	Kinesiological Instrument for Normal and Altered Reaching Movements
LED	Light Emitting Diode
MEDARM	Motorized Exoskeleton Device for Advanced Rehabilitation of Motor function
PRE	Progressive-Resistive Exercise
ROM	Range of Motion

Variables

α	parameter used to select spherical joint axis orientation (also link angle in section 3.3 only)
β	parameter used to select spherical joint axis orientation
δ	cable pretension force in cable-drive system
ϵ	channel width for trajectory assistance algorithm
η	gear ratio
θ, $\dot{\theta}$, $\ddot{\theta}$	joint angle, velocity, acceleration
$\theta_{(M=0)}$	joint angle at which singularity occurs
ξ	cable force in cable-drive system

τ	torque
f	end-point force
k	spring constant for wall stiffness in trajectory assistance algorithm
l	link length
r	pulley radius in cable-drive system (also link length in section 3.3 only)
s	cable length change in cable-drive system
z	rotary joint axis unit vector
A	cable length - joint angle transformation matrix for cable-drive system
B	cable force - joint torque transformation matrix for cable-drive system (structure matrix)
B^*	dimensionless structure matrix
M	kinematic manipulability (volume of parallelepiped)
M_{max}	maximum manipulability
R^*	cable-drive pulley radius matrix

Chapter 1: Introduction

1.1 Motivation

Stroke is a leading cause of disability in Canada, leaving people with limited ability to perform activities of daily living. More than 300,000 people currently live with the effects of stroke, and there are 50,000 new occurrences every year [1]. Stroke arises from a sudden interruption in blood flow to the brain or a rupture of blood vessels in the brain. Consequently, some parts of the brain do not receive sufficient oxygenated blood, causing death of neurons in this region, and thus a loss of brain function. Impairments may involve loss of a combination of sensory, motor and/or cognitive functions and may manifest as weakness, reduced coordination, diminished ability to think, communicate, and make decisions, as well as difficulties in touch, vision and/or hearing. Also, a stroke can modify behaviour and personality. The degree of dysfunction arising from stroke is variable, depending highly on the location and size of the lesion. Lesions are typically localized to one side of the brain, therefore loss of function is predominantly related to the opposite side of the body [2].

Providing stroke survivors with the treatment that they need to regain motor function is a tremendous challenge for physiotherapists. Not only is the process physically laborious for the therapist, but also it requires time and personnel resources that the health care system struggles to provide. Unfortunately, it means that patients are usually not able to get as much therapy as they need. Overall, stroke care costs the Canadian health care system $2.7 billion every year [1]. This will only increase as the population continues to age.

Robotic technology is emerging as a tool to assist therapists with assessing stroke patients and providing the necessary therapy. One of the main goals of robotic therapy units is to increase the efficiency of the recovery process. In order to provide therapy

at the same level as a therapist, a robot must be able to perform functional movement training for the patient. A major problem with current robotic devices is that upper-limb mobility is poorly replicated. In fact, there are few devices that can provide any type of control of the shoulder girdle. The shoulder girdle is a critical part of upper-limb motion and stability [3], and is commonly recruited to make compensatory movements following stroke [4] and thus should not be ignored. Without direct control at the shoulder girdle, it is not possible to prevent compensatory movements, nor is there a means to properly regain strength and coordination of the shoulder girdle. It seems that a next step for robotic technology in a rehabilitation setting is to develop a robot that can more closely match the mobility of the human shoulder.

1.2 Research Contributions

The fundamental goal of this thesis is to develop a means of providing direct control of the shoulder girdle. As a result of this research, two new robotic devices have been designed from scratch based on several novel design concepts. The first is a new robotic exoskeleton device designed specifically to target five degrees of freedom (DOF) in the human shoulder complex. This robot is called MEDARM (Motorized Exoskeleton Device for Advanced Rehabilitation of Motor function). The second device is a simpler planar version of MEDARM, called Planar MEDARM, which was designed to gain practical experience with the novel design features of MEDARM in a simpler more controlled manner. The planar device also served as a means to test the feasibility of the new design concepts to extend the capabilities of the existing KINARM stroke assessment device [5]. KINARM is a 2DOF robotic exoskeleton that attaches to the upper-limb, allowing measurement and/or manipulation of the shoulder and elbow joints in the horizontal plane. Along with other features, Planar MEDARM adds a third DOF at the wrist. Planar MEDARM has been fully assembled and its performance has been tested using several variants of the actuation system.

Several novel design concepts have been developed through the design process for these two devices. The fundamental basis of operation of both robots is a new cable-driven curved track mechanism that can remotely actuate a joint. This new mechanism allows coupling of a limb joint that cannot be driven by equipment located along the axis of rotation. In fact, this concept is the central component of a patent application that has been filed [6].

Another major accomplishment is the development of an intuitive algorithm to design a spherical joint while ensuring that all design criteria are satisfied. The technique was developed to choose the relative orientation of the three joint axes that make up MEDARM's glenohumeral joint. The technique has general applicability to the design of spherical joints, but is particularly well-suited for exoskeleton devices. Additionally, the designs of both robots use some unique ideas to incorporate simple adjustments for people of different size. For example, quick-release clamps have been implemented on both robots to allow easy clamping/unclamping of adjustable components.

The designs presented in this thesis will be a step toward the development of devices that can give stroke patients a better chance at regaining independence.

1.3 Outline

The following provides a brief description of each chapter in this thesis.

Chapter 2: Literature Review

This chapter reviews some of the background literature to illustrate the motivation for this project. Topics include a description of the mechanics and models of the human upper-limb, and a summary of the current state of conventional and robotic upper-limb stroke rehabilitation and assessment. A comprehensive list of existing robotic devices is provided to create a clear picture of the areas in need of improvement.

Chapter 3: Technical Background

This chapter is dedicated to describing several techniques and equations that are important to this project. These descriptions include a full description of cable-drive robot mechanics, a detailed explanation of techniques used to select a cable-routing structure, and 4-bar linkage mechanics.

Chapter 4: MEDARM

The design of MEDARM is described in detail in this chapter, beginning with the design requirements. Mechanical design components including the curved track system, joint design, and user interface are detailed. The actuation and transmission systems are explained, along with the models and simulations developed to assist with the selection of components.

Chapter 5: Planar MEDARM

This chapter is dedicated to Planar MEDARM, and shares a similar tone with the MEDARM chapter. While many aspects of the design are similar, there are some different design objectives, and thus the involved mechanisms require slightly different design. These differences are highlighted and described as necessary.

Chapter 6: Performance Evaluation

This chapter outlines the evaluation of Planar MEDARM's performance in terms of several fundamental performance characteristics. In fact, five variations of Planar MEDARM's transmission system were tested to gain a full understanding of its performance. Suggestions for improvement are discussed. Moreover, some basic rehabilitation applications are explored and implemented with Planar MEDARM including a basic motion guidance algorithm that does not require force sensing.

Chapter 7: Conclusions and Future Work

The thesis closes with an overview of the project achievements and suggestions for future research.

Chapter 2: Literature Review

2.1 Human Upper-Limb Mechanics

The human upper-limb can be sub-divided into five main components: the shoulder girdle, the shoulder joint, the elbow, the wrist, and the hand (fingers). Modeling the kinematics of these joints is a challenge due to the significant variations among people, particularly at the shoulder complex. Relative motion of the joints are typically non-linear [7], and even in the simplest case of the elbow, the range of motion depends on the overall orientation of the limb. Also, upper-limb injuries or motor impairment can alter motion in substantial ways.

While motion of the biomechanically simpler lower-limb has been studied extensively, there is relatively little data available for upper-limb motion. Most available kinematic data for the upper-limb was collected for specific purposes, and measured using non-standardized techniques. As such, it is difficult to combine the results from different studies in a meaningful way. For rehabilitation, functional range of motion is an important quantity. This often manifests as a minimum range of motion required to achieve functional tasks. The following briefly discusses the elbow, the shoulder joint and the shoulder girdle in terms of their structure, mobility and range of motion (for the purposes of this thesis, wrist and hand motion will not be discussed). Range of motion (ROM) for the joints were obtained as averages from a number of sources [7–12], and are listed as a typical minimum (functional) and maximum.

2.1.1 The Joints

The Elbow

The elbow is a compound joint consisting of three bones and two articulations as shown in Fig. 2.1. The humerus of the upper-arm connects to the radius and ulna of the forearm through the humeroradial and humeroulnar joints. The humeroradial

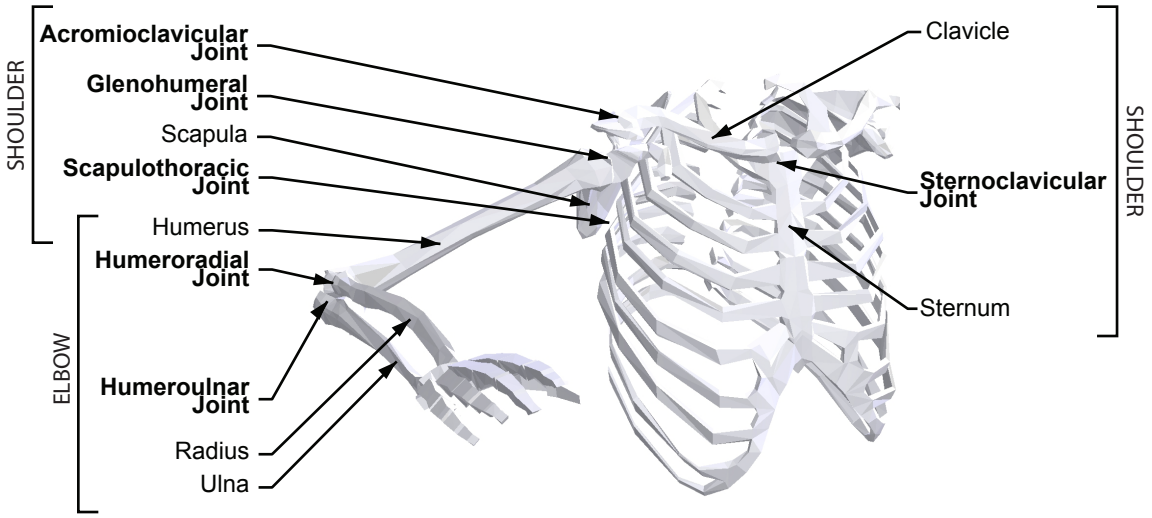

Figure 2.1: An illustration of the skeletal structure and articulations of the upper-limb. Articulations are labelled with bold text, and bones are labelled with normal text.

joint can be approximated by a ball-and-socket joint with three degrees of freedom (3DOF) while the humeroulnar joint is best described as a hinge joint with 1DOF. The bones form a closed kinematic chain, restricting the elbow joint to 2DOF overall [3]. Elbow motions are described by the following terminology (Fig. 2.2a):

- FLEXION (EXTENSION) – Motion of the forearm toward (away from) the upper-arm. Functional ROM $\sim 110°$; up to $140°$.
- PRONATION (SUPINATION) – Rotation of the forearm such that the palm faces downward (upward), orienting the wrist (sometimes considered part of wrist motion). Functional ROM $\sim 120°$; up to $160°$.

The Shoulder

The human shoulder is a complex structure that produces extraordinary range of motion and stability. As shown in Fig. 2.1, the shoulder is composed of four bones (humerus, scapula, clavicle, and sternum) and four articulations (sternoclavicular, acromioclavicular, scapulothoracic , and glenohumeral joints). The shoulder girdle

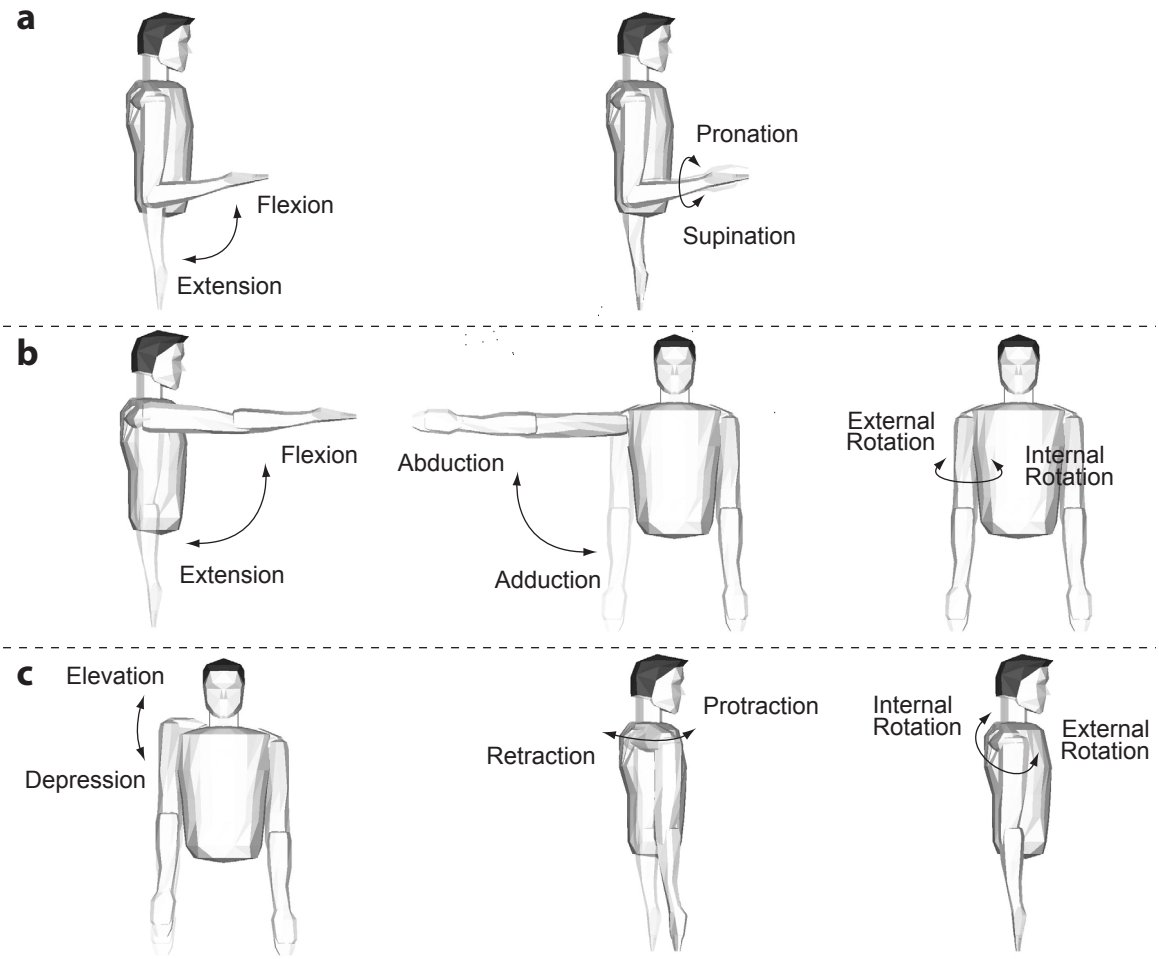

Figure 2.2: Diagrams illustrating the terminology used to describe the degrees of mobility of (**a**) the elbow, (**b**) the shoulder joint and (**c**) the shoulder girdle (except translation).

connects the arm to the body and supports, positions and orients the proximal end of the humerus in space. The shoulder joint is responsible for orientating the humerus. Overall, the shoulder is a redundant 7DOF system, providing stability and mobility that is unmatched by any other part of the body [3, 13].

The Shoulder Joint. The humerus is connected to the scapula at the gleno-humeral joint (Fig. 2.1), which can be approximated as a ball-and-socket joint with 3DOF. However, there can be translation of the humeral head in its socket during motion, but this is most significant for motions near the edge of the joint's ROM [3]. The motions of the humerus can be described by the following terminology (Fig. 2.2b):

- FLEXION (EXTENSION) – Forward motion of the upper-arm upwards (downwards) and to the front (back) with the elbow facing the front/back. Functional ROM $\sim 90°$; up to $140°$.
- ABDUCTION (ADDUCTION) – Sideways motion of the upper-arm upwards (downwards) and away from (toward) the mid-line of the body with the elbow facing front/back. Functional ROM $\sim 120°$; up to $150°$.
- INTERNAL (EXTERNAL) ROTATION – Rotation of the humerus around its longitudinal axis, turning it inward toward (outward away from) the body. Functional ROM $\sim 90°$; up to $120°$.

The Shoulder Girdle. The shoulder girdle is composed of three articulations (Fig. 2.1). The sternoclavicular joint connects the clavicle to the sternum, and can be approximated by a ball-and socket joint (3DOF). It is the only bony connection of the shoulder to the rest of the skeletal system. The scapula connects to the clavicle through the acromioclavicular (or claviculoscapular) joint, which also has 3DOF. The kinematic chain is closed by the scapulothoracic articulation which connects the scapula to the torso. However, the scapulothoracic "joint" is not a typical joint as it floats on the back of the rib cage between layers of muscle. The scapula moves over the rib cage, but since the ribs are not planar, scapular motion is neither pure rotation nor pure translation. Since the shoulder girdle is a closed kinematic chain, the motion of the joints are intimately coupled to give 4DOF overall. The terminology that describes the overall motion of the shoulder girdle – motion of the proximal humerus joint centre with respect to the body – is listed below [3] (Fig. 2.2c). Functional ROM data is not available for the shoulder girdle, thus the typical maximum is listed.

- ELEVATION (DEPRESSION) – An upwards (downwards) shrugging motion in which the scapula moves up (down) along the rib cage. ROM up to $50°$.
- PROTRACTION (RETRACTION) – A forward (backward) horizontal motion in which the scapula moves away from (toward) the spine. ROM up to $50°$.

- INTERNAL (EXTERNAL) ROTATION – A tipping motion of the scapula in which the inferior (superior) tip of the scapula moves backwards, away from the ribs. For most movements, this is small, and at most, the ROM up to 15°.
- LONGITUDINAL TRANSLATION – Displacement of the glenohumeral joint centre toward the sternoclavicular joint centre (not shown in Fig. 2.2c). The displacement is significant only for large humeral elevations, and can be up to 20% of the normal joint separation [9].

While the shoulder girdle has 4DOF overall, a large majority of its motion is well-described by 2DOF (elevation/depression and protraction/retraction). The contribution of the remaining 2DOF to the motion is minimal. Range of motion for the shoulder girdle is difficult to determine because it is a nonlinear function of the humeral orientation. For example, there is little contribution to humeral elevation from the shoulder girdle until high elevations where the ratio of glenohumeral to scapular motion becomes approximately 1.7:1 [7].

2.1.2 Kinematic Modeling of the Upper-Limb

A mathematical model of upper-limb motion is invaluable when designing a robotic exoskeleton. It can be used for determining size and strength of mechanical components, and also for developing appropriate motion controllers for the robot. The minimum requirement for simulation is to build a kinematic model of the limb, however, it is also useful and sometimes necessary to include the dynamics. Detailed dynamic models can also be built which include muscle properties.

It is common to model the elbow as two intersecting revolute joints, and the shoulder joint as three intersecting revolute joints. This model makes the reasonable assumption that the glenohumeral joint is a perfect ball-and-socket joint and that there is no translation within the joint. Shoulder girdle motion is more challenging, because its characteristics depend on the curvature of the rib cage, which varies widely

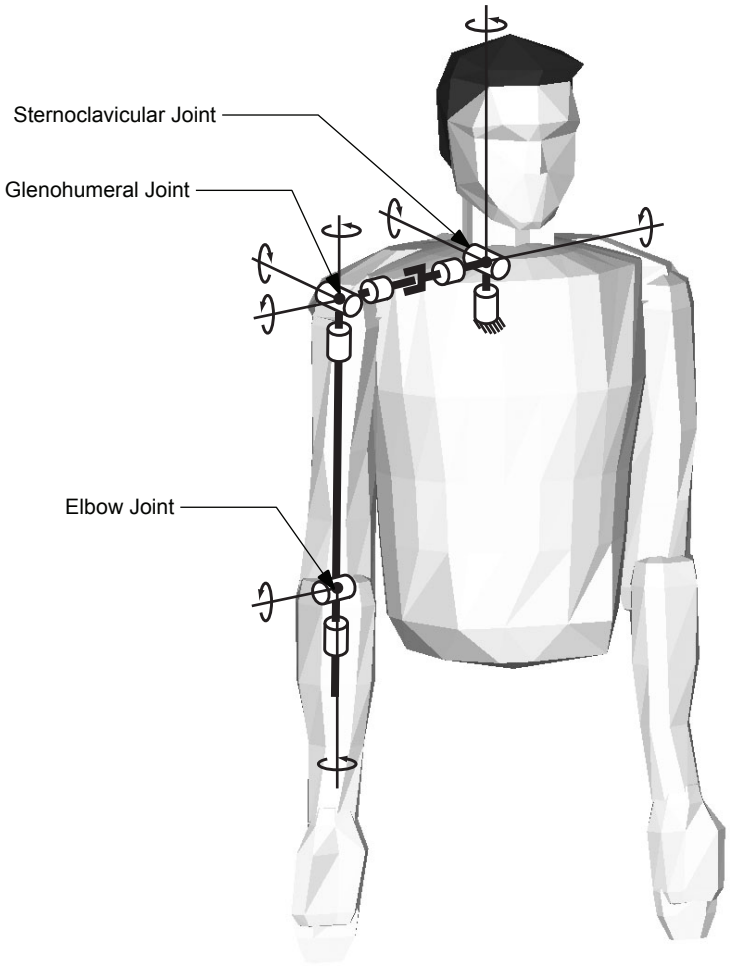

Figure 2.3: A model of the upper-limb. The 4DOF of the shoulder girdle are modeled as three intersecting revolute joints centred on the sternoclavicular joint, and a single translational joint connecting to the glenohumeral joint. The glenohumeral joint is represented by three intersecting revolute joints, and the elbow by two intersecting revolute joints.

among individuals of different size and shape. Rather than describing the position of the scapula and clavicle directly, models of the shoulder girdle usually describe the motion of the glenohumeral joint centre with respect to the sternoclavicular joint (fixed on the torso). For many applications, this is a reasonable approximation which allows the system to be treated as a serial chain, as shown in Fig. 2.3. Here, the shoulder girdle is modeled as a ball-and-socket joint (3DOF) at the sternoclavicular joint which is joined to the glenohumeral joint by a translational joint [9]. The glenohumeral joint itself is also a ball-and-socket joint as described above.

2.1.3 Upper-Limb Anthropometry

Anthropometry is the study of human body measurement. Any machine or device that functions closely with the human upper-limb, including the robots designed in this thesis, must take anthropometric measurements of the limb into account. Body dimensions vary among individuals, therefore anthropometric measurements are typically organized in tables for specific population. A value designated as 50^{th} percentile means that it is the median value across the population, and a 95^{th} percentile value means that only 5 percent of the population have a larger value.

Measurements can vary significantly with gender, age, race, disability level, and occupation among others, therefore data should be carefully chosen to be appropriate for its purpose. From a rehabilitation robotics perspective in Canada, it might be most appropriate to use data that encompasses both genders and the socioeconomic and ethnic diversity of today's society. Also, if stroke patients are considered, age must also be factored into the choice of data as most incidents occur after the age of 55 [1]. It is important to note that one must be cautious about interpreting the anthropometric measurements. For example, it is incorrect to imagine that a person that is 50^{th} percentile in terms of height is 50^{th} percentile in all other respects [14].

Size and Mass

In general, the average length or mass of a body segment can be estimated as a fraction of total standing height, H, or total mass, M, respectively. Table 2.1 summarizes height and mass measurements for 5^{th}, 50^{th} and 95^{th} percentile male/female

Table 2.1: Anthropometric measurements of height and mass for North American civilians (50/50 male/female, approx. 50 years of age) [14].

Subject Size	**Height (m)**	**Mass (kg)**
5th	1.54	58.5
50th	1.68	75
95th	1.83	110

Table 2.2: Body segment parameters expressed in terms of total standing height, H, or total mass , M [15]. Distances are measured from joint centres.

Segment	**Segment Mass / *M***	**Segment Length / *H***	**Centre of Mass/ Segment Length (Proximal End)**	**Segment Density (kg/m^3)**
Upper-arm	0.028	0.186	0.436	1070
Forearm	0.016	0.146	0.430	1130
Hand	0.006	0.108	0.506	1160
Forearm + Hand	0.022	0.254	0.394	1140

North American civilians (approx. 50 years of age). Table 2.2 summarizes upper-limb segment lengths, segment centres of mass, segment masses, and segment densities as a function of the height and mass measurements [15].

2.2 Upper-Limb Stroke Rehabilitation

It is possible to regain partial or complete motor function after stroke through various rehabilitation therapy programs. An integral component of rehabilitation, however, is assessment. Not only is an initial assessment performed to determine what therapy should be provided, but patients are assessed throughout the therapy program to monitor progress. In this section, current assessment and therapy techniques will be summarized, including both conventional and robotic strategies.

2.2.1 Assessment

Conventional Assessment

Before providing a patient with any kind of stroke therapy, the extent of the motor impairments must first be assessed thoroughly. This can be a challenging task because it is often not clear whether the impairments are a result of sensory or motor deficits. The traditional system involves leading the patient through functional assessment programs, which typically involve scoring the patient across a range of very specific functional tests. The final score is used to gauge the level of functional deficits, and also to determine the best course of treatment. The tests are usually performed

several times throughout the therapy program, in part to monitor progress, but also to re-evaluate the course of the treatment plan.

There are several scoring systems available for functional assessment including the Chedoke McMaster Stroke Assessment [16], the Fugl-Meyer (F-M) Score [17, 18], and the Functional Independence Measure (FIM) [19]. A problem with most of the tests is that they are not completely objective, and require judgement from the therapist or personal accounts on ability. In order to increase reliability and repeatability, a points system is used, and often it is simply a matter of whether or not the patient can make a specific movement. In these cases, there is no middle ground, and the result is that the scores tend to be insensitive to subtle differences in motor ability. Even the most sensitive score does not provide quantitative analysis of movement. A thorough functional assessment may not provide enough information to correctly determine the appropriate course of therapy for a patient.

Manual testing requires significant one-on-one attention from a therapist, and as a result, it is a time-consuming and expensive process. There is a need to improve the assessment and diagnostic process as a whole.

Robotic Assessment

Robotic technology has the potential to become an invaluable assessment tool for physiotherapists [20, 21]. First of all, robots have the ability to provide sensitive and inherently objective quantitative assessments of both the kinematics and the dynamics of movement. This can be used to measure performance and monitor the recovery progress with much more sensitivity and reliability than traditional functional scores [22–25]. Moreover, robots can make controlled movements with ease and precision. It is a simple matter to incorporate a robot into a virtual environment which can be designed to mimic conventional and also novel situations. The result is the ability to provide a set of reliable standardized tests which can quantitatively observe motor impairments. Robotic technology can also be fully automated, which would allow a

single therapist to supervise multiple patients simultaneously, significantly easing the burden on the health care system.

2.2.2 Therapy

Conventional Therapy

It is possible to regain partial or complete motor function through individualized rehabilitation programs. In general, early treatment provides the best outcome, but unfortunately, complete recovery is not common. Usually, more treatment with longer and/or more frequent sessions provides a better outcome [26]. It was previously thought that significant functional gains are possible only within the first 3 to 6 months following stroke, but functional improvements have been shown in patients more than one year post stroke [27, 28].

The ultimate goal is to restore a patient's ability to perform activities of daily living. Traditionally, therapists taught compensatory movements such as using redundant joints of the body (i.e. using torso motion to assist with reaching) or fractionation of movements into several simpler movements [4, 27]. While compensation allows patients to rapidly regain some degree of independence, a strong reliance on compensation promotes learned non-use of the impaired limb which slows or inhibits functional recovery [29, 30].

Current rehabilitation programs tend to focus instead on reducing the degree of permanent disability [31]. Recovery of motor function has recently been linked to motor learning that occurs during repetitive, frequent and intensive movements [32, 33]. This increased sensorimotor activity takes advantage of neural plasticity, in which adjacent or other areas of the brain reorganize and compensate for lost function in damaged brain regions [29]. Nevertheless, it is agreed that exercising and practicing a variety of functional multi-joint movements with the impaired arm is an important part of therapy for stroke patients [34]. Therefore, typical therapy programs focus on training with repetitive movements using a range of techniques such as restriction,

gravity compensation, manual guidance, and progressive-resistive exercise.

Restriction. A key technique used in upper-limb stroke rehabilitation is restriction. In daily life, a stroke patient is likely to facilitate movement of the affected limb by making compensatory movements of the shoulder girdle [35] and/or torso [30]. Often, the patient will also use the unaffected limb to perform tasks. Constraint-induced movement therapy (CIMT), is an effective technique in which the non-paretic arm is constrained, forcing use of the paretic limb to perform tasks. This technique helps to prevent learned non-use [36]. However, CIMT does not prevent incorrect movements of the trunk and/or shoulder girdle. Unfortunately, this technique cannot be used for patients with severe impairment because the patient must be able to move their paretic arm to some degree to perform exercises and daily activities.

Gravity Compensation. In the initial stages of treatment, a patient is typically very weak and therefore can have difficulty overcoming gravity during movement. In fact, in the presence of gravity, a stroke patient's impaired arm workspace can be less than 5% of their normal workspace [37]. In the past, therapists have used passive sling systems to reduce the effects of gravity on the limb during therapy, making it significantly easier for the patient to move his/her arm freely in space. Unfortunately, this system can easily lead to injury arising from over-extension of the limb joints if the patient is not strong enough to stop a movement.

Guidance and Assistance. In conventional programs, one or more therapists manually assist the patient by repeatedly guiding the affected limb(s) through a variety of functional tasks such as picking up or moving an object. A therapist can help the patient achieve the appropriate muscle responses by tapping, stroking, holding or guiding as necessary [38]. As the patient's recovery progresses, assistance from the therapist is required less frequently. Bilateral movement training is another technique that involves the use of the normal arm to assist the impaired arm by making collaborative and/or mirror-image reaching movements. Studies of this technique in-

dicate immediate performance improvements of the impaired limb when compared with unilateral movements [39, 40].

Resistance. Another component of a typical treatment program is progressive-resistive exercise (PRE), which is a form of strength training in which the patient makes movements against resistance [41]. The therapist increases the resistance as the patient progresses. The idea is that increased muscle force output can lead to increased muscle power and endurance, which are linked to improved performance in activities of daily living [42].

Motivation. Success of these contrasting treatment programs suggests that movement variety is beneficial to the recovery process [34]. A patient will be more motivated to take part in the program if they are engaged and interested in the program [27]. This can be achieved through task variety, encouragement and high levels of feedback and interactivity. For example, if patients feel or see that they are making progress, they will be more motivated.

Although these conventional techniques have proven effectiveness, a significant drawback is that they require extensive one-on-one attention from one or more therapists. As such, recovery is severely limited by staffing, time, and budget constraints: thus, it is becoming more difficult to give patients the time and attention that they require for maximum recovery. Even with sufficient time and budget, therapists can tire easily when manually moving heavy paretic limbs, and with no means to quantitatively record patient progress, it is a challenge to properly monitor functional ability. Unfortunately, therapists are often forced to resort to shorter, less intense therapy programs that focus on teaching compensatory techniques rather than on recovering motor function [4, 21, 27].

Robotic Therapy

With the aging population comes the increased incidence of stroke, and the increased need for motor rehabilitation. This is straining the capabilities of the health

care and rehabilitation system. There is no doubt that improvements are required to provide the high quality care that patients need. The possibility of using robotic devices as a more efficient means of providing therapy has been at the forefront of stroke rehabilitation research in the past 15 years [20, 21]. Robotic systems provide a compelling solution which has significant potential as another tool in the arsenal of a trained physiotherapist.

Robotic devices present a number of benefits over traditional therapy techniques, and thus have significant potential in clinical settings. Perhaps the most significant advantage is that robots can repeat and monitor movements precisely without making mistakes and without getting tired. An additional benefit is that robots cannot be distracted or show discouragement. Robots can be programmed to perform many motions ranging from simple to complex trajectories. Furthermore, a robot can provide any level and duration of assistance and can apply novel loads that cannot be applied easily by hand [21, 43]. This clearly removes the strenuous labour from the therapist, allowing him/her to focus on other important tasks such as treatment planning and progress monitoring. Overall, this process facilitates treatment standardization.

An enormous amount of quantitative kinematic and dynamic information (including joint and end-point positions, velocities, accelerations, forces/torques, etc...) can be obtained about every movement. This is the key benefit of robotic assessment, but it is also useful for therapy. Based on this information, robots can provide visual, auditory and/or kinesthetic feedback to the patient as needed during movement.

Efficiency is another area in which robotic therapy systems excel. When appropriately designed, a single device can be used for both assessment and therapeutic purposes for a range of motor impairments, and can be used for any level of disability since the robot can provide as much or as little assistance as necessary. This reduces the need to move patients between different pieces of equipment during a therapy session. Also, commissioning multiple robots would allow a single therapist to work

with multiple patients simultaneously. In fact, it has been shown that providing automated therapy with as little as 25% supervision from a therapist has no negative effects on functional outcome [44]. Furthermore, at-home systems would allow patients to practice more frequently on their own time on a daily basis [31]. A therapist would be able to monitor progress and update programs remotely, thus enforcing practice at times other than during organized sessions. Not only will the patient be able to spend more time practicing movements, but the therapist will be able to spend time with more patients. Other opportunities such as group therapy (one therapist leading multiple patients) also become feasible using robotic technology.

Robots can replicate or even extend many of the traditional manual therapy techniques as described earlier. Some of the key concepts are briefly introduced below.

Restriction. Exoskeletal robots have the unique benefit of being able to isolate specific joints. Not only does this mean that these joints can be individually actuated, but also they can be restrained or locked in any given configuration. Thus, the patient is truly constrained to use the unlocked joints. Robots have a distinct advantage over CIMT because they can target assistance to specific joints.

Gravity Compensation. A robot can be configured to provide active gravitational compensation. First of all, robots can be built to avoid joint over-extension, reducing the chance of injury when compared with passive sling systems. Second, a robot with active gravity compensation can counteract gravity with high accuracy at all configurations, providing a much more realistic environment for the patient. Third, for exoskeleton robots, gravity compensation can be applied to specific joints or movements that require assistance. Finally, the level of compensation can be gradually reduced on a joint-by-joint basis as the patient becomes stronger and more able to deal with gravitational forces on his/her limb.

Guidance and Assistance as Needed. A robot can be programmed to provide any level of motion assistance. The limb can be moved through any trajectory,

and it is easy for a robot to learn a new trajectory for a specific individual. The robot can encourage the patient to stay on a desired path [45, 46] with or without any assistance to move along that path. Guidance can be used for passive exercises designed to extend the range of motion of specific joints [47], or for bilateral training in which the unaffected arm is used to drive the position of the impaired arm in a mirror-image fashion. There are many ways to encourage physiological movement patterns while providing only the assistance that is necessary, some of which can sense the patient's intentions [48–54]. Once the robot knows what the patient is trying to do, it can automatically facilitate accomplishment of that goal, while giving the patient a chance to contribute as much as he/she can toward that goal.

Resistance. Most robotic systems have already tested robotic progressive resistive exercise [19, 28, 55]. It is straightforward to implement velocity-dependent loads (or viscous loads) that involve applying opposing torques/forces that increase as the velocity increases. This creates a feeling of moving through a viscous material, and requires the patient to push harder, thus increasing his/her strength. The system can be easily adapted to target specific joints and muscle groups. The robot acts like a high-tech weight training machine.

Motivation. Feedback is a key part of motivating patients, and with robotic technology and virtual reality, there are many ways to convey information to the patient. The main goal is to provide a way for the patient to interact with or become immersed in the system, keeping him/her interested and motivated. Feedback can be visual, tactile, auditory or any combination of these. Useful information might include start/stop time, trajectory to follow, actual trajectory, position error, force output, and success rate, among many other kinematic, dynamic and/or task related variables. It can be provided in the form of a simple display, or as a full virtual reality system in which the patient can see and feel objects. Robots can apply abstract and unusual force fields that cannot be applied manually by a therapist. Examples include

joint-dependent forces (i.e. torque at a joint depends on the motion of a different joint) and bilateral-dependent forces (force on one arm is dependent on movement of the other). Another possibility is to simulate a force acting at the hand as if the patient were picking something up. Also, tasks in which both limbs collaborate to move a single virtual object are possible [56]. The ability of the robot to simulate different force-fields is limited only by imagination (and perhaps hardware capabilities). Tasks can include typical daily tasks or games specifically designed to target certain motor deficits [57–63]. In whatever way the feedback is presented, the interaction must be clear and interesting and must ultimately provide a challenging but enjoyable experience that improves the user's motor ability.

Limitations of Robots. Robotic devices are certainly not free from limitations. Safety is always top priority when there is such close interaction between human and machine. Robots are powerful, and can be dangerous without implementing appropriate safety mechanisms. For example, simple position control strategies that rigidly adhere to specified trajectories could be dangerous for patients with limited range of motion, forcing the limb to positions that could injure the user. Moreover, patients and therapists alike may not feel safe (safe design does not ensure a feeling of safety [38]), which can heavily influence acceptance of robotic technology in clinical environments. Fortunately, these safety systems exist, and when implemented correctly, robots can be safe and comfortable for both patients and therapists [64].

A robot that closely mimics upper-limb motion will be able to train with more realistic functional movements. Perhaps the most significant limitation is that it is a challenge for robotic devices to match the mobility of the human upper-limb. In particular, the human shoulder complex is a structure with extraordinary mobility that is challenging to describe, let alone replicate [3]. The evolution of robot design ensures that innovative technologies will continue to close the gap between robot and human mobility.

Another important aspect of robot design which can be easily overlooked is the robot-human interface. The main issue is the large variation in patient size and shape. Robots are typically designed to fit a range of people, but it is a challenge to account for all unique patient situations. The set-up process should be quick and simple, to improve the overall effectiveness and efficiency of the treatment.

Patient pain, distraction, refusal of cooperation and/or other unexpected situations make it difficult for robots to formulate appropriate responses. In particular, it is hard for robots to provide qualitative feedback to patients. For example, robots do not offer compassion or sympathy. However, it is likely that more techniques will be developed to overcome this problem by the wealth of quantitative data available to robots to provide more types of useful feedback to patients.

Robotic technology has the potential to provide immense benefits to the rehabilitation field, but there is still room for improvement. Fortunately, ongoing research continues to provide more capable robots that are better equipped to deal with the unique demands of rehabilitation.

2.2.3 Existing Devices for the Upper-Limb

There are two main categories of robotic mechanisms used in rehabilitation: end-effector and exoskeleton. In the end-effector category, the user grasps the end-effector of the robot (a handle). This handle is the only point of attachment of the robot to the user. The systems are simple and versatile, but cannot target specific joints of the limb because the handle can apply forces only to the attachment point. As a result, it is not possible to monitor the complete kinematics of the limb because the precise joint centres of the limb are unknown. Patient set-up is quick because there is no need to make any precise alignments. An exoskeleton system is built to couple its joints with the limb joints, allowing the degrees of mobility of the limb to be isolated and trained independently. However, exoskeleton robots are typically much

Table 2.3: Summary of existing end-effector robotic rehabilitation systems. By nature of their design type, there is no way to know the limb joint kinematics.

Robot	Mobility	Shoulder Girdle Control	Description
MIT-MANUS (InMotion2)	2DOF + 3DOF	n/a	rehabilitation robot pioneer, mature design, commercial product (Interactive Motion Technologies Inc.), simple, backdriveable, horizontal plane only with 3DOF wrist attachment [65–67]
MIME	6DOF	n/a	high mobility, strong evidence of efficacy [19], bimanual mode, not backdriveable [68]
WAM	4DOF (or 7DOF with handle)	n/a	backdriveable, lightweight, cable-driven, commercial product (Barrett Technology Inc.), no limb support [69]
ARM Guide	1DOF	n/a	linear reaching movements (forearm trough), adjustable orientation, non-functional movements since only 1DOF [70]
REHAROB	Dual 6DOF	n/a	2 independent industrial robots, 6DOF control of both upper-arm and forearm, not backdriveable, incoordination of robots could injure elbow [71]
(unnamed)	Dual 3DOF	n/a	similar to REHAROB, pneumatically driven, backdriveable, limited to slow speed [72]
MACARM	6DOF	n/a	parallel structure, cable-driven, powerful, limited workspace due to interference with cables [73]
GENTLE/s	3DOF	n/a	backdriveable, passive gravity compensation using slings [45]
MariBot	5DOF	n/a	forearm sling, orientation controlled by wires (3DOF), position controlled by planar 2DOF mechanism, swinging motion possible [74]
(unnamed)	3DOF	n/a	wrist position controlled by orthogonal cables, mounts to wheelchair, no limb support [75]
EMUL	3DOF	n/a	actuated using electrorheological fluid, backdriveable, no limb support [57]

Table 2.4: Summary of existing exoskeleton robotic rehabilitation systems.

Robot	**Mobility**	**Shoulder Girdle Control**	**Description**
KINARM	2DOF (1 shoulder, 1 elbow)	no	highly backdriveable, light-weight, commercial product (BKIN Technologies), bimanual operation, assessment, horizontal plane [5]
MULOS	5DOF (3 shoulder, 2 elbow)	no	battery operated, wheelchair compatible, maximized workspace, not backdriveable [76, 77]
WREX	5DOF (3 shoulder, 2 elbow)	no	passive (no actuation), complete gravitational compensation, not easily adjustable for different people [78]
Armeo (T-WREX)	5DOF (3 shoulder, 2 elbow)	no	modified WREX (see above), commercial product (Hocoma AG), with position sensors, stronger [58, 79]
PNEU-WREX	5DOF (3 shoulder, 2 elbow)	no	pneumatically actuated version of T-WREX, only slow movements [80]
Sarcos Master Arm	7DOF (3 shoulder, 2 elbow, 2 wrist)	no	hydraulically driven, commercial product (Sarcos, Inc.), not backdriveable [81]
RUPERT	5DOF (2 shoulder, 2 elbow, 1 wrist)	no	lightweight, pneumatic drive (slow motion only), backdriveable, incomplete shoulder joint motion [82]
(unnamed)	7DOF (3 shoulder, 2 elbow, 2 wrist)	no	pneumatic drive (slow motion only), backdriveable [83]
CADEN 7	7DOF (3 shoulder, 2 elbow, 2 wrist)	no	partially cable-driven, three motors located on forearm, to be controlled by EMG [84]
MGA Exoskeleton	5DOF (4 shoulder, 1 elbow)	1DOF	not backdriveable, motors mounted directly to joints [85]
(unnamed)	9DOF (5 shoulder, 2 elbow, 2 wrist)	2DOF	large and heavy, hydraulic or cable-driven [86]

Table 2.5: Summary of existing hybrid (part end-effector and part exoskeleton) robotic rehabilitation systems.

Robot	Mobility	Shoulder Girdle Control	Description
(unnamed)	8DOF (shoulder, elbow, wrist)	n/a	simple interface, high mobility, powerful, not backdriveable, unknown shoulder motion [87]
ARMin	7DOF (4 shoulder, 2 elbow, 1 wrist)	1DOF†	allows small misalignment, backdriveable, †1DOF at shoulder girdle coupled to 1DOF at shoulder (no independent control of shoulder girdle) [88–90]

more complex due to the close interaction with the user. Also, these robots must be adjustable to accommodate users of different size, and because each joint of the robot must be aligned with the patient, the set-up time is longer.

Tables 2.3, 2.4 and 2.5 summarize several of the most relevant existing end-effector and exoskeleton robots designed specifically for rehabilitation. The list is not exhaustive. Many other systems have been designed for purposes other than rehabilitation [91–101]. Most of these devices were designed as exoskeletons for tele-robotic or virtual reality applications. While these devices share many of the characteristics necessary for rehabilitation robot design, they cannot be used directly for rehabilitation applications due to their low power and complex set-up procedures. However, their insights into backdriveability, human-robot interfacing, actuation and sensing are important.

It is clear from Tables 2.3, 2.4 and 2.5 that there has been little work done with the shoulder girdle. Without control of the shoulder girdle, it is not possible to use the device to fully assess or rehabilitate the upper-limb. The devices that do consider the shoulder girdle are either incomplete, dependent on another DOF, or too heavy and slow to be useful in a clinical setting. There is no question that more work must be done to more closely replicate upper-limb motion.

Chapter 3: Technical Background

To facilitate the description of the new robots designed for this thesis, it is useful to summarize some technical background. In particular, both robots make use of open-ended cable-drive transmissions, which require special mathematical transformations to relate motion of the cables to motion of the robot's joints. The first two sections describe these transformations as applied to this project. For more detailed derivations and descriptions, the reader is referred to the original sources [102, 103]. The final section of this chapter details the relationships between the joints that make up a 4-bar linkage. Both robots make use of a novel 4-bar linkage to replicate motion of the upper-limb, therefore it is important to be able to describe the motion.

The relationships and techniques presented in this chapter are fundamental components of the new robots. In fact, the techniques were used to make some important design choices. It will be apparent in the chapters to come that these fundamental ideas serve as the foundation for modifications made to account for the novel design features of the new robots.

3.1 Cable-Driven Robot Mechanics

A mathematical model that describes the mechanics of a robot is important for modeling and control of the robot. Below is the general vector form of the equations of motion for a rigid serial manipulator:

$$M(\boldsymbol{\theta})\ddot{\boldsymbol{\theta}} + C(\boldsymbol{\theta}, \dot{\boldsymbol{\theta}})\dot{\boldsymbol{\theta}} + G(\boldsymbol{\theta}) + \boldsymbol{\tau_f} + \boldsymbol{\tau_{ext}} = \boldsymbol{\tau} \tag{3.1}$$

where $\boldsymbol{\theta}$, $\dot{\boldsymbol{\theta}}$ and $\ddot{\boldsymbol{\theta}}$ are the angular position, velocity, and acceleration vectors for all joints. Matrix $M(\boldsymbol{\theta})$ and vectors $C(\boldsymbol{\theta}, \dot{\boldsymbol{\theta}})\dot{\boldsymbol{\theta}}$ and $G(\boldsymbol{\theta})$ represent the mass/inertia, centrifugal/Coriolis, and gravitational properties of the manipulator. $\boldsymbol{\tau}$, $\boldsymbol{\tau_f}$ and $\boldsymbol{\tau_{ext}}$ are torques exerted on the system as a result of actuation, viscous/static friction,

and external forces (including torques applied by a human user) in joint space. Several techniques are available to determine these equations for a given manipulator, including Lagrangian Mechanics and the recursive Newton-Euler formulation [103].

Equation (3.1) can be used directly if the actuators for each joint are mounted to their respective joint axes. However, for alternate transmission systems such as the open-ended cable-drive transmission, additional transformations are required in order to model the robot. The extra computation required for cable-drive transmission systems is often outweighed by several compelling advantages over traditional transmissions. Perhaps the most obvious advantage is that all actuators are remotely located on the base of the robot, which significantly reduces the mass, inertia, and size of the manipulator. This also means that the power-to-weight ratio of the actuators is increased, and when coupled with the fact that joint torques are shared among the cables, it means that the robot can often function with smaller actuators. Therefore cable-drive transmissions are good options for actuating exoskeleton-type rehabilitation robots, and therefore it is important to understand how to determine their kinematics and dynamics, and how such systems can be modeled and controlled.

The additional transformations needed to control the robot arise from the fact that the number of joints needing control (n) is less than the number of actuators (m). As open-ended systems can apply force through positive tension only, it is necessary to have an antagonistic cable routing scheme to achieve motion in both rotation directions and to prevent the cables from becoming loose. As such, a minimum of $n + 1$ cables are necessary for complete control, but as many as $2n$ cables can be used [103]. Furthermore, since the cables are routed along the entire length of the mechanism through a series of pulleys, their motion affects multiple joints. There are also multiple ways to route the cables around the joints while still providing full ability to move in all directions. A method to determine the most suitable cable routing scheme is discussed in Section 3.2.

Before getting into the mathematical description of open-ended cable-drive systems, it is useful to consider how cable-drive systems operate in practice. One end of each cable is fixed to a link on the mechanism, and the cables are wound around free-moving pulleys at each joint back to the base of the system. At any point along the mechanism, idler pulleys can be used to guide the cables around corners (in or out of plane). The other end of each cable is then fixed to a pulley which is coupled to a motor. Rotating one or more joints of the mechanism will cause the cables to either wind up or unwind at each joint. The motor pulley will wind up or unwind any net change in cable length as a result of the joint rotation. There is a precise relationship between a joint rotation and the net change in length of the cables (i.e. rotation of the motors) which will be described in Section 3.1.1. The motors apply a constant force on the cables in a specific proportion to maintain tension in the cables (see Section 3.1.2). In this case, all forces are balanced around each joint, and the net joint torques are all zero. If one or more cables are pulled with additional force, the balance of force around the joints is disrupted, and net torques are created at one or more joints. Once again, there is a precise relationship between the forces applied to the cables and the torques that are created at the joints, and this will be described in Section 3.1.2.

3.1.1 Relating Joint Angles and Cable Displacements

The following describes how to relate joint space and cable space for the non-planar 2DOF manipulator shown in Fig. 3.1a. Note that the guide pulleys that are required to guide the cables from the pulleys on joint axis 1 to the pulleys on joint axis 2 are shown as simplified schematics for the sake of clarity. The system has $n = 2$ orthogonal joints, and is actuated by $m = 3$ cables. Pulley $c1$ is fixed to link 1, and pulleys $a2$ and $b2$ are fixed to link 2. Pulleys $a1$ and $b1$ are free to rotate about joint axis 1. In general, each pair of pulleys separated by a common link is called a pulley

pair. When the routing is parallel-type, positive rotation of one joint creates positive rotation of the next joint (Fig. 3.2a), and when the routing is cross-type, positive rotation of one joint creates negative rotation of the next joint (Fig. 3.2b).

The first step is to draw the mechanism as a planar schematic representation (Fig. 3.1b), in which all joints are displayed in a two-dimensional representation. In this notation, all joints are "flattened" into a plane by sequentially twisting each joint axis about the common normal defined by its joint axis and the adjacent joint axes. This system transforms the cable routing into a more readable diagram, while maintaining the cable routing structure. The schematic can be further simplified by writing a separate schematic for each of the three cables (Fig. 3.1c). In these representations, it is standard practice to define the positive direction as counter-clockwise.

At this point, it is easy to picture the antagonistic nature of the cable system by considering Fig. 3.1b. If cables a and b are each pulled with a force of 1 unit, two things happen. First, there will be no net torque about joint 2 because the cables are applying equal force to each side of link 2, canceling each other out. Second, there will be a negative net torque about joint 1 because both cables act on the same side of link 1. To maintain a balance in the system, a force of 2 units must be applied to cable c to counteract the forces applied by cables a and b. As another example, to create a positive torque about joint 2 with zero torque at joint 1, is it clear that a force must be applied to cable b. However, to balance the forces around joint 1, an equal force must also be applied to cable c.

The relation between joint angles, $\boldsymbol{\Delta\theta}$, and cable displacements, $\boldsymbol{s}$, can be determined by using a systematic technique [102, 103]. Cable displacements generally affect motion at multiple joints, thus this must be accounted for in the expressions. The final goal is to be able to relate cable displacements to joint angles, therefore it is necessary to obtain an expression for each cable.

Consider the 2DOF example in Fig. 3.1. Starting from a fixed base, links and

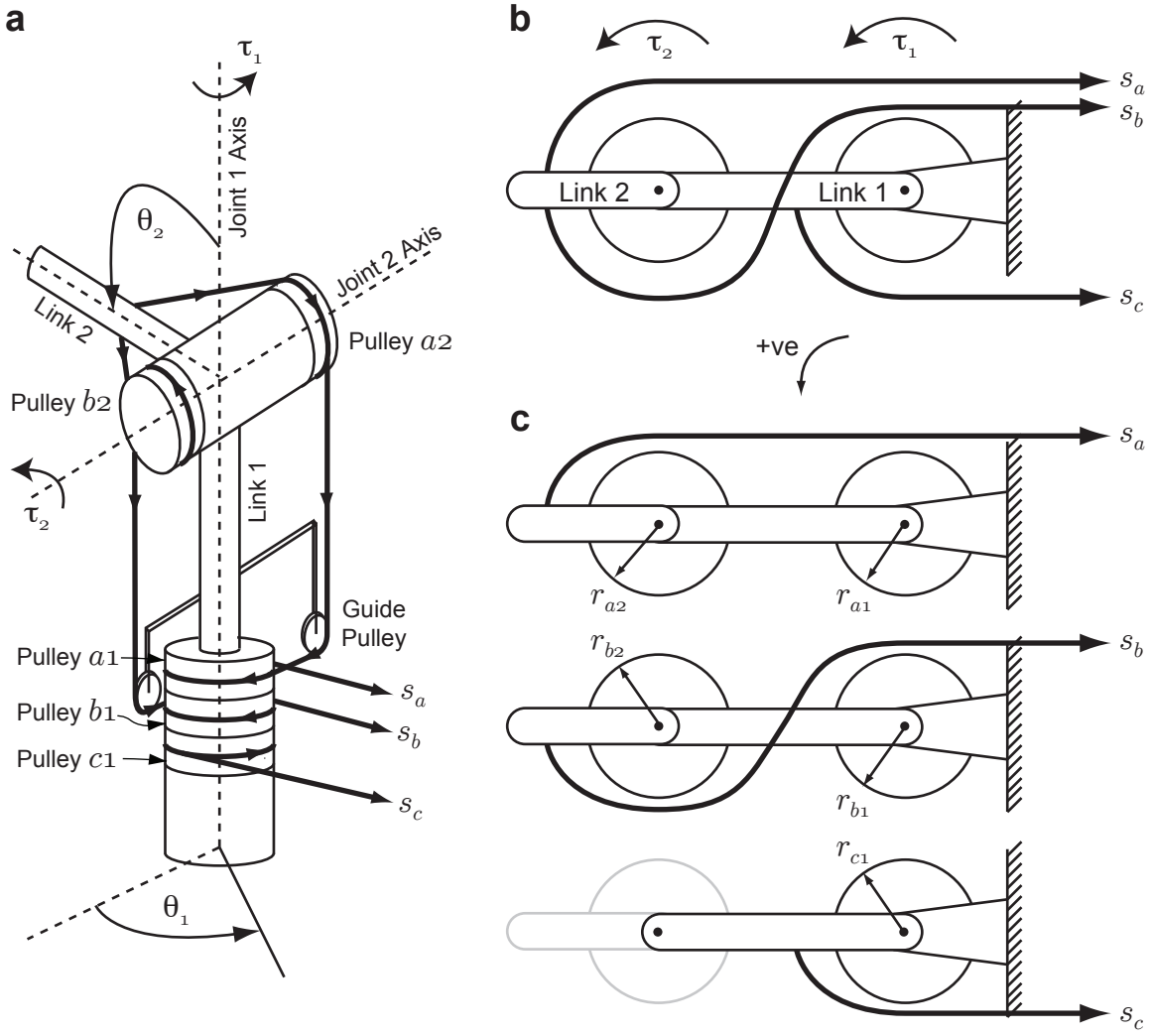

Figure 3.1: Planar schematic representation of a 2DOF spatial manipulator. (**a**) 3D view (with simplified guide pulleys guiding the cables from joint 1 to joint 2), (**b**) standard planar representation and (**c**) separate diagram for each cable. Note that positive rotation and torque are defined as pointing out of the page.

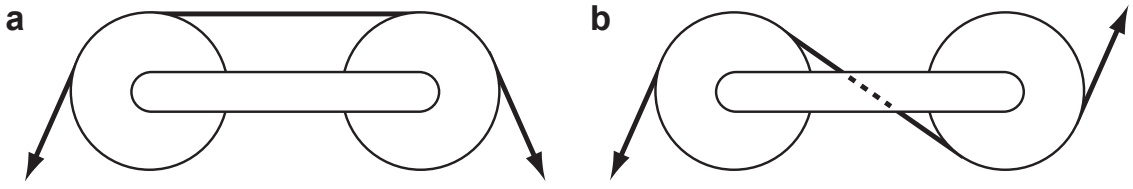

Figure 3.2: The two possible pulley pair types: (**a**) parallel, and (**b**) cross-type

joints are numbered from 0 to n. The cables are designated by letters, starting with 'a'. The pulleys are labeled with a letter to denote the cable that passes across, and a number to denote the joint on which it is mounted. The pulleys for cable a are labelled $a1$ and $a2$, for cable b they are labelled $b1$ and $b2$, and for cable c it is labelled $c1$.

The cable length change, s, that occurs when a joint angle is changed by angle $\Delta\theta$, is given by the arc length equation:

$$s = \pm r\Delta\theta \tag{3.2}$$

where r is the radius of the pulley guiding the cable at that joint.

If a cable is routed along more than one joint, the total cable length change is simply a combination of the arc length changes for each of the joints. However, whether the contribution from a specific joint is added or subtracted depends on whether or not the pulley winds up or unwinds cable during the rotation. This in turn depends on which direction the cable is routed along that pulley. Overall, the sign is positive if a pull of the cable creates a positive rotation of the pulley, otherwise the sign is negative.

For the 2DOF example in Fig. 3.1, the three cable length changes are given by:

$$s_a = -r_{a1}\Delta\theta_1 - r_{a2}\Delta\theta_2 \tag{3.3}$$

$$s_b = -r_{b1}\Delta\theta_1 + r_{b2}\Delta\theta_2 \tag{3.4}$$

$$s_c = r_{c1}\Delta\theta_1 \tag{3.5}$$

Writing in matrix form [102, 103]:

$$\boldsymbol{s} = \begin{bmatrix} s_a \\ s_b \\ s_c \end{bmatrix} = \begin{bmatrix} -r_{a1} & -r_{a2} \\ -r_{b1} & r_{b2} \\ r_{c1} & 0 \end{bmatrix} \begin{bmatrix} \Delta\theta_1 \\ \Delta\theta_2 \end{bmatrix} = A \begin{bmatrix} \Delta\theta_1 \\ \Delta\theta_2 \end{bmatrix} = A\boldsymbol{\Delta\theta} \tag{3.6}$$

Matrix A is a 3×2 transformation matrix that relates joint angles to cable displacement lengths. Note that A is not a square matrix, indicating that the number of joints is less than the number of actuator cables.

3.1.2 Relating Joint Torques and Cable Forces

It is also necessary to find the relationship between joint torques, $\boldsymbol{\tau}$, and cable forces $\boldsymbol{\xi}$. Using the principle of virtual work [103], it can be shown that:

$$\boldsymbol{\tau} = B\boldsymbol{\xi} \tag{3.7}$$

where the matrix $B = A^T$ is called the structure matrix; each column represents the routing of a single cable. If pulleys mounted on the same joint axis have the same radius, it is possible to decompose the structure matrix into two components [103]:

$$B = R^* B^* \tag{3.8}$$

where R^* is an $n \times n$ diagonal matrix describing pulley sizes in the mechanism, and B^* is an $n \times m$ matrix describing the cable routing in terms of ± 1's and 0's. B and B^* are useful in selecting a suitable routing structure for the system (see Section 3.2).

The relationship between cable force and joint torque for the 2DOF manipulator is as follows:

$$\boldsymbol{\tau} = \begin{bmatrix} \tau_1 \\ \tau_2 \end{bmatrix} = \begin{bmatrix} -r_{a1} & -r_{b1} & r_{c1} \\ -r_{a2} & r_{b2} & 0 \end{bmatrix} \begin{bmatrix} \xi_a \\ \xi_b \\ \xi_c \end{bmatrix} = B\boldsymbol{\xi} = A^T\boldsymbol{\xi} \tag{3.9}$$

In most cases, the pulleys located at each joint are indeed the same size. Thus $r_{a2} = r_{b2} = r_2$, and $r_{a1} = r_{b1} = r_{c1} = r_1$, and the matrix B can be written in the form of (3.8)

$$B = \begin{bmatrix} -r_1 & -r_1 & r_1 \\ -r_2 & r_2 & 0 \end{bmatrix} = \begin{bmatrix} r_1 & 0 \\ 0 & r_2 \end{bmatrix} \begin{bmatrix} -1 & -1 & 1 \\ -1 & 1 & 0 \end{bmatrix} \tag{3.10}$$

To implement a robot with this type of transmission, it is essential to determine what cable forces are required to achieve a given set of joint torques. However, a problem arises from the fact that the mapping from torques to forces is not unique, and also that cable forces must always be positive (otherwise, the cables will become slack). Pseudo-inverse techniques could be employed, but could be computationally expensive to calculate and discard all cases resulting in negative force. An alternative

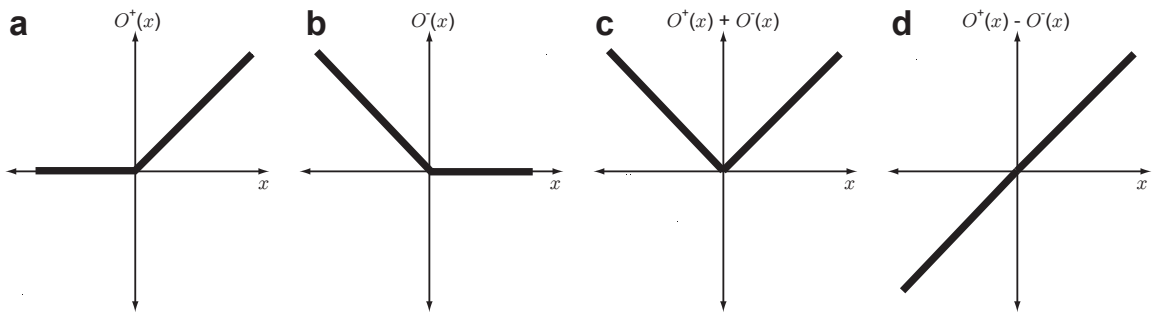

Figure 3.3: Diagrams of the rectifying operators used for the torque resolver technique. (a) depicts operator (3.11), (b) depicts operator (3.12), (c) depicts operator (3.13) and (d) depicts operator (3.14)

technique has been previously developed called the "torque resolver technique" [102] which finds a practical solution for the cable forces. This method also incorporates a bias force, δ, which allows pretension of the cables. In order to use this technique, some "rectifying" operators must first be defined:

$$O^+(x) = \begin{cases} x & \text{for } x \geq 0 \\ 0 & \text{for } x < 0 \end{cases} \tag{3.11}$$

$$O^-(x) = \begin{cases} 0 & \text{for } x \geq 0 \\ -x & \text{for } x < 0 \end{cases} \tag{3.12}$$

The above operators can be expressed in some useful forms:

$$O^+(x) + O^-(x) = |x| \tag{3.13}$$

$$O^+(x) - O^-(x) = x \tag{3.14}$$

Operators (3.11)-(3.14) are illustrated in Fig. 3.3.

The technique is best described by the above 2DOF example. The first step is to write (3.9) in the form of separate equations using the simplified form of B:

$$\frac{\tau_1}{r_1} = -\xi_a - \xi_b + \xi_c \tag{3.15}$$

$$\frac{\tau_2}{r_2} = -\xi_a + \xi_b \tag{3.16}$$

Equation (3.16) is considered first, because it contains only two unknowns: ξ_a and ξ_b. Both ξ_a and ξ_b are always positive (by definition) and pull in opposite directions

(when one pulls, the other is zero), therefore operators (3.11) and (3.12) can be used to split (3.16) into two equations.

$$\xi_a = O^- \left(\frac{\tau_2}{r_2} \right) + \delta_{ab} \tag{3.17}$$

$$\xi_b = O^+ \left(\frac{\tau_2}{r_2} \right) + \delta_{ab} \tag{3.18}$$

where δ_{ab} is an arbitrary positive pretension force, and because the magnitude of δ_{ab} is the same in both (3.17) and (3.18), there will be no net torque as a result of this pretension force. The subscript, ab, is simply an indicator that only cables a and b have been considered thus far.

Next, substitute (3.17) and (3.18) into (3.15), rearrange, and use (3.13) to simplify:

$$\frac{\tau_1}{r_1} = -\left[O^+ \left(\frac{\tau_2}{r_2} \right) + O^- \left(\frac{\tau_2}{r_2} \right) \right] - 2\delta_{ab} + \xi_c = -\left| \frac{\tau_2}{r_2} \right| - 2\delta_{ab} + \xi_c \tag{3.19}$$

There are now only two unknowns (ξ_c and δ_{ab}), therefore the operators (3.11) and (3.12) can be applied again.

$$\delta_{ab} = \frac{1}{2} O^- \left(\frac{\tau_1}{r_1} + \left| \frac{\tau_2}{r_2} \right| \right) + \frac{1}{2}\delta_{abc} \tag{3.20}$$

$$\xi_c = O^+ \left(\frac{\tau_1}{r_1} + \left| \frac{\tau_2}{r_2} \right| \right) + \delta_{abc} \tag{3.21}$$

where δ_{abc} is another arbitrary positive bias force. The subscript abc indicates that all three cables have now been considered. Substituting (3.20) into (3.17) and (3.18), the final three equations for cable force as a function of joint torque are:

$$\xi_a = O^- \left(\frac{\tau_2}{r_2} \right) + \frac{1}{2} O^- \left(\frac{\tau_1}{r_1} + \left| \frac{\tau_2}{r_2} \right| \right) + \frac{1}{2}\delta_{abc} \tag{3.22a}$$

$$\xi_b = O^+ \left(\frac{\tau_2}{r_2} \right) + \frac{1}{2} O^- \left(\frac{\tau_1}{r_1} + \left| \frac{\tau_2}{r_2} \right| \right) + \frac{1}{2}\delta_{abc} \tag{3.22b}$$

$$\xi_c = O^+ \left(\frac{\tau_1}{r_1} + \left| \frac{\tau_2}{r_2} \right| \right) + \delta_{abc} \tag{3.22c}$$

The bias force, δ_{abc}, is included to ensure that tension is present in the cables at all times. The bias can be scaled arbitrarily provided it is positive, and will have no effect on the joint torque output of the mechanism.

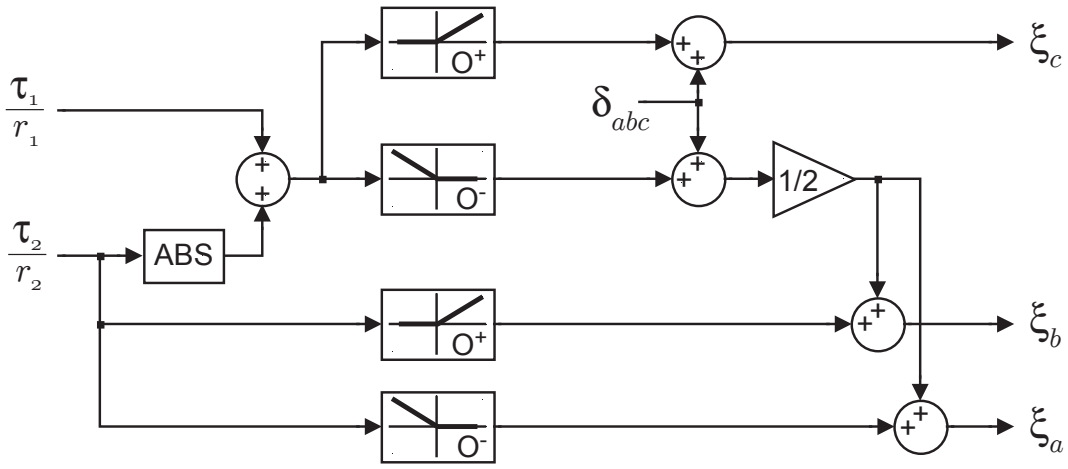

Figure 3.4: Torque resolver implementation schematic which transforms desired joint torques, τ_i, into associated tendon forces, ξ_i. The formulation also includes the required bias force, δ_{abc}.

A possible implementation for this transformation is shown in Fig. 3.4, which shows a graphical schematic of (3.22a)-(3.22c) for the 2DOF example in this section.

3.2 Cable Routing Structure Selection

For any open-ended cable-drive transmission with more than 2DOF, there are multiple cable routing structures that will provide complete actuation of all the joints. While there is only one unique cable routing scheme for a 2DOF manipulator, there are five for 3DOF, eleven for 4DOF, and so forth [102]. To increase the efficiency of the transmission, it is important to choose the routing scheme that provides the most even distribution of forces among the cables. Also, careful choice of cable routing can reduce the actuator requirements. The cable routing structure can have an influence on the friction, the apparent inertia, and the stiffness as seen at the joints. There are two main parameters that can be calculated from the structure matrix, B, of each routing scheme, which can be useful in choosing a suitable routing structure for a given manipulator.

For a multi-joint mechanism, powered by $n + 1$ cables, there are many possible

cable routes that can achieve full motion. Different cable routings share the forces differently among the cables in order to apply the same joint torques. If the forces are not shared equally, the system cannot operate efficiently, and can even result in severe antagonism between cables. It is possible to choose a structure that minimizes the relative differences in tension across all cables. This means not only that the forces are evenly distributed across all cables, but also that the maximum required force is minimized [102].

Parameter 1: In order to control the mechanism in joint space, it is necessary to calculate the forces from a given set of joint torques using the inverse of Equation 3.7. Since there are more cables than joints, there are infinite solutions. These solutions can be written as the sum of a particular solution plus a homogeneous solution [103]:

$$\boldsymbol{\xi} = B^{+}\boldsymbol{\tau} + \lambda \boldsymbol{H} \tag{3.23}$$

where $B^{+} = B^{T}(BB^{T})^{-1}$ is the pseudo-inverse of B, λ is a constant and $\boldsymbol{H}$ is the homogeneous solution ($B\boldsymbol{H} = 0$, therefore $\boldsymbol{H}$ is the null space of B). Each entry in $\boldsymbol{H}$ corresponds to the force in a cable. The value of λ will have no effect on the joint torques, $\boldsymbol{\tau}$, but must be chosen such that the solution does not contain negative cable forces at any configuration. This solution can be interpreted in the sense that for any cable drive system, when the cable forces are applied in the correct proportion (scalar multiple of $\boldsymbol{H}$), there will be no motion at any of the joints.

It is important to select a routing scheme in which the ratio of cable forces in the homogeneous solution is close to unity (for the 2DOF case with three cables, $\boldsymbol{H} = [1, 1, 1]^{T}$ is ideal). As the ratio between entries in $\boldsymbol{H}$ increases, antagonism between the cables becomes more severe, causing larger forces on the pulleys. The result is increased actuator torque requirements and reduced efficiency of the system.

This parameter can also be used to determine the ratio of pretension forces that must be applied to prevent the cables from becoming slack. In fact, this ratio appears in (3.22a)-(3.22c) from the 2DOF example from Section 3.1.2. The bias force, δ_{abc},

appears in each equation and is proportional to the homogeneous solution, $\boldsymbol{H}$. In this example (which has only one possible routing scheme), $\boldsymbol{H} = [1, 1, 2]^T$, thus the maximum antagonism ratio is 2.

Parameter 2: Another characteristic that is critical in choosing an appropriate routing scheme is maximum force required in the cables. Ideally, the forces are distributed evenly among the cables, but in most instances, the distribution is not even. Therefore, the ratio between the cable with the highest maximum force and the cable with the least maximum force becomes a useful indicator of manipulator performance. Choosing a routing scheme that minimizes this ratio of maximum cable forces can provide significant reductions in the actuator torque requirements.

The ratio can be found by considering the force manipulability ellipsoid for the cable system [102, 104]. In the context of cable-drive systems, the force manipulability ellipsoid characterizes the cable forces that are required to generate a set of joint torques, $\boldsymbol{\tau}$, given by:

$$\boldsymbol{\tau}^T \cdot \boldsymbol{\tau} = 1 \tag{3.24a}$$

$${\tau_1}^2 + {\tau_2}^2 = 1 \tag{3.24b}$$

To find the maximum forces in the cables for the conditions given by (3.24), there are a number of steps [102]. These will be summarized for the 2DOF case with three cables, but the technique can easily be expanded to work with higher DOF. Refer to [102] for a more detailed description.

The technique begins by considering (3.7) using the simplified structure matrix, B^* (considering only the routing structure and not the pulley radii for clarity).

$$\boldsymbol{\tau} = B^* \boldsymbol{\xi} \tag{3.25}$$

If $\xi_a = 0$ is substituted into (3.25), the relationship simplifies as follows:

$$\begin{bmatrix} \tau_1 \\ \tau_2 \end{bmatrix} = \begin{bmatrix} -1 & -1 & 1 \\ -1 & 1 & 0 \end{bmatrix} \begin{bmatrix} \xi_a \\ \xi_b \\ \xi_c \end{bmatrix} \Rightarrow \begin{bmatrix} -1 & 1 \\ 1 & 0 \end{bmatrix} \begin{bmatrix} \xi_b \\ \xi_c \end{bmatrix} \tag{3.26}$$

which means that the column of B^* corresponding to the first cable is removed. This solution describes the intersection of the force manipulability ellipsoid with the coordinate plane defined by ξ_b and ξ_c. Physically, this means that the cable does not contribute to the joint torques, and is on the verge of becoming slack. The idea is that the remaining cables *may* experience maximum tension as a result.

Equation (3.26) is now two equations and two unknowns, and it is simple to solve for the remaining two cable forces in terms of the joint torques:

$$\xi_b = \tau_1 \tag{3.27a}$$

$$\xi_c = \tau_1 + \tau_2 \tag{3.27b}$$

This process is repeated, for the cases in which $\xi_b = 0$ and $\xi_c = 0$, removing the column corresponding to that cable, and solving for the remaining cable forces. In the end, there are n expressions of the above form for each of the m cables ($n \times m = 2 \times 3 = 6$ in total for this example). The typical form for the i^{th} cable is as follows:

$$\xi_i = X\tau_1 + Y\tau_2 \tag{3.28}$$

where X and Y are coefficients resulting from B^*. Next, the Cauchy-Schwarz Inequality is used to find the maximum force. The form of the inequality is:

$$\xi_i^2 = (X\tau_1 + Y\tau_2)^2 \leq (X^2 + Y^2)({\tau_1}^2 + {\tau_2}^2) \tag{3.29}$$

Combining (3.24) and (3.29), the result simplifies to:

$$\xi_i \leq \sqrt{X^2 + Y^2} \tag{3.30}$$

Equation (3.30) is applied to each of the 6 expressions to obtain the maximum force in each case. The results are proportional to the maximum forces on the cables for the joint torque vector given by (3.24).

In the final step, the largest of the n values calculated for each cable is selected as the maximum force for that cable, and written into a vector form. The vector for

the 2DOF example is $[1, 1, \sqrt{2}]^T$, which means that the maximum force ratio among cables (highest maximum to lowest maximum) in the given cable routing scheme is 1.41. For systems with higher DOF, this ratio varies significantly between routing schemes, which indicates that some schemes require several times more actuator power to achieve the same result. Thus carefully selecting the cable routing scheme allows the use of lighter, smaller and cheaper motors.

3.3 Four-Bar Linkage Mechanics

A 4-bar linkage is a simple mechanism that consists of four rigid links connected by revolute joints (see Fig. 3.5). They have a multitude of uses in a range of applications requiring rotation or oscillation. Typically, one link is fixed (link 1). The other links are known as the input link (link 4), the follower link (link 2), and the coupler or floating link (link 3). When a torque is applied to link 4, the mechanism will move.

The resulting motion of the linkage depends highly on the relative lengths of the four links, and also which of these lengths are fixed. A special class of four-bar linkages are called Grashof linkages [105]. Linkages in this class have a special characteristic

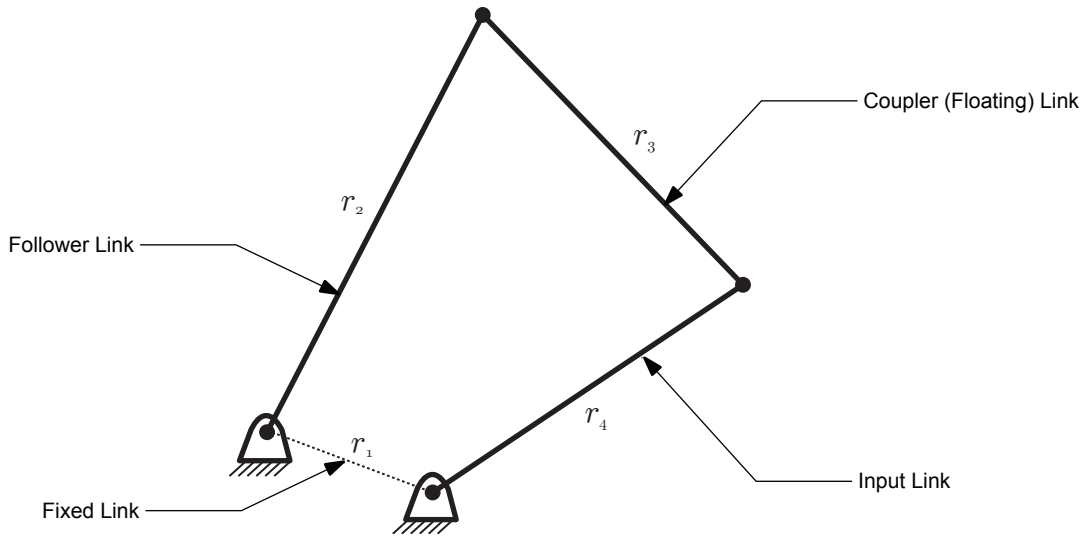

Figure 3.5: A schematic of a 4-bar linkage. In this case, it is a Grashof linkage with its shortest link fixed, therefore both links 2 and 4 can rotate a full 360°.

that allows continuous motion (360° rotation) of links adjacent to the shortest link. To be a part of this class, the following relationship between the link lengths must hold true:

$$r_{shortest} + r_{longest} < r_{middle_1} + r_{middle_2} \tag{3.31}$$

The shortest link can be in any one of four positions relative to the fixed link, which can have a profound effect on the kinematics of the overall system. If the shortest link is the fixed link, a unique case arises. In this case, both the input and follower links have the ability to make unrestricted 360° rotations. Therefore, it is not possible to run into a singularity with this configuration. Fig. 3.5 is an example of a Grashof linkage of this special type because $r_1 + r_2 < r_3 + r_4$, and the shortest link (link 1) is fixed. For robotic 4-bar linkage designs that require a large range of motion, a Grashof linkage may be a suitable choice. However, for devices with smaller range of motion, non-Grashof linkages can be perfectly suitable. The following mathematical derivations apply to any 4-bar linkage.

3.3.1 Kinematic Analysis

The links making up the 4-bar linkage are coupled together, and as a result, knowledge of the motion of one link (i.e. the input) will determine the motion of the other links. To analyze the kinematics of such a linkage, it is simplest to first describe the links in vector form:

$$\boldsymbol{r_2} + \boldsymbol{r_3} = \boldsymbol{r_1} + \boldsymbol{r_4} \tag{3.32}$$

where the vectors are as defined in Fig. 3.6. These vectors can also be written in complex form:

$$r_2 e^{i\alpha_2} + r_3 e^{i\alpha_3} = r_1 e^{i\alpha_1} + r_4 e^{i\alpha_4} \tag{3.33}$$

where r_1, r_2, r_3, and r_4 are the link lengths, and α_1, α_2, α_3, and α_4 are the four joint angles, as labeled in Fig. 3.6. All link lengths and α_1 are known constants.

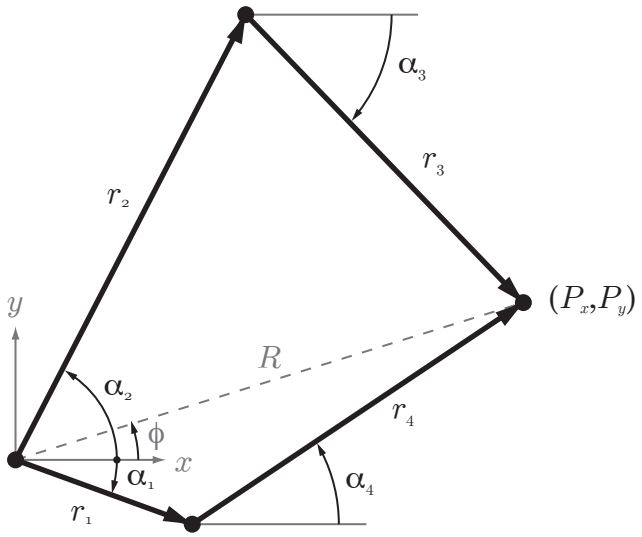

Figure 3.6: A vector schematic of a 4-bar linkage. Each angle and link length is labelled, and the end-point of the vector pairs is labelled (P_x, P_y).

Position

The position of all links of the mechanism depends on the input angle, which in this case is α_4. The following describes how to solve for α_2 and α_3, given α_4.

Equation (3.32) and Fig. 3.6 indicate that there are two different vector paths that can be used to describe the common endpoint, (P_x, P_y). These two paths can be written in terms of the x and y components P_x and P_y, respectively:

$$P_x \longrightarrow r_2 \cos\alpha_2 + r_3 \cos\alpha_3 = r_1 \cos\alpha_1 + r_4 \cos\alpha_4 \tag{3.34}$$

$$P_y \longrightarrow r_2 \sin\alpha_2 + r_3 \sin\alpha_3 = r_1 \sin\alpha_1 + r_4 \sin\alpha_4 \tag{3.35}$$

So there are two equations to describe P_x and P_y. However, α_4 is the input and thus its position is known, which means that all variables contained in one of the paths are known. Therefore x and y components of the endpoint, P_x and P_y, can be written in terms of these known values:

$$P_x = r_1 \cos\alpha_1 + r_4 \cos\alpha_4 \tag{3.36}$$

$$P_y = r_1 \sin\alpha_1 + r_4 \sin\alpha_4 \tag{3.37}$$

What is left is a system of two equations:

$$r_2 \cos\alpha_2 + r_3 \cos\alpha_3 = P_x \tag{3.38}$$

$$r_2 \sin\alpha_2 + r_3 \sin\alpha_3 = P_y \tag{3.39}$$

which can be solved for the two unknowns: α_2 and α_3.

The first step is to rearrange both (3.38) and (3.39) as follows:

$$\cos\alpha_2 = \frac{P_x - r_3 \cos\alpha_3}{r_2} \tag{3.40}$$

$$\sin\alpha_2 = \frac{P_y - r_3 \sin\alpha_3}{r_2} \tag{3.41}$$

To find α_3, (3.40) and (3.41) must be squared, then added, and rearranged to give:

$$P_y \sin\alpha_3 + P_x \cos\alpha_3 = \frac{{P_x}^2 + {P_y}^2 + {r_3}^2 - {r_2}^2}{2r_3} \tag{3.42}$$

At this point, it is useful to define point (P_x, P_y) in terms of two new variables:

$$R = \sqrt{{P_x}^2 + {P_y}^2} \tag{3.43}$$

$$\phi = \arctan\left(\frac{P_y}{P_x}\right) \tag{3.44}$$

so that P_x and P_y can be defined as follows:

$$P_x = R\cos\phi \tag{3.45}$$

$$P_y = R\sin\phi \tag{3.46}$$

Next, substitute (3.45) and (3.46) into the left side of (3.42).

$$R\sin\phi\sin\alpha_3 + R\cos\phi\cos\alpha_3 = \frac{{P_x}^2 + {P_y}^2 + {r_3}^2 - {r_2}^2}{2r_3} \tag{3.47}$$

After simplifying with a trigonometric sum-difference identity, substituting (3.43) and (3.44), and then solving for α_3, the solution is obtained:

$$\alpha_3 = \arctan\left(\frac{P_y}{P_x}\right) - \arccos\left(\frac{{P_x}^2 + {P_y}^2 + {r_3}^2 - {r_2}^2}{2r_3\sqrt{{P_x}^2 + {P_y}^2}}\right) \tag{3.48}$$

Finding α_2 is found from (3.40) and (3.41):

$$\alpha_2 = \arctan\left(\frac{\sin\alpha_2}{\cos\alpha_2}\right) = \arctan\left(\frac{P_y - r_3\sin\alpha_3}{P_x - r_3\cos\alpha_3}\right) \tag{3.49}$$

where, for both (3.48) and (3.49), P_x and P_y are defined by (3.36) and (3.37).

Velocity

To find the angular velocity of the unknown joints, $\dot{\alpha}_2$ and $\dot{\alpha}_3$ knowing $\dot{\alpha}_4$, it is simplest to consider the complex notation. Start by taking the time derivative of (3.33).

$$i\dot{\alpha}_2 r_2 e^{i\alpha_2} + i\dot{\alpha}_3 r_3 e^{i\alpha_3} = 0 + i\dot{\alpha}_4 r_4 e^{i\alpha_4} \tag{3.50}$$

To find $\dot{\alpha}_3$, multiply (3.50) by $e^{-i\alpha_2}$:

$$i\dot{\alpha}_2 r_2 + i\dot{\alpha}_3 r_3 e^{i(\alpha_3-\alpha_2)} = i\dot{\alpha}_4 r_4 e^{i(\alpha_4-\alpha_2)} \tag{3.51}$$

Use the identity, $e^{i\beta} = \cos\beta + i\sin\beta$ to expand (3.51). To get the final solution, equate the real parts and solve for $\dot{\alpha}_3$.

$$\dot{\alpha}_3 = \dot{\alpha}_4 \left(\frac{r_4 \sin(\alpha_4 - \alpha_2)}{r_3 \sin(\alpha_3 - \alpha_2)} \right) \tag{3.52}$$

Similarly, $\dot{\alpha}_2$ can be found by multiplying (3.50) by $e^{-i\alpha_3}$. The final solution is:

$$\dot{\alpha}_2 = \dot{\alpha}_4 \left(\frac{r_4 \sin(\alpha_4 - \alpha_3)}{r_2 \sin(\alpha_2 - \alpha_3)} \right) \tag{3.53}$$

Acceleration

The procedure to find the angular acceleration of the unknown joints, $\ddot{\alpha}_2$ and $\ddot{\alpha}_3$ knowing $\ddot{\alpha}_4$, begins with the second derivative of (3.33).

$$i\ddot{\alpha}_2 r_2 e^{i\alpha_2} - \dot{\alpha}_2{}^2 r_2 e^{i\alpha_2} + i\ddot{\alpha}_3 r_3 e^{i\alpha_3} - \dot{\alpha}_3{}^3 r_3 e^{i\alpha_3} = 0 + i\ddot{\alpha}_4 r_4 e^{i\alpha_4} - \dot{\alpha}_4{}^4 r_4 e^{i\alpha_4} \tag{3.54}$$

Following the same steps as for the velocity analysis, the final solutions are:

$$\ddot{\alpha}_3 = \frac{\ddot{\alpha}_4 r_4 \sin(\alpha_4 - \alpha_2) + \dot{\alpha}_4{}^2 r_4 \cos(\alpha_4 - \alpha_2) - \dot{\alpha}_2{}^2 r_2 - \dot{\alpha}_3{}^2 r_3 \cos(\alpha_3 - \alpha_2)}{r_3 \sin(\alpha_3 - \alpha_2)} \tag{3.55}$$

$$\ddot{\alpha}_2 = \frac{\ddot{\alpha}_4 r_4 \sin(\alpha_4 - \alpha_3) + \dot{\alpha}_4{}^2 r_4 \cos(\alpha_4 - \alpha_3) - \dot{\alpha}_3{}^2 r_3 - \dot{\alpha}_2{}^2 r_2 \cos(\alpha_2 - \alpha_3)}{r_2 \sin(\alpha_2 - \alpha_3)} \tag{3.56}$$

3.3.2 Force Analysis

Force analysis can be used to relate the forces and torques within the linkage given a known external input torque. The first step is to create a free body diagram of the linkage. Fig. 3.7 shows the free body diagram for the linkage for the case in which gravity is not included (i.e. for a planar system).

The next step is to write the static equilibrium equations for each movable link. There will be three equations for each link (x-force, y-force, and moment), and because link 1 is fixed, there are 9 equations total:

$$F_{12x} + F_{32x} = 0 \tag{3.57a}$$

$$F_{12y} + F_{32y} = 0 \tag{3.57b}$$

$$\boldsymbol{\tau_2} + \boldsymbol{r_2} \times \boldsymbol{F_{32}} = 0 = \tau_2 + r_2 \cos\alpha_2 F_{32y} - r_2 \sin\alpha_2 F_{32x} \tag{3.57c}$$

$$F_{23x} + F_{43x} = 0 \tag{3.57d}$$

$$F_{23y} + F_{43y} = 0 \tag{3.57e}$$

$$\boldsymbol{r_3} \times \boldsymbol{F_{43}} = 0 = r_3 \cos\alpha_3 F_{43y} - r_3 \sin\alpha_3 F_{43x} \tag{3.57f}$$

$$F_{34x} + F_{14x} = 0 \tag{3.57g}$$

$$F_{34y} + F_{14y} = 0 \tag{3.57h}$$

$$\boldsymbol{\tau_4} + \boldsymbol{r_4} \times \boldsymbol{F_{34}} = 0 = \tau_4 + r_4 \cos\alpha_4 F_{34y} - r_4 \sin\alpha_4 F_{34x} \tag{3.57i}$$

where the moment equations describe the net moments acting on the link about an endpoint of the link. The links are attached, thus the internal reaction forces can be simplified using $F_{ijx} = -F_{jix}$ and $F_{ijy} = -F_{jiy}$. After making these simplifications, the resulting system of 9 equations and 9 unknowns can be solved for the forces and moments. One of the solutions relates input torque, τ_4, to output torque, τ_2:

$$\tau_4 = -\left(\frac{r_4 \sin(\alpha_4 - \alpha_3)}{r_2 \sin(\alpha_2 - \alpha_3)}\right)\tau_2 \tag{3.58}$$

Equation (3.58) can be interpreted as the external torque that would be required at joint 4 to keep the mechanism from moving (to keep it in static equilibrium) if an

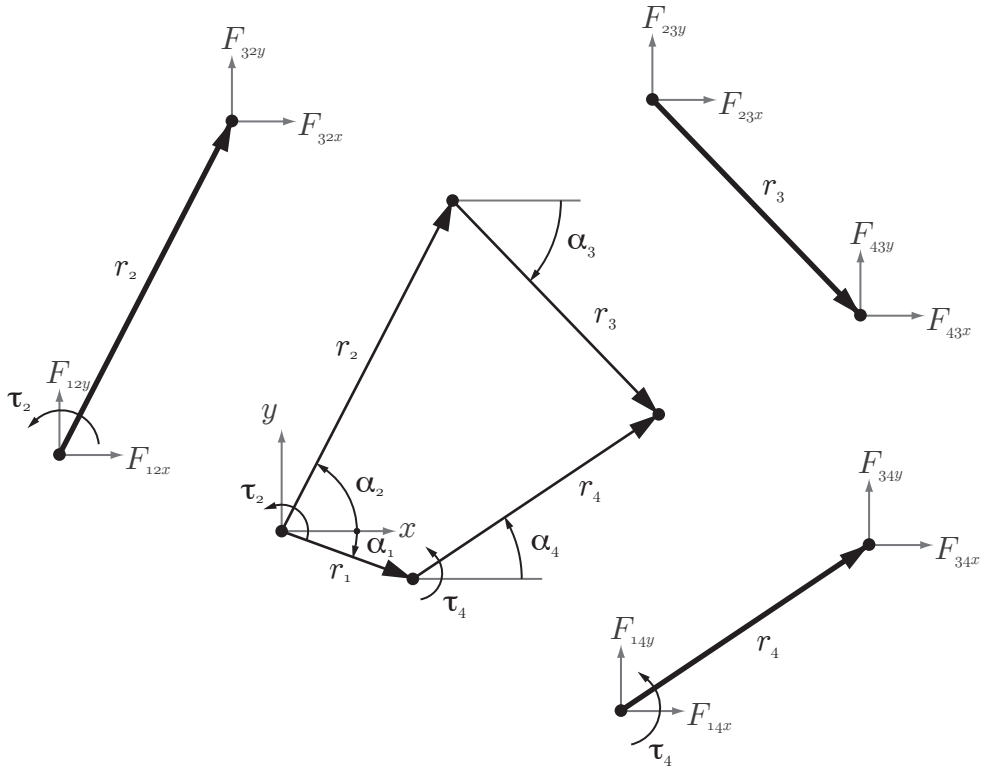

Figure 3.7: Free body diagrams for a 4-bar linkage. The diagram for each link is shown independently, and is offset from the central 4-bar linkage diagram.

external torque was applied at joint 2. Another useful interpretation appears if (3.58) is multiplied by -1:

$$\tau_4 = \left(\frac{r_4 \sin(\alpha_4 - \alpha_3)}{r_2 \sin(\alpha_2 - \alpha_3)} \right) \tau_2 \tag{3.59}$$

in which case (3.59) can be interpreted as the external torque that must be applied at joint 4 to produce a known equivalent torque about joint 2. The interpretation in (3.59) will be used in later chapters. In either case, it is clear that the applied torque depends on the position of the linkage.

In the special case of a parallelogram, $r_1 = r_3$, $r_2 = r_4$, $\alpha_1 = \alpha_3$ and $\alpha_2 = \alpha_4$, therefore (3.59) simplifies to $\tau_4 = \tau_2$. The applied torque no longer depends on the position of the linkage.

Chapter 4: MEDARM

MEDARM (Motorized Exoskeleton Device for Advanced Rehabilitation of Motor function) has been designed for rehabilitation and assessment of the shoulder complex. However, the shoulder girdle has not been well addressed by rehabilitation robots. The shoulder girdle is a part of upper-limb motion [4], and because it is often recruited for compensatory movements [32], it should be a part of robotic rehabilitation.

The main goal with MEDARM is to replicate the DOF of the upper-limb that are involved in coarse reaching movements. This means that independent control should be provided to all five main DOF of the shoulder complex, and one DOF at the elbow (the second DOF at the elbow, pronation/supination, is involved with fine control and hand orientation). Several other features have also been incorporated. First, the joint axes are arranged to mimic natural upper-limb motion without reaching singularity, and while maintaining high kinematic manipulability. Second, the robot is able to reduce to 2DOF planar motion in any plane, which will simplify some therapy and assessment programs. Third, MEDARM is driven by a novel combination of four-bar linkage and cable-drive system that enables remote actuation of the joints. Finally, the device has a simple attachment and alignment procedure for the user.

This chapter begins by introducing the key design objectives used to create MEDARM's final mechanical design. A detailed technical description of the proposed design for MEDARM is then provided.

4.1 MEDARM Design Objectives

MEDARM was designed with specific therapeutic functionality in mind. A set of design objectives required to achieve the desired functionality were outlined and then grouped into two categories: robot-user interface and technical design. Not sur-

prisingly, there is significant overlap between these categories. This section describes these objectives in terms of these groupings. The objectives are summarized in Table 4.1, where each goal is identified by number for future reference within the chapter.

4.1.1 Therapeutic Functionality Objectives

MEDARM is intended to assist a therapist with the delivery of rehabilitation services to stroke patients with upper-limb motor deficits. A key part of the design process involves specifying the types of tasks the robot should be able to perform.

The fundamental requirement for any upper-limb rehabilitation robot is to be able to perform basic therapy tasks that would otherwise be performed manually by a therapist. A significant part of typical therapy programs includes full or partial assistance with functional reaching movements [32]. Repeating and practicing these functional movements is part of the motor learning process, and is thus important for recovering the ability to perform activities of daily living. Patients with motor impairments may initially require full assistance, but the level of required assistance decreases as function is regained. As such, MEDARM should be able to replicate functional movements with any level of assistance (Th.1), and should move passively with the patient when assistance is not needed (Th.2).

Another important function of a rehabilitation robot is gravity compensation. Overcoming the forces of gravity during motion is difficult for weak patients, and removing these forces can make it easier for a patient to perform reaching movements [37]. However, it is difficult for a therapist to manually eliminate the effect of gravity. Sling systems can be used, but they do not compensate equally across the upper-limb workspace. MEDARM should be designed to provide any level of gravity compensation for all reaching movements (Th.3).

One of the advantages of robotic technology is the ability to present the user with virtual environments. The simplest case would be to apply simple resistive loads.

Table 4.1: A summary the design objectives for MEDARM. Th.X stands for therapeutic functionality objectives, RI.X stands for robot-user interface objectives, and Te.X stands for technical objectives.

Number	**Objective**
Th.1	Replicate functional movements with any level of assistance.
Th.2	Move passively with the patient when assistance is not needed.
Th.3	Provide any level of gravity compensation for all reaching movements.
Th.4	Simulate a range of virtual environments.
Th.5	Allow joint-based control of the patients limb.
Th.6	Operate simultaneously as a therapy device and an assessment system.
Th.7	Reduce to planar motion.
Th.8	Replicate basic fundamental movements with as simple a mechanism as possible.
RI.1	Safety: joint limits, comfort, etc...
RI.2	Coarse reaching movements replication. Independent control 6DOF of upper-limb: 2DOF at the sternoclavicular joint, 3DOF at the glenohumeral joint and 1DOF at the elbow (flexion/extension).
RI.3	Range of motion (ROM) should at least match the functional ROM (Section 2.1.1) .
RI.4	Fully adjustable to accommodate a wide range of users (1.4m and 2.0m in height).
RI.5	Attachment system should be quick and simple.
RI.6	Robot should be unobtrusive (i.e. place mechanism away from the users head).
Te.1	Singular configurations must be avoided over the entire upper-limb workspace.
Te.2	Manipulability of the mechanism should be maximized.
Te.3	Mechanism must not collide with itself or the user.
Te.4	Generate joint torques sufficient to move the arm of a large user (up to 2.0m height and 115kg weight) with an end-point speed of up to 1.0m/s without any assistance from the user.
Te.5	Backdriveable.
Te.6	High power-to-weight ratio.
Te.7	Low friction.
Te.8	Low inertia, lightweight.

This type of progressive-resistive exercise is a key component of regaining strength and coordination [41]. Therefore, MEDARM should be able to simulate a range of environments (Th.4), including movement through viscous fluids and picking up objects. Other complex environments can be designed to encourage proper coordination and to prevent compensation by limiting or locking motion at specific joints. Movements may also be purposefully restricted to simpler single-joint or planar motions to reduce abnormal muscle synergies, or to perform functional assessment. MEDARM should thus be designed to allow joint-based control of the patient's limb (Th.5).

Another aspect of rehabilitation programs is patient monitoring and assessment. Since robots provide ongoing quantitative measurements of movement and are inherently objective, they show significant potential as diagnostic and assessment tools [22, 24, 25]. Thus, MEDARM should be able to operate simultaneously as a therapy device and an assessment system (Th.6). The robot should be able to transparently observe and record movements throughout the treatment program. This would provide an ongoing measure of progress, and this data could be stored for future use.

Simplification of movements can facilitate assessment (simpler equations of motion), and thus a useful feature would be the restriction of movement to planar motion. There is also clinical value in providing assessment and movement training of some of the fundamental upper-limb movements such as flexion/extension and abduction/adduction. These movements provide a consistent means of monitoring range of motion, and they can be used to target specific muscle groups during exercise. MEDARM should be designed to reduce to planar motion (Th.7) and to replicate basic fundamental movements with as simple a mechanism as possible (Th.8).

4.1.2 Robot-User Interface Objectives

Anytime a robot is used intimately with a person, there are a number of design considerations that must be met. The fact that people vary in size, shape, and motor

ability makes it a tremendous challenge to accommodate everyone's needs.

Safety (RI.1), of course, is of utmost importance, therefore MEDARM should have hardware and software limits to ensure that joints are not overextended. Other kinematic and dynamic limits should also be considered. A secure and comfortable attachment to the user should be maintained with minimal pinching, rubbing, stretching or twisting. This is particularly important in a rehabilitation setting because elderly users and patients with motor impairments are often more susceptible to injury from forced movements. Moreover, these users typically have more sensitive and supple skin, and/or have limited ability to sense their environment.

To provide realistic functional training, a rehabilitation robot must be able to closely mimic natural motion of the upper-limb. However, few robotic devices can replicate motion of the entire shoulder complex. Therefore, a fundamental goal for the design of MEDARM is to provide independent control for all 5DOF of the shoulder complex: 2DOF at the sternoclavicular joint, 3DOF at the glenohumeral joint (RI.2). In addition, 1DOF at the elbow (flexion/extension) must also be included in order to make reaching movements, bringing the total to 6DOF. Collectively, these 6DOF should at least match the functional ROM as outlined in Section 2.1.1 (RI.3).

MEDARM should be fully adjustable to accommodate a wide range of users (RI.4) with limb segments of varying length, width and shape as summarized in Tables 2.1 and 2.2 from Section 2.1.3. It is not sufficient to design only for the range of 5^{th} to 95^{th} percentile individuals, as there is still 10% of the population that cannot fit in the device. The vast majority of the adult population falls between the range of 1.4m and 2.0m in height [14], therefore the mechanisms link lengths should be adjustable to fit this range of people.

There is a strong argument for minimizing patient set-up time. The overall effectiveness of the robotic treatment will be reduced if the setup time is long and uncomfortable for the patient, and complicated for the therapist. Therefore, the attachment

system should be quick and simple (RI.5), while still maintaining adjustability for a range of people. Issues relating to patient comfort should also be considered. As much as possible, the robot should be unobtrusive (RI.6). For example, placing the mechanism away from the users head is more comfortable for the user, and will not interfere with movements.

4.1.3 Technical Objectives

The design of the mechanism itself also plays a critical role in the overall capabilities of the robot. The relative placement and orientation of the joint axes influences the robot's performance. More specifically, singular configurations must be avoided over the entire upper-limb workspace to prevent the loss of one or more DOF (Te.1). Furthermore, manipulability of the mechanism (the ability to position and orient it's end-effector within the workspace [104]) should be maximized over the workspace to reduce actuator requirements and improve the ability of the robot to move passively (Te.2). Finally, the mechanism must not collide with itself or the user at any point in the workspace (Te.3).

MEDARM should be able to drive a user's arm through a variety of functional movement patterns. Thus, as an upper-limit, MEDARM's actuation system should be able to generate enough torque at each joint to move the arm of a large user (up to 2.0m height and 115kg weight) with an end-point speed of up to 1.0m/s [8] without any assistance from the user (Te.4). At the same time, it is important that the system can be used passively as an assessment tool. In order for the robot to be powerful enough for therapy while achieving a high level of transparency (i.e. the feeling that the robot is not present) for assessment purposes, the robot must be backdriveable (Te.5) with a high power-to-weight ratio (Te.6) and low friction (Te.7). Making the mechanism as small and lightweight as possible (Te.8) without losing the structural rigidity required to provide movement assistance will also contribute to transparency.

4.2 MEDARM Design Overview

MEDARM is an exoskeleton. An exoskeleton design was chosen because it is the only way to independently control all DOF in the shoulder complex, otherwise the redundancy of the joints would make it impossible to isolate motion of the glenohumeral joint from motion of the shoulder girdle. Another advantage of the exoskeleton design is that grasping a handle is not necessary, leaving the hand available for functional training, if desired.

The design of MEDARM is shown in Fig. 4.1. The robot is mounted to a support structure, and the user is wheeled into position using a movable chair. There is space for the operator to get beside the exoskeleton during the set-up procedure. MEDARM consists of two main subsystems: the shoulder/elbow mechanism (4DOF to move the upper-arm and forearm), and the shoulder girdle mechanism (2DOF to move the glenohumeral joint relative to the torso). The shoulder/elbow mechanism itself consists of a 3DOF spherical joint centred at the user's glenohumeral joint and a single rotary joint at the elbow. It is actuated entirely by a cable-drive transmission which is powered by five electric motors located on the base of the system. The shoulder girdle mechanism is based on a novel curved track mechanism which allows the exoskeleton to be located behind the user. It is driven directly by two motors, although all cables for the shoulder/elbow mechanism are routed along the shoulder girdle mechanism to the base in such as way that they assist the two motors.

Each of the six individual joint motions are depicted in Fig. 4.2. Fig. 4.2a and Fig. 4.2b illustrate the 2DOF of the shoulder girdle mechanism. Joints 1 and 2 correspond to elevation/depression and protraction/retraction, respectively. Fig. 4.2c, Fig. 4.2d, Fig. 4.2e, and Fig. 4.2f show the 4DOF of the shoulder/elbow mechanism. Together, joints 3, 4 and 5 provide 3DOF at the glenohumeral joint, and joint 6 provides flexion/extension of the elbow.

The system is designed to be lightweight and backdriveable in order to minimize

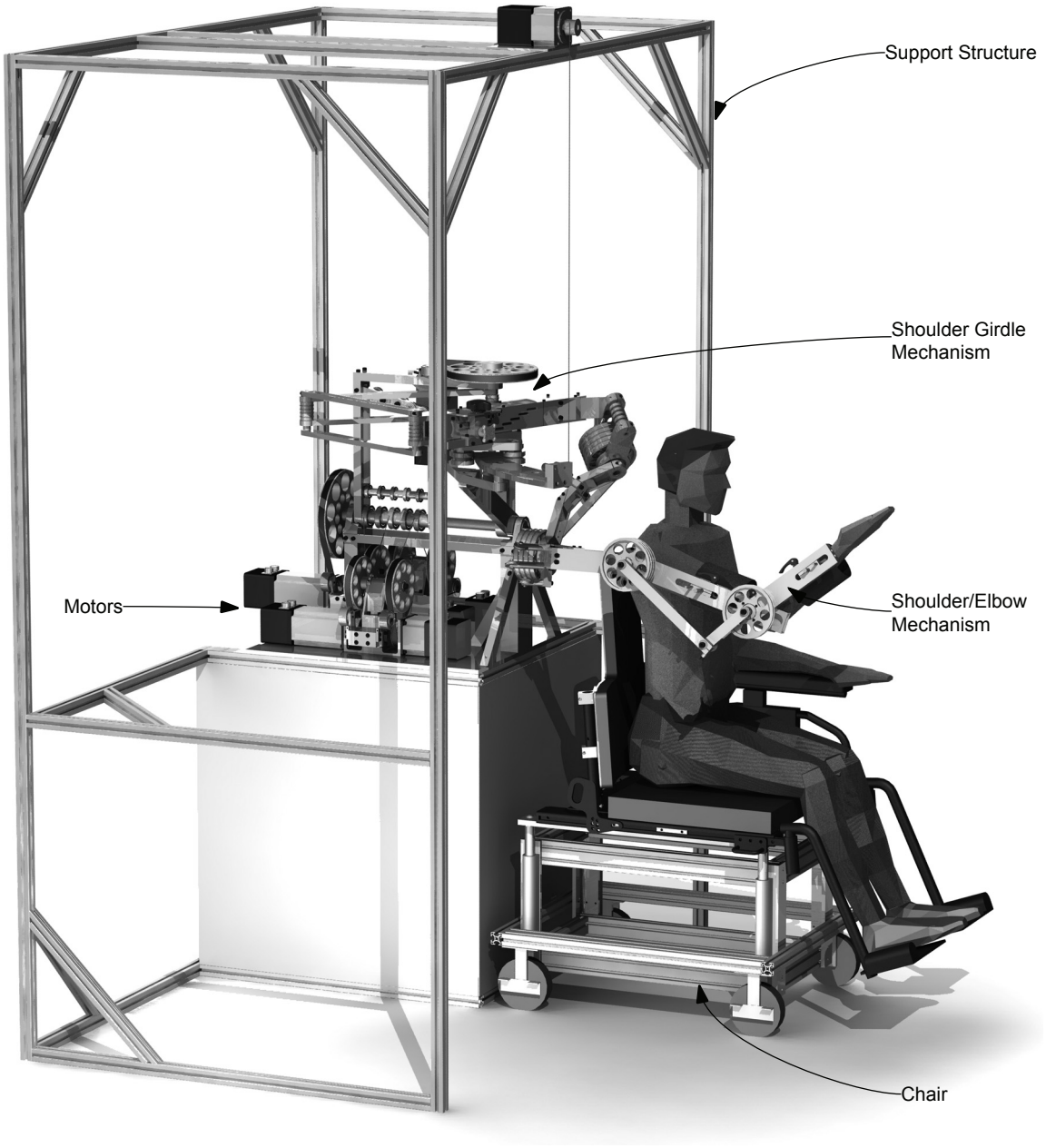

Figure 4.1: MEDARM system consists of a 6DOF robotic exoskeleton mounted onto a support structure. The motors and electronics are mounted underneath the robot, and external gravity compensation is provided by a motorized vertical cabling system. A movable chair is used to bring the user into alignment with the system.

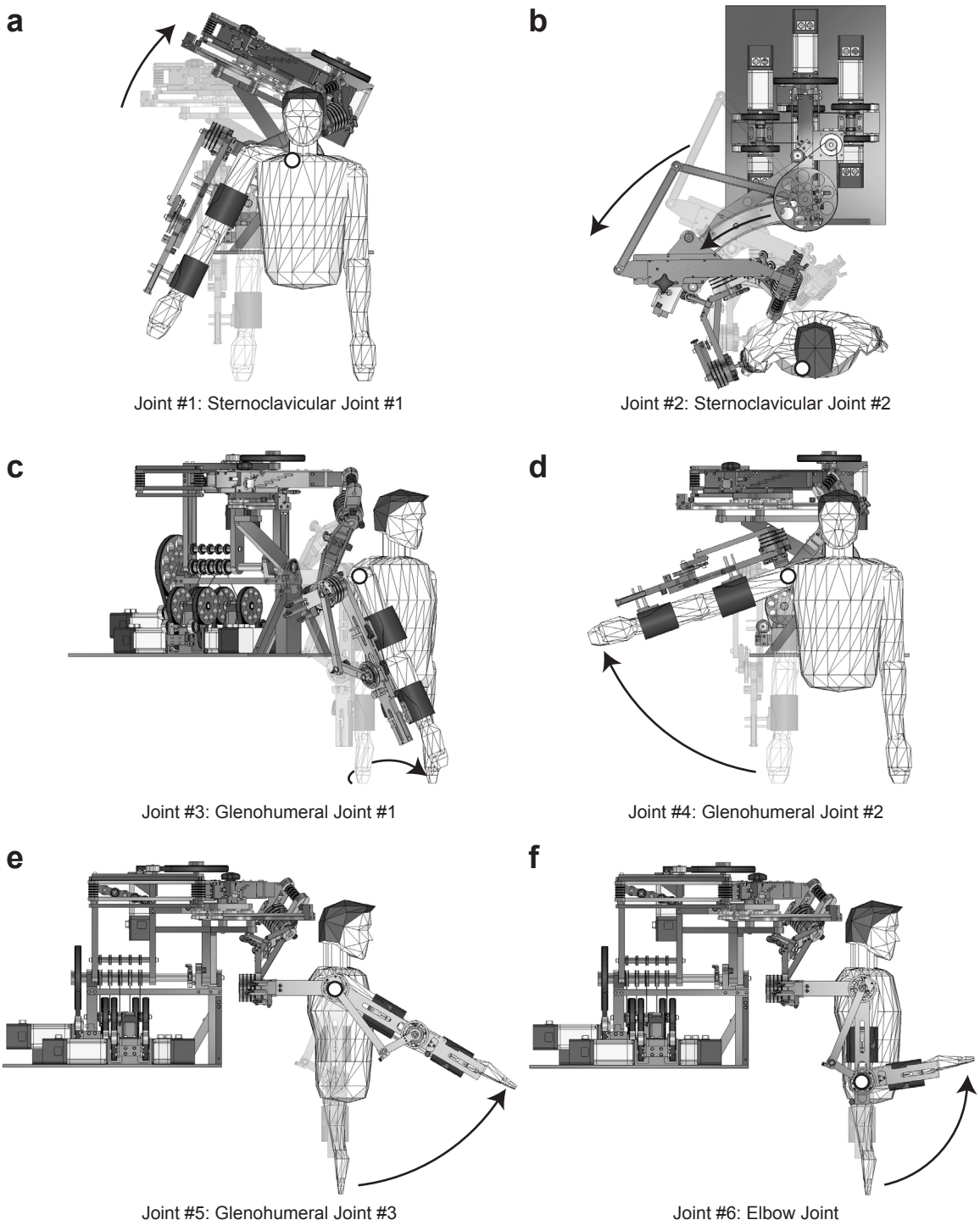

Figure 4.2: Diagrams illustrating the individual DOF in MEDARM. The joint centres are indicated by the white circles. (a) Joint 1 and (b) Joint 2 are centered on the sternoclavicular joint, and mimic elevation/depression and protraction/retraction, respectively. (c) Joint 3, (d) Joint 4, and (e) Joint 5 together replicate the 3DOF of the glenohumeral joint. When operating individually, Joint 4 provides abduction/adduction, and Joint 5 provides flexion/extension. (f) Joint 6 provides flexion/extension of the elbow joint.

the robot's influence on natural upper-limb motion. The mechanism is attached to the lateral side of the user's arm using two adjustable inflatable arm cuffs, which are the only points of physical attachment to the user. There are several adjustments to account for users of different size. The following sections describe the technical details of MEDARM's mechanism design and its actuation system.

4.3 MEDARM Mechanical Design

There are several important features of the mechanical design that contribute to the uniqueness of MEDARM's design. The first is the shoulder girdle mechanism, which uses a novel virtual 4-bar linkage to drive one of the joints. The next is the glenohumeral joint, which has been designed to avoid singularities and to maximize manipulability using a procedure that was developed specifically for MEDARM. Also, the joints of the shoulder/elbow mechanism are specially designed to contain several functions in a compact form. And finally, the method of attaching and aligning the user in the exoskeleton has some unique features designed specifically to simplify the user set-up procedure. These design features will be discussed in detail in this section.

4.3.1 Shoulder Girdle Mechanism

The shoulder girdle is challenging to replicate for several reasons. Shoulder girdle motion is difficult to characterize because it is a complicated closed-loop mechanism with 4DOF. Most of the motion can be replicated by considering the sternoclavicular joint as the base. Unfortunately, the sternoclavicular joint is difficult to access with conventional mechanisms because the body and head interfere significantly with just about any choice of joint axis orientation. The result is that equipment must be placed over and around the head, and the equipment ends up being large and very bulky to accommodate the large variations in patient size and shape.

MEDARM's shoulder girdle mechanism provides 2DOF about the sternoclavicular

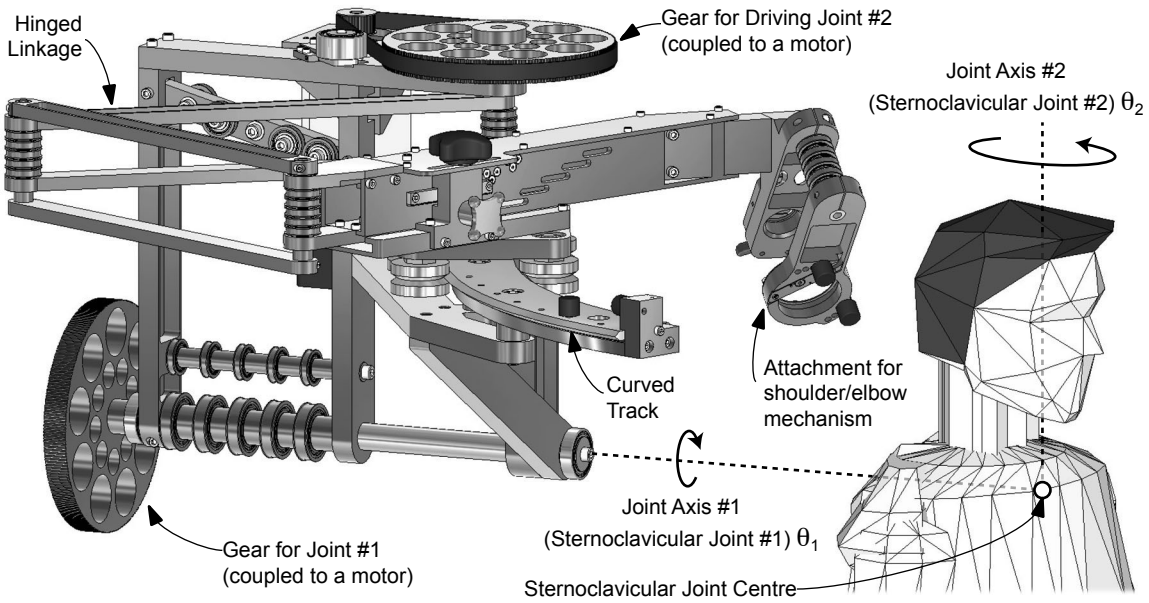

Figure 4.3: A CAD drawing of the shoulder girdle mechanism. The two joint axes intersect at the user's sternoclavicular joint as indicated by the hollow circle. The second joint is a translation along a curved track as part of a virtual 4-bar linkage, producing a rotation about the vertical axis.

joint centre: elevation/depression and protraction/retraction (Fig. 4.3). Its unique curved track mechanism allows the equipment to be located behind the user, with minimal equipment near the head. The mechanism includes adjustments to accommodate users of different size, as will be discussed in Section 4.3.4. The mechanism supports the complete shoulder/elbow system including the user's arm, and guides the driving cables to the joints. As a result, the mechanism is structurally strong.

The first joint axis is fixed to the base structure behind the user, with its axis pointing forward in the horizontal plane. It is a conventional rotary joint that provides elevation/depression motion.

The second joint axis is vertically aligned, and intersects the first joint axis at the user's sternoclavicular joint centre, allowing protraction/retraction motion. However, it is not a typical rotary joint. Details of the mechanism are illustrated in Fig. 4.4. The heart of the mechanism is a curved track that is aligned with the user's sternoclavicular joint (see Fig. 4.4a). A low-friction carriage runs along this track, so all

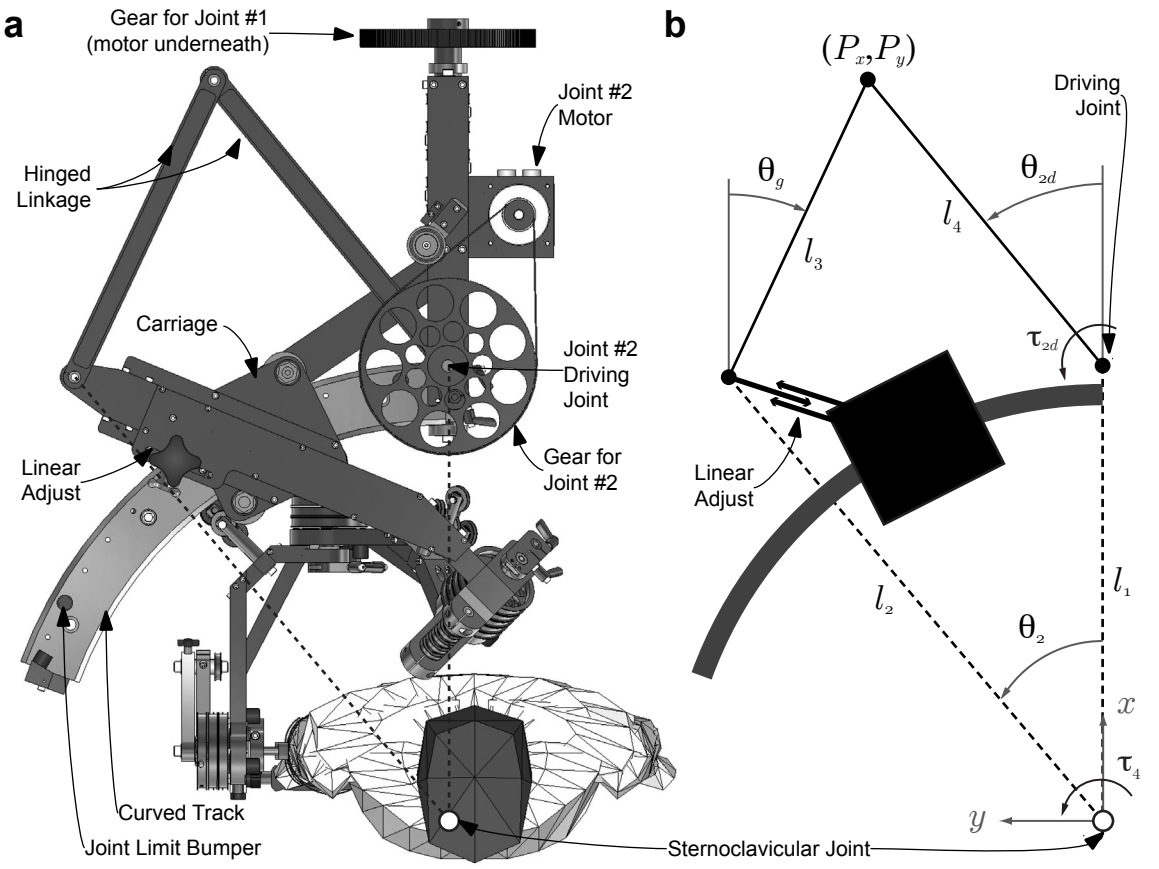

Figure 4.4: (a) A top view CAD drawing of the virtual 4-bar mechanism that drives the second shoulder girdle joint. (b) A schematic of the virtual 4-bar linkage. The links and angles can be related to Fig. 3.6 as follows: $\alpha_1 = 0$, $l_1 = 0.55$m $(= r_1)$, $l_3 = 0.40$m $(= r_3)$, and $l_4 = 0.45$m $(= r_4)$. $l_2 (= r_2)$ changes length depending on the linear adjustment as shown. $\theta_2 (= \alpha_2)$ is the joint 2 angle, and $\theta_{2d} (= \alpha_4)$ is the joint 2 driving joint angle.

equipment placed on the carriage will rotate about the sternoclavicular joint of the user. The carriage is attached to a two-link hinged linkage, which closes the mechanical loop. When the hinged linkage is driven, the carriage will translate along the curved track, rotating about the sternoclavicular joint axis. The resulting motion is identical to a 4-bar linkage as shown in Fig. 4.4b, but, no structural elements are required near the sternoclavicular joint axis (see dashed lines). Links l_1 and l_2 are virtual links, thus the system can be thought of as a virtual 4-bar linkage. Motion about the sternoclavicular joint is coupled to the driving joint, which is offset from the sternoclavicular joint axis. As described in Section 3.3, knowledge of the motion

of the driving joint allows knowledge of the motion of the sternoclavicular joint. It should be noted that this 4-bar linkage is not a Grashof linkage. Since this mechanism does not require a large range of motion, a non-Grashof linkage is sufficient.

The benefits of this track system are significant. First, it facilitates placing equipment behind the user rather than above the user's head, which is safer and more comfortable for the user, and also easier for the operator to set up. Second, as will be discussed in Section 4.4, the hinged driving linkage also functions as a routing system for the cables from the shoulder/elbow mechanism by guiding them through to the base of the robot. Any change in cable length as a result of shoulder girdle motion is easily accounted for in the cable length calculations (see Section 4.4.1). Without this linkage, the motors of the cable-drive system would have to be mounted to the carriage, which would be far too heavy for the track system.

Locks and Joint Limits

Both joints incorporate joint locks and range of motion limits. The locks are simple clamps that swivel into place and clamp directly to the joint shaft (similar to the locks shown in Section 4.3.3. In the case of the curved track mechanism, the lock is fixed to the driving joint shaft.

Range of motion limits are screws with large rubber-coated heads. These bumpers prevent the linkages from exceeding a chosen minimum and maximum joint rotation. The screws can be inserted into two of a series of holes that change the range of motion by 10° for the first joint, and 5° for the second joint. The bumpers for the curved track are located on the curved track itself, and prevent the carriage from moving beyond the desired range (see Fig. 4.4).

4.3.2 Glenohumeral Joint Axis Orientation

MEDARM mimics glenohumeral joint motion using a spherical joint made from three consecutive joint axes that intersect at the glenohumeral joint centre. Fig. 4.5

shows the final design of the spherical joint which was selected using a new procedure developed specifically for this purpose. The method is described in this section.

A major drawback for a spherical joint of this type is that its range of motion is limited by wrist singularities which occur whenever the three joint axes align in a common plane [104, 106]. The kinematic manipulability of the mechanism decreases as the mechanism approaches a singularity. When the mechanism reaches a singular configuration, the manipulability becomes zero. Physically, this means that one of the joint's 3DOF is lost, and that the mechanism can no longer be fully controlled in all directions. While singularities cannot be removed, the relative orientation of the three joint axes can be chosen so that the singular configurations occur outside the desired workspace. In fact, the relative orientation and order of the three joint axes also influences the size of the functional workspace, the manipulability of the

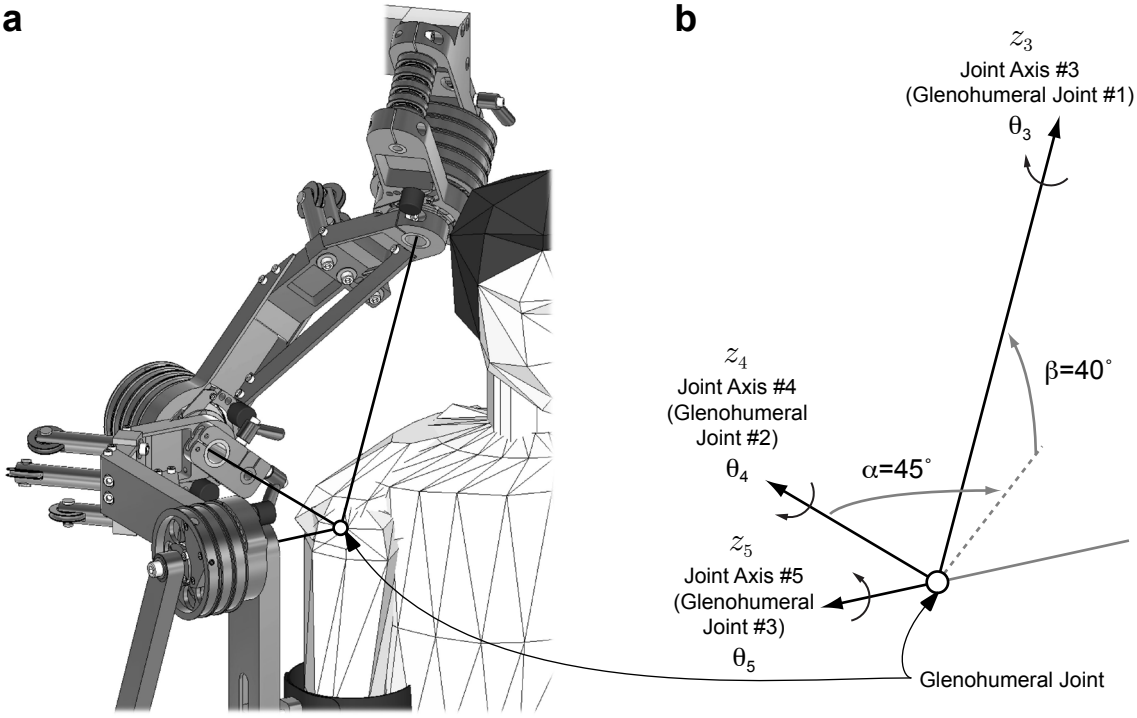

Figure 4.5: (a) A CAD drawing of the final spherical joint design used to replicate glenohumeral joint motion. It is shown in its zero configuration. The joint is made up of three intersecting revolute joint axes that are arranged to meet the design criteria. (b) A close-up view of the three intersecting joint axes showing their relative orientations.

mechanism, and also the likelihood of collision with itself or a user. Therefore, in order to mimic the entire range of motion of the human upper-limb, MEDARM's glenohumeral joint must be carefully designed.

Several robotic devices have now been designed to incorporate the glenohumeral joint [76, 79, 84, 89], but the method used to choose the orientation of the joint axes is not clear. Therefore, a simple and visually intuitive procedure has been developed to choose the relative orientation of the three joint axes that make up MEDARM's spherical joint, while ensuring that all design constraints are satisfied. While the technique was developed specifically to find the best configuration for MEDARM, it is designed in such a way that it can be applied to the design process for other spherical joints of this type. The graphical nature of the approach is easy to follow, which makes the inherent performance and design trade-offs more readily understandable.

This method is based on simple calculations of the volume of the parallelepiped defined by three unit vectors pointing in the directions of the three joint axes of the spherical joint. This volume can be expressed as a scalar value using the *box product* (or instead, *scalar triple product*) equation:

$$M = \boldsymbol{z_3} \cdot (\boldsymbol{z_4} \times \boldsymbol{z_5}) \tag{4.1}$$

where M is the volume of the parallelepiped and $\boldsymbol{z_i}$ is the i^{th} joint axis (the order of the vectors is not important in this equation).

In the context of this application, M is the kinematic manipulability (hereafter, simply manipulability) of the mechanism. Although M is not the same as the manipulability that could be calculated using the Jacobian matrix of the spherical joint [107], M shares many of the same practical outcomes. For example, when $M = 1$, the joint axes are orthogonal and manipulability (volume) is at its maximum, and when $M = 0$, the joint axes are coplanar, indicating a singularity (i.e. a degree of freedom is lost). Using M as a measure of manipulability also has an important benefit. M provides a meaningful physical interpretation that is easy to visualize

(volume), which is not always possible with the traditional measures [104]. Overall, M provides a practical, easy-to-understand measure of manipulability that does not require knowledge of the Jacobian matrix. This itself has the added benefit for the design phase of a spherical joint because it allows more freedom to quickly rearrange the order and orientation of the joint axes without having to update the Jacobian matrix for each arrangement.

The technique consists of three main steps, which can be summarized as follows. First, the joint axes are defined mathematically, using elementary rotation matrices that transform each joint axis to the base reference frame in terms of two *parameters*. Next, the set of possible combinations of these *parameters* is narrowed down to a small subset in order to reduce the computational requirements. Finally, the combination of *parameters* is iterated until the joint meets all design requirements. The procedure, as applied to MEDARM, will be described in the remainder of this section.

STEP 1: Mathematical Set-up. The first and most important step in the procedure is to define the base reference frame (frame 2, because the spherical joint is mounted to the end-point of the shoulder girdle linkage, which is link 2). All calculations require knowledge of the position of each joint axis expressed in this reference frame. The spherical joint will be aligned with a user's right glenohumeral joint, therefore the base frame origin is defined as the joint centre as indicated by the open circle in Fig. 4.6a. Positive $\boldsymbol{x_2}$, $\boldsymbol{y_2}$ and $\boldsymbol{z_2}$ are defined as pointing to the right, forward, and upwards, respectively.

Next, the zero-configuration of the three joint axes, $\boldsymbol{z_3}$, $\boldsymbol{z_4}$ and $\boldsymbol{z_5}$ must be clearly defined relative to frame 2 (see Fig. 4.6b). For the purposes of this method, the joint axis vectors point toward the mechanical equipment associated with the spherical joint, thus it is important to define the vectors accordingly. The orientations of joints 4 and 5 are dictated by design constraints Th.7 and Th.8. In order to achieve simplified planar shoulder/elbow motion (Th.7), joint 5 must be parallel to the elbow

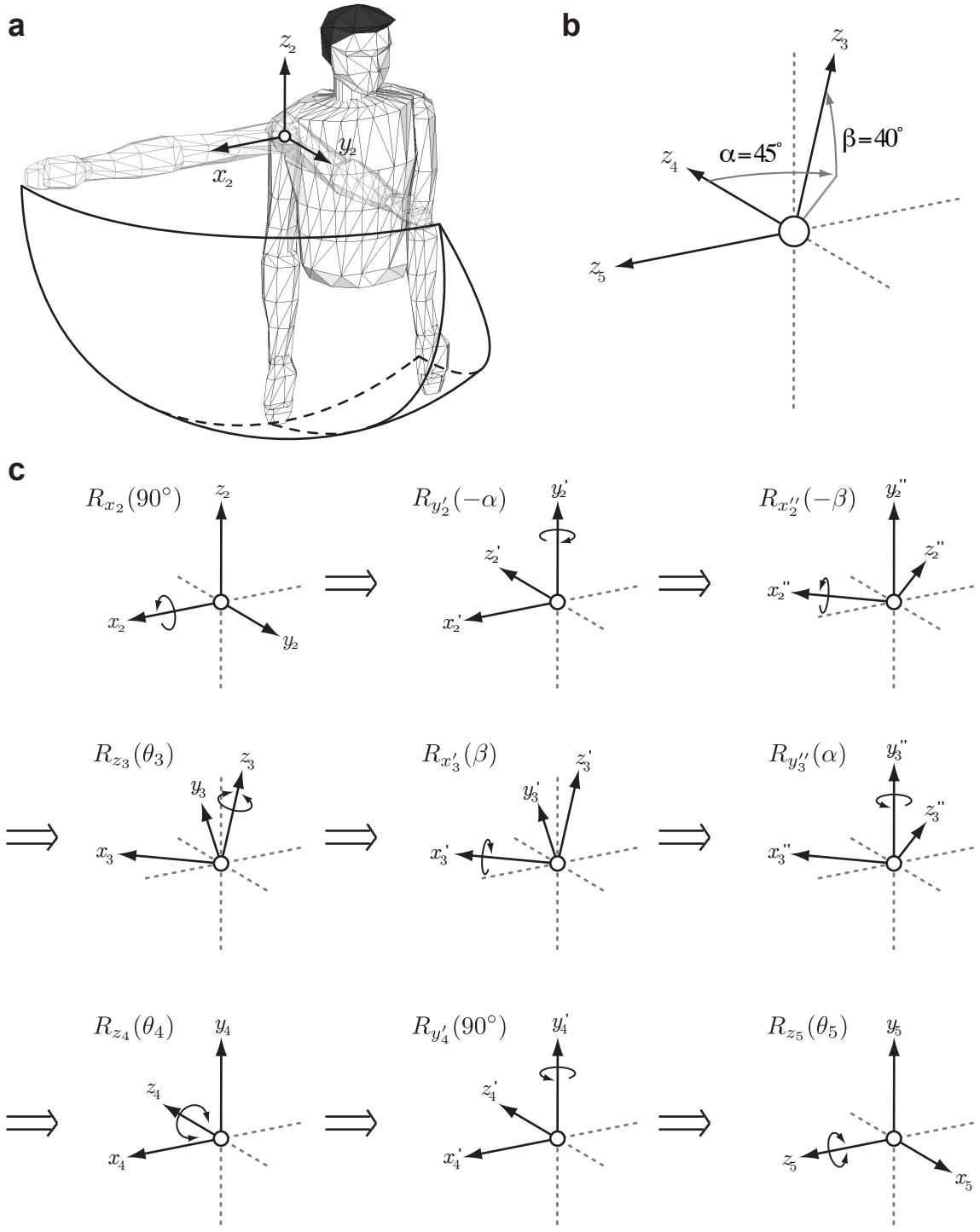

Figure 4.6: (a) The desired workspace of the glenohumeral joint allows abduction/flexion into the horizontal plane, and also additional adduction when the shoulder girdle is elevated. The base frame of reference, frame 2, is centred on the right glenohumeral joint centre as indicated by the open circle. (b) The three joint axes, $\boldsymbol{z_3}$, $\boldsymbol{z_4}$ and $\boldsymbol{z_5}$, are shown in their zero-configuration. $\boldsymbol{z_3}$ is defined in terms of two *parameters*, α and β, which describe its position relative to the base frame. (c) Graphical representation of the rotations used for equations (4.2)-(4.5).

joint axis (joint 6), which means that $\boldsymbol{z_5}$ must be aligned with $\boldsymbol{x_2}$. This choice also satisfies objective Th.8 because flexion/extension can be performed solely with joint 5. The orientation of joint 4 is also dictated by design requirement Th.8. In order for abduction/adduction to be controlled by a single joint, $\boldsymbol{z_4}$ must be aligned with $\pm\boldsymbol{y_2}$. However, since equipment would interfere with the user (i.e. the exoskeleton would get in the way of limb motion) if aligned with $+\boldsymbol{y_2}$, $\boldsymbol{z_4}$ must be aligned with $-\boldsymbol{y_2}$.

The orientation of the joint 3 axis is dictated by the requirements that singularity be avoided, that manipulability be maximized and that collision with the body be avoided. There are many possible solutions, and the best one should be chosen. $\boldsymbol{z_3}$ must lie somewhere in the octant bounded by $-\boldsymbol{x_2}$, $-\boldsymbol{y_2}$ and $\boldsymbol{z_2}$ so that the exoskeleton can be positioned behind the user. Otherwise, singularity or collision with the body would definitely occur. The orientation of $\boldsymbol{z_3}$ relative to the base frame can be fully defined by two parameters, α and β, which describe the orientation of joint axis 3 relative to joint axis 4 (Fig. 4.6b). It is these parameters that will be selected to meet the design requirements. α is the angle from $\boldsymbol{z_4}$ to the projection of $\boldsymbol{z_3}$ on the horizontal plane (gray line). β is the upward angle from the horizontal plane. For $\boldsymbol{z_3}$ to remain within this octant, the values of α and β must lie between 0° and 90°.

Now that the zero-configuration is defined, each of $\boldsymbol{z_3}$, $\boldsymbol{z_4}$ and $\boldsymbol{z_5}$ must be expressed mathematically in terms of the base frame. This can be done by concatenating a series of elementary rotation matrices. There are multiple solutions to achieve the same overall result. Equations (4.2)-(4.4) describe the rotations chosen for this example.

$$\boldsymbol{z_3^2} = R_{x_2}(90°)R_{y_2'}(-\alpha)R_{x_2''}(-\beta)\boldsymbol{z_3^3} \tag{4.2}$$

$$\boldsymbol{z_4^2} = R_{x_2}(90°)R_{y_2'}(-\alpha)R_{x_2''}(-\beta)R_{z_3}(\theta_3)R_{x_3'}(\beta)R_{y_3''}(\alpha)\boldsymbol{z_4^4} \tag{4.3}$$

$$\boldsymbol{z_5^2} = R_{x_2}(90°)R_{y_2'}(-\alpha)R_{x_2''}(-\beta)R_{z_3}(\theta_3)R_{x_3'}(\beta)R_{y_3''}(\alpha)R_{z_4}(\theta_4)R_{y_4'}(90°)\boldsymbol{z_5^5} \tag{4.4}$$

where $\boldsymbol{z_i^j}$ refers to the i^{th} joint axis expressed in the j^{th} frame, θ_i is the rotation angle of joint i, and $R_k(\phi)$ is a rotation about the *current* k-axis by angle ϕ. Note that in this example, it was chosen to perform the sequential rotations about the *current* k-axis, therefore the rotation matrices are post-multiplied [104]. Fig. 4.6c shows these rotations graphically in the appropriate order. By following the order of rotations as shown, it becomes clear why some joint axes are related by several intermediate steps.

Similarly, any point, $\boldsymbol{P}$, in frame 5 (i.e. any point on the humerus, such as the elbow joint location) can be transformed to the base frame (frame 2) using (4.5).

$$\boldsymbol{P^2} = R_{x_2}(90^\circ)R_{y_2'}(-\alpha)R_{x_2''}(-\beta)R_{z_3}(\theta_3)R_{x_3'}(\beta)R_{y_3''}(\alpha)R_{z_4}(\theta_4)R_{y_4'}(90^\circ)R_{z_5}(\theta_5)\boldsymbol{P^5} \tag{4.5}$$

Notice in (4.2)-(4.5), that the vectors expressed in the base frame are a function of the joint angles, θ_3, θ_4 and θ_5, as well as the two *parameters*, α and β. Manipulability can now be calculated as a function of α and β for the entire workspace by substituting (4.2)-(4.4) into (4.1).

STEP 2: Reduce Possibilities. Manipulability could be calculated for the entire workspace of the joint for all possible combinations of α and β, but this is not necessary. Without first narrowing down the possible combinations, it becomes a challenging exercise of trial and error. Therefore, the next step in this technique reduces the set of possible combinations by eliminating all combinations of α and β that do not meet the design requirements for a single simplified configuration. θ_3 and θ_5 are fixed into a configuration which allows θ_4 to follow a motion with well known design constraints. By the very nature of the spherical joint, the singular configuration will occur at some value of θ_4 because it is the only way in which the three joint axes will become coplanar.

The simple motion was chosen to be abduction. With $\theta_3 = \theta_5 = 0$, M is calculated as θ_4 is varied through its entire range, as shown in Fig. 4.7a. Each point represents the endpoint of a vector with magnitude equal to M, pointing radially from

the glenohumeral joint centre in the direction of the humerus during the abduction motion. The plot contains two important quantities. The first is the singular abduction angle, $\theta_{4(M=0)}$, which can be identified mathematically as the point at which the manipulability is zero. A singular configuration also occurs in the opposite direction at $\theta_4 = \theta_{4(M=0)} - 180°$. The negative value is important because the joint can be adducted into this negative range when the shoulder girdle is elevated. The second quantity to be obtained from Fig. 4.7a is the maximum manipulability, M_{max}.

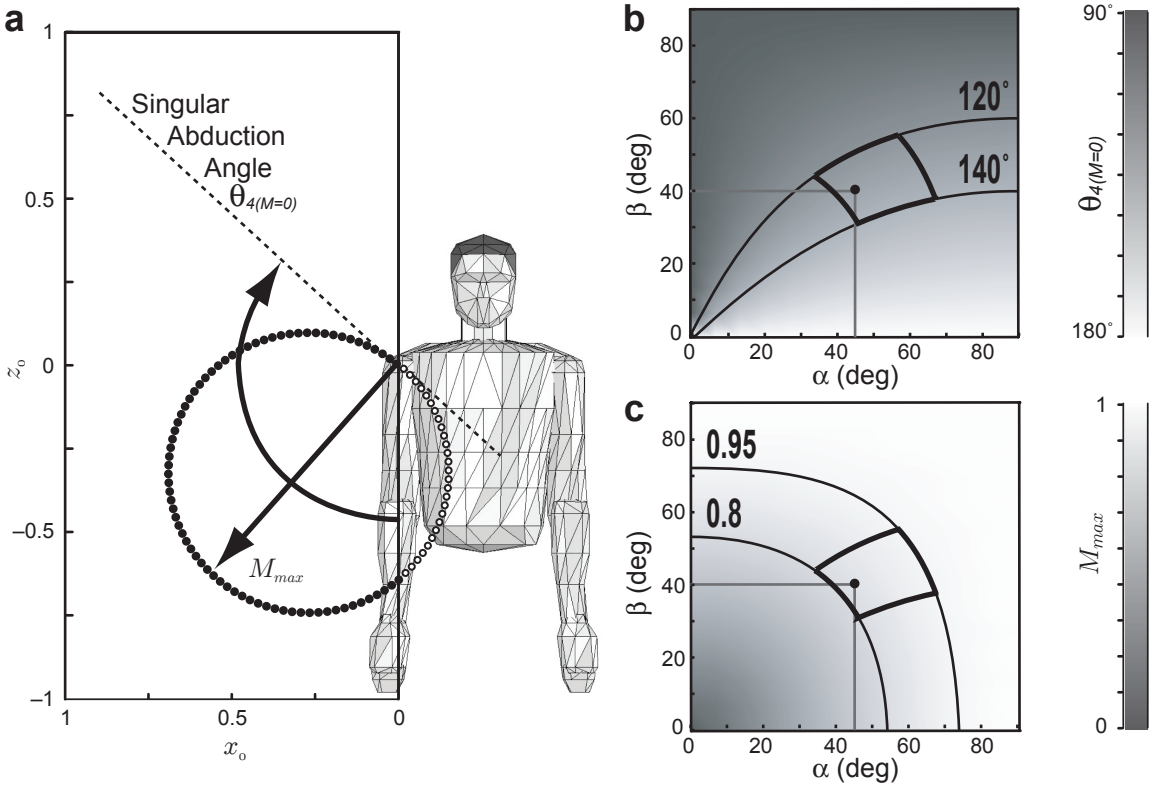

Figure 4.7: (a) A plot of manipulability, M, for a given combination of α and β (here, $\alpha = 45°$, $\beta = 40°$) as θ_4 is varied. θ_3 and θ_5 are fixed at 0°, so the motion is equivalent to shoulder abduction. Each point represents the endpoint of a vector with magnitude equal to M, pointing radially from the glenohumeral joint centre (base frame origin) in the direction of the humerus. The closed and open circles denote abduction (positive motion) and adduction (negative motion) from the rest position, respectively. The abduction angle at which singularity occurs, $\theta_{4(M=0)}$, and the maximum manipulability, M_{max}, can both be determined from this plot. Plots of (b) $\theta_{4(M=0)}$ and (c) M_{max} for all combinations of α and β between 0° and 90°. A range of α and β combinations that provides a suitable compromise between $\theta_{4(M=0)}$ and M_{max} is shown by contour lines, and the overlap is highlighted. The final choice of $\alpha = 45°$ and $\beta = 40°$ is indicated by the black dot.

The next step is to calculate $\theta_{4(M=0)}$ and M_{max} for all combinations of α and β. These values are plotted as a function of α and β in Figs. 4.7b and 4.7c in which the colour bars indicate the values of $\theta_{4(M=0)}$ and M_{max}, respectively. Now it is possible to choose a range of values of α and β which reach a compromise between $\theta_{4(M=0)}$ and M_{max} by drawing contour lines on both plots. According to design constraints, θ_4 typically does not exceed 90° or -30°. To avoid singularity within the abduction/adduction motion, it was chosen to keep $\theta_{4(M=0)}$ within the contours representing 120° and 140° (Fig. 4.7b). It turns out that configurations based on the combinations of α and/or β that produce the highest M_{max} are also more likely to collide with the user's body because the joint axes align more closely with the body. A range of $0.8 \leq M_{max} \leq 0.95$ strikes a reasonable compromise as shown in Fig. 4.7c. The manipulability is still high, but collisions are avoided.

The overlapping area between the contours becomes the reduced set of α and β combinations that satisfy the design requirements for the simple motion considered in this step (in this case, abduction). The number of possible combinations is only a few percent of the original set, which significantly reduces the amount of trial and error computations.

STEP 3: Iterations. The final step of the process is iterative, requiring a manual check after each iteration to make sure that the design constraints are satisfied. First, a combination of α and β within the range identified in step 2 is chosen. Next, M is calculated for the entire reachable workspace by varying each of θ_3, θ_4 and θ_5 across their ranges in increments of 2.5°. The result can be plotted as shown in Fig. 4.8a, which is simply an extension of Fig. 4.7a to the entire three-dimensional workspace. At this point, several checks are made to determine if this particular combination of α and β produces acceptable results across the entire workspace. The magnitude of M should be checked to see if there are any configurations within 10° of singularity (i.e. $M < 0.15$, which can be found directly from (4.1)) and if the distribution of M

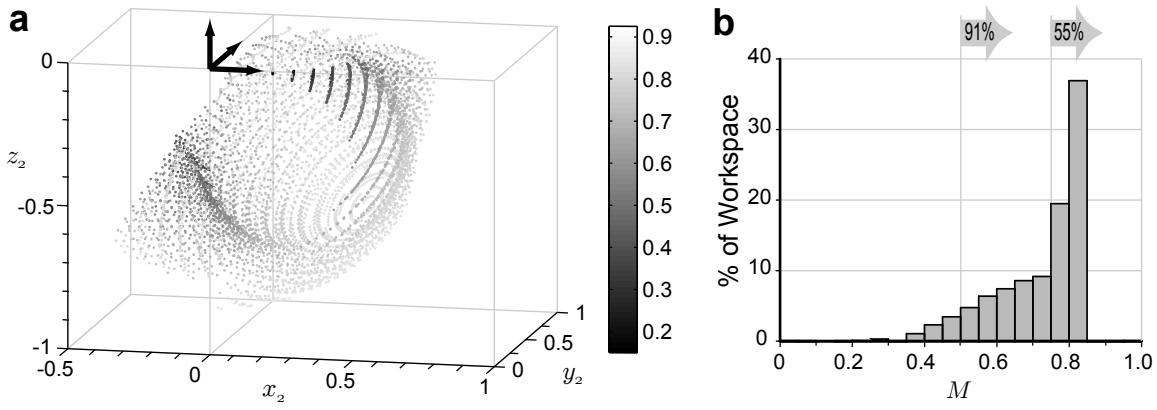

Figure 4.8: (a) A three-dimensional extension of Fig. 4.7a in which the manipulability, M, is plotted radially in the direction of the humerus over the workspace for $\alpha = 45°$ and $\beta = 40°$. Points farther away from the origin indicate higher manipulability, and singular locations are represented by points at the origin. M is evenly distributed over a large majority of the workspace, indicated by the almost spherical surface. M does decrease near the limits of the workspace, as can be seen by the few points lying closer to the origin, but no points come within 10° of singularity. (b) A histogram of the distribution of manipulability across the workspace. For this mechanism, $M_{max} = 0.84$, and the mean over the entire workspace is $M \simeq 0.73$. More than 91% of the possible configurations of the mechanism have $M > 0.5$, and more than 55% of the possible configurations have $M > 0.75$

across the workspace is even. Finally, it should be determined whether there could be any collisions of the mechanism with itself or the user. If any of these checks indicates a problem, a new combination of α and β must be chosen and the process repeated. Once a combination of α and β produces satisfactory results, the process is complete.

After several iterations, the final selected values of $\alpha = 45°$ and $\beta = 40°$ were obtained for MEDARM. Considering the entire workspace, more than 91% of the possible configurations of the mechanism have $M > 0.5$, and more than 55% of the possible configurations have $M > 0.75$ (see Fig. 4.8b). The maximum manipulability is 0.84, and the mean is $M = 0.73$. The spherical-like surface in Fig. 4.8a indicates that M is evenly distributed across the majority of the workspace. Only the extreme limits of the workspace exhibit a lower manipulability, and no configurations exist within 10° of singularity configurations. The high-manipulability region is nearly centred in the workspace, corresponding to the most functionally relevant area of the workspace.

4.3.3 Joint Design

There are several important components that make up a joint in the exoskeleton. At the most basic level, the joints must withstand significant forces and moments, and guide the driving cables as necessary for actuation. Some joints must also contain a secondary encoder, joint limits and/or a clamp to lock the joint in place. Fig. 4.9 shows an exploded view of joint 4. This joint was chosen to highlight the features

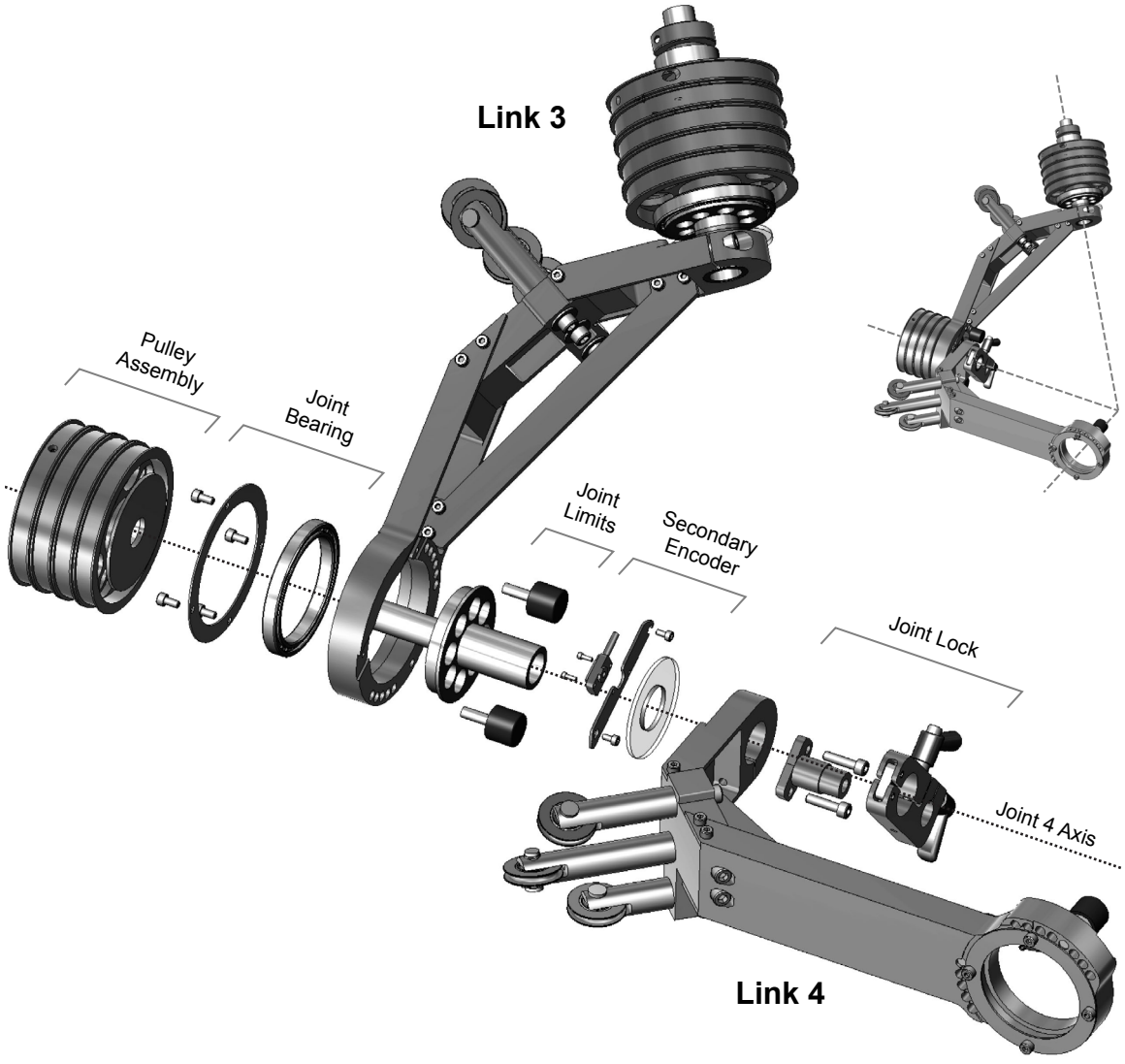

Figure 4.9: An exploded view of MEDARM's joint 4. The small inset at the top right shows the joint in its normal configuration. The joint consists of several components including the pulley assembly, the bearing, joint limits, a secondary encoder, and a lock.

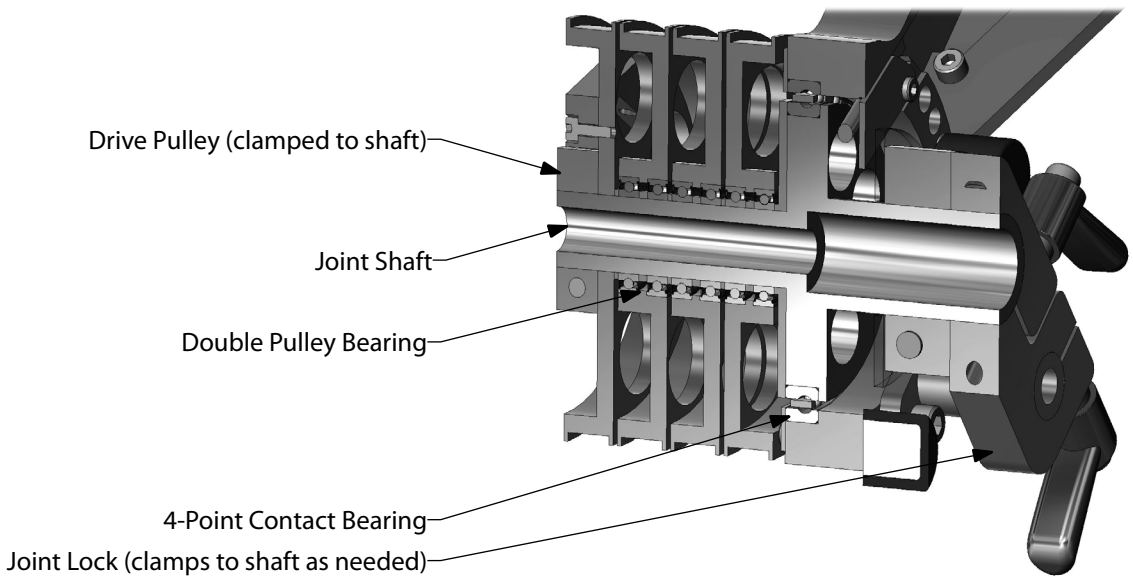

Figure 4.10: The section view shows the detail of the joint construction. The joint bearing and the free pulley bearings are clearly illustrated.

common to most of MEDARM's joints, and gives an idea of the consideration put into the design of each joint.

Each joint of the exoskeleton requires a low friction bearing system that provides rigidity against all forces and non-axial moments. In addition to withstanding non-axial gravitational and inertial moments during motion, the joints must withstand substantial non-axial moments resulting from forces applied by the cables and pulleys (these values were obtained using the dynamic model described in Section 4.4.3). Standard bearings must be used in pairs to resist this type of moment. Four-point contact bearings are highly resistant to non-axial moments and therefore it is not necessary to use them in pairs. Use of four-point contact bearings in MEDARM has resulted in a thin and lightweight exoskeleton that would not be possible with standard bearings.

Another necessity for a cable-driven system is a set of pulleys for guiding the cables around the joint. Fig. 4.10 shows a detailed section view of the pulley assembly. Each joint requires one pulley to be fixed to the joint shaft using a shaft collar clamp so

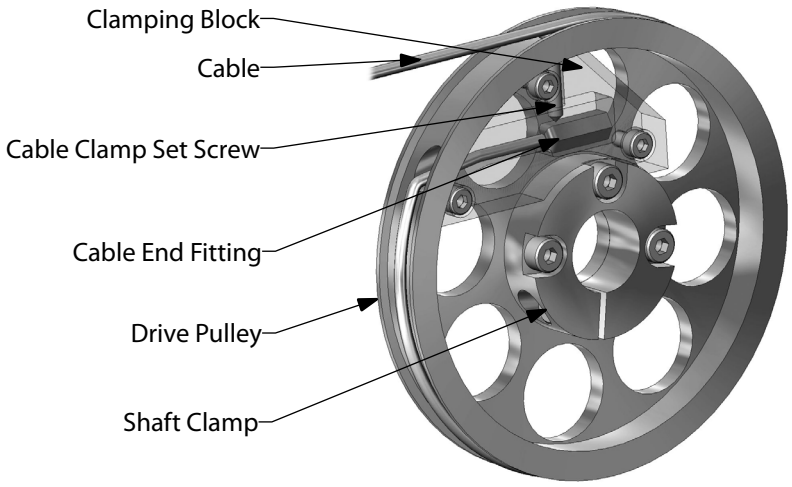

Figure 4.11: The drive pulley clamps to the joint shaft. The cable is fed through a hole in the pulley into a clamping block (made partially transparent in this view). A single set screw is used to lock the cable fitting into place so that it cannot be pulled out.

that it can apply torque directly to the joint. This drive pulley is the end-point for a cable, therefore the end of the cable is clamped to the pulley using a clamping block (Fig. 4.11). The cable fits through a hole in the pulley surface and is held in place by the clamping block so that it cannot be pulled out. A single set screw holds the fitting in place. Each of the remaining pulleys are attached to the shaft via a pair of small bearings so that they are free to rotate around the shaft.

Built into the joint are several other important features. The first is adjustable mechanical joint range of motion limits. These are simply two rubber-covered bolts that screw into holes in one of the links, preventing the adjacent link from moving beyond a maximum and minimum range of motion. In fact, there are a series of holes in which these bumpers can be inserted. Consecutive holes change the range of motion by an increment of 5° or 10°, depending on the joint.

The second feature of the joint is a high-resolution optical encoder. A glass scale centred about the joint axis, is mounted to one link, and an optical sensor is mounted to the other. The system provides direct measurement of the joint kinematics with high resolution and adds zero friction. These encoders will hereafter be referred to as

secondary encoders, since the main encoders are located on the motors.

The third feature is a lock for the joint. It clamps directly to the shaft, and can swivel in and out of place as needed. The joint can be locked at any rotation angle.

4.3.4 User Attachment and Alignment

The exoskeleton must be aligned with the sternoclavicular, glenohumeral and elbow joints of the user, and adjusted to fit arms of different lengths. A harness attaches the user's torso to a chair which provides the three translational adjustments necessary to align the user's sternoclavicular joint with the mechanism's fixed shoulder girdle joint centre. Once aligned, the chair is locked to the main structure.

Next, the mechanism must be aligned with the user's glenohumeral joint centre. As before, three spatial adjustments are required to shift the robot's glenohumeral joint centre relative to its sternoclavicular joint centre. The 2DOF of the shoulder girdle mechanism can be used to provide two of the adjustments, thus only one additional adjustment is necessary. The single manual linear adjustment provides the ability to change the distance between the sternoclavicular joint centre and the glenohumeral joint centre. This linear adjustment (see Fig. 4.12) shifts the cable-drive system relative to the carriage in the direction approximately aligned with the horizontal projection of the clavicle and is then clamped to the carriage. It is important to note that there are no attachment points to the user on the shoulder girdle mechanism.

This adjustment scheme has the benefit of simplifying the structure of the mechanism, and also the set-up procedure. Otherwise, three consecutive translational adjustments would be required, making the system significantly larger, heavier and more complicated. Using the shoulder girdle mechanism to provide this adjustment moves the exoskeleton away from its home configuration. Fortunately, the 3DOF spherical joint of the shoulder/elbow mechanism can compensate by rotating until the mechanism is aligned with the user's limb. Relying on the shoulder/elbow

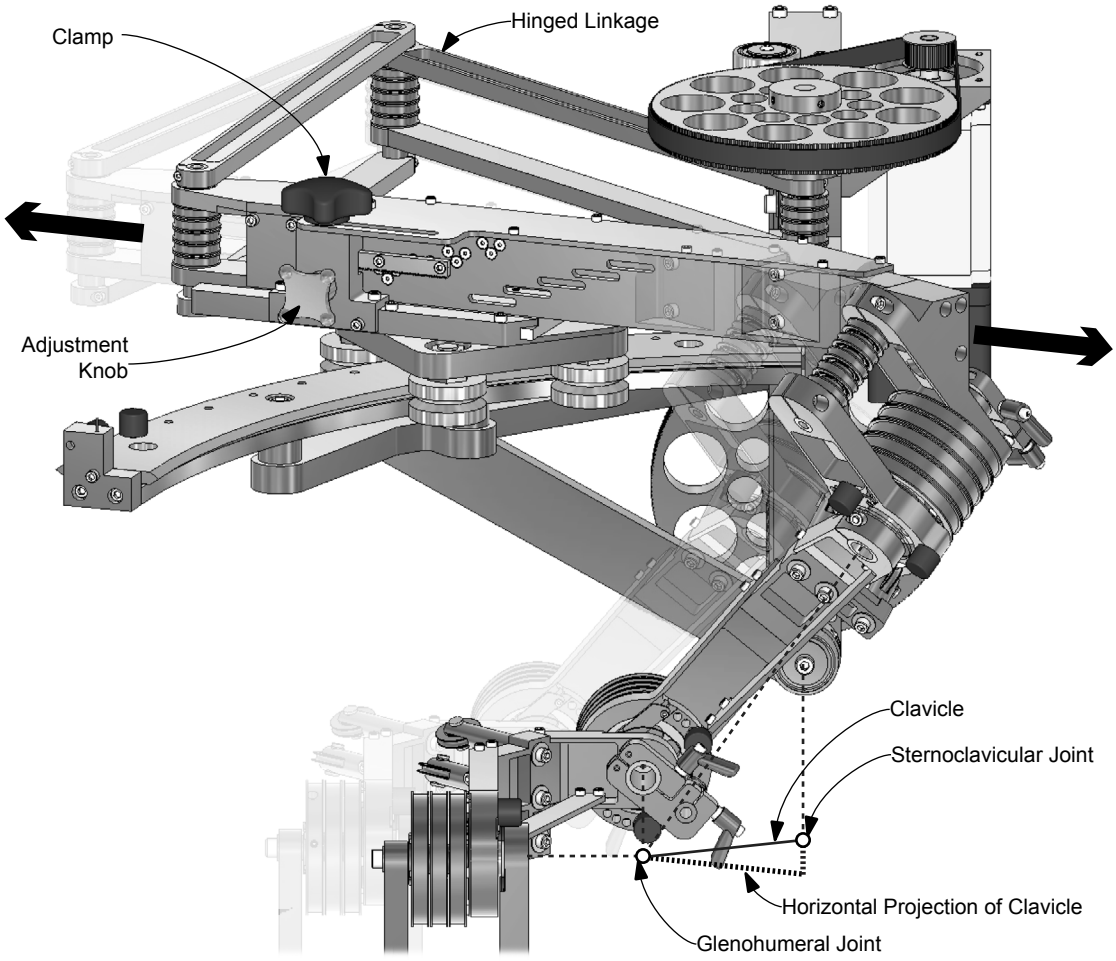

Figure 4.12: A diagram showing the single linear horizontal adjustment on the shoulder girdle mechanism. The arrows indicate the adjustment direction, which is approximately aligned with the horizontal projection of the clavicle. The mechanism slides as a knob is turned, and is clamped tight with a second knob.

mechanism to compensate tends to push the spherical joint away from its optimal configuration, decreasing the range of motion of the mechanism in some directions. However, the adjustment range is typically small (2° or 3° at most), therefore the singularities and manipulability of the mechanism will not be significantly altered.

A design issue that arises when adjusting a cable-drive system is that it is necessary to maintain tension in the cables at all times. Adjusting the link length must not change the cable length, otherwise tension would be lost. Routing the cables along the hinged driving linkage (see Fig. 4.12) ensures that the cable length does not change

and that tension is maintained.

The exoskeleton system attaches to the user in two places: the upper-arm and the forearm (Fig. 4.13a). These attachments keep the exoskeleton aligned with the limb at all times. The proposed design is to strap the limb into a rigid half-cylindrical trough using an inflatable Velcro strap similar to a blood pressure cuff. Once strapped in, the cuff is inflated to provide a secure fit that is customized to the user. On the lateral side of the cuffs is a single rigid connection to the exoskeleton structure. The cuff will be attached to the subject before connecting to the exoskeleton, which is easier for the operator, and more comfortable for the user. An important difference from many previous arm cuff designs is that the arm cuff does not have a fixed size

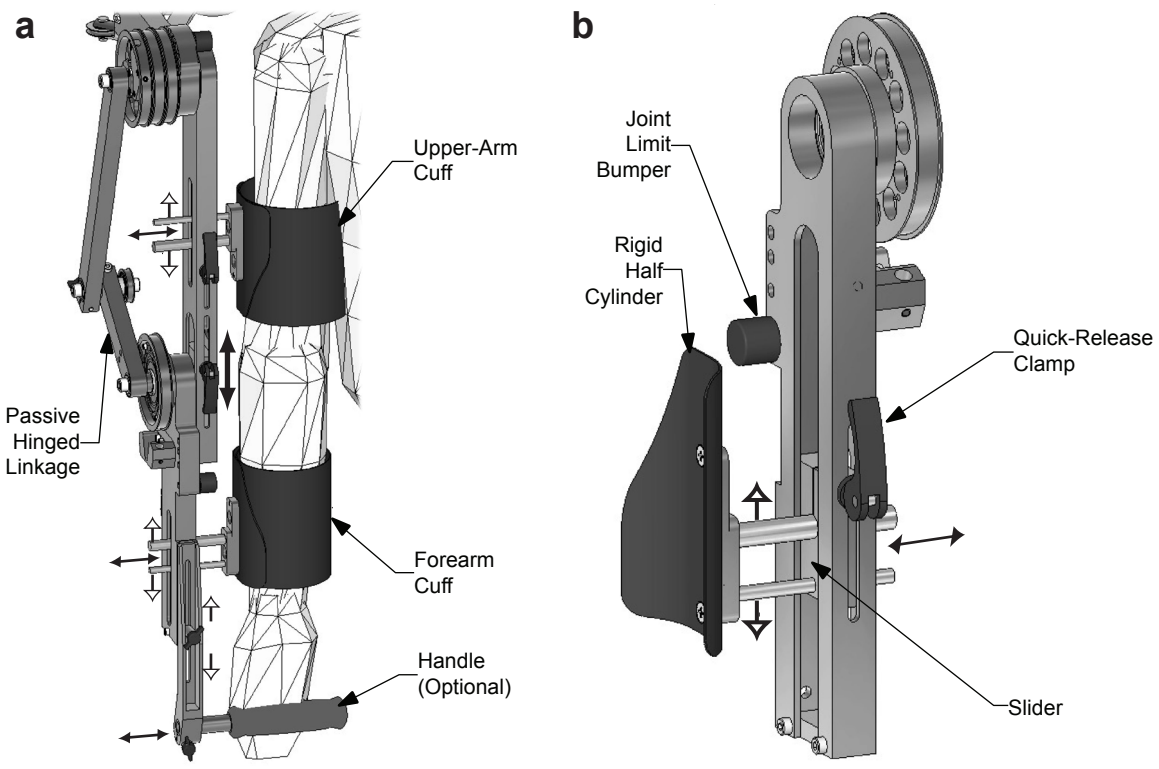

Figure 4.13: (a) A drawing illustrating the arm cuff attachments and adjustments. Each cuff has two translational adjustments to correctly align the limb segments relative to the mechanism structure: perpendicular to the link (small arrows) and parallel to the link (hollow arrows). A fifth adjustment (large arrow) moves the location of the elbow joint to change the length of the upper-limb link. A possible handle attachment is shown (it is optional) and can also be adjusted parallel and perpendicular to the link. (b) A close-up of the cuff attachment, showing the quick-release clamp.

cuff through which the user must put his/her arm. This allows simpler set up, and also is compatible with a larger variety of arm sizes.

A total of five adjustments are required to ensure that the user's arm is properly aligned with the exoskeleton (see Fig. 4.13a). Each cuff is adjustable along the length of the exoskeleton (for limbs of different length) and perpendicular to the exoskeleton (for limbs of different width). The cuff is attached by inserting it into a slider which can move freely along the exoskeleton. A single quick-release clamp (see Fig. 4.13b, similar to those used to clamp bicycle components) simultaneously clamps the cuff to the slider and the slider to the exoskeleton (see Fig. 4.13b). To accommodate users with different arm lengths, a similar slider and clamp is used to locate the elbow joint along the upper-arm link. A passive hinged guide was added to the upper-arm link of the robot to ensure that cable tension is not lost when adjusting the arm length.

One of the advantages of exoskeleton robots is that the user's hand is free to perform grasping or other functional tasks during the reaching movements. Using a handle would restrict the hand from being used during the movement. However, if grasping is not needed, it might be useful to include a handle for the patient to grasp. The handle shown in Fig. 4.13a is a possible design that allows for two adjustments: one parallel to the link, and one perpendicular.

Exoskeleton type devices always require more set up time than their end-effector type counterparts. However, given its mobility and adjustability, MEDARM has a relatively simple set up procedure. In fact, once the chair is locked in place, only four clamps are required to secure all eight adjustments (with no handle). This will keep set up time to a minimum, allowing the user to receive a longer therapy session.

4.4 MEDARM Actuation System

MEDARM is actuated by a set of electric motors which are geared using timing belts. The shoulder/elbow mechanism is driven entirely by cable-drive transmission

system which provides a large power-to-weight ratio. The shoulder girdle mechanism is driven directly, but since the cables are guided along the mechanism to the four distal joints, they influence the required torques from the shoulder girdle motors. The following describes the proposed actuation system in detail.

4.4.1 Cable-Drive System

The four joints of the shoulder/elbow mechanism are actuated by electric motors with an open-ended cable drive transmission. Cable-drive systems have a number of advantages which are described in Section 3.1. MEDARM in particular benefits from the design in a number of ways. First and foremost, the cable drive system allows an immense reduction of weight on the exoskeleton. In fact, all motors are placed on the base of the system, so the exoskeleton can be lightweight. It also means that the cable forces are reduced and the motors can be smaller. The result is a high power-to-weight ratio, which is part of what makes actuation of MEDARM possible. Fig. 4.14 shows the cable routing scheme chosen for MEDARM.

The cable routing scheme choice has a significant effect on the performance of the device. In fact, for this 4DOF system ($n = 4$) actuated by five motors ($m = 5$), there are 11 possible unique cable routing structures [102]. These 11 structures were analyzed as described in Section 3.2 to choose a suitable routing scheme. Table 4.2 summarizes the results for the 11 schemes (arbitrarily labeled by roman numerals). Scheme "ii" was chosen (see Fig. 4.14b) because the antagonism ratio is 2, and the maximum force ratio is 2.45 which is the best combination of the two parameters. The scheme chosen for MEDARM will thus provide the most even distribution of forces, and with minimized actuator requirement of all possible routing schemes.

Section 3.1.1 describes the relationship between joint angles and cable lengths for an open-ended cable-drive system such as MEDARM. However, the cables are routed along the shoulder girdle mechanism, and therefore, the cable lengths change as the

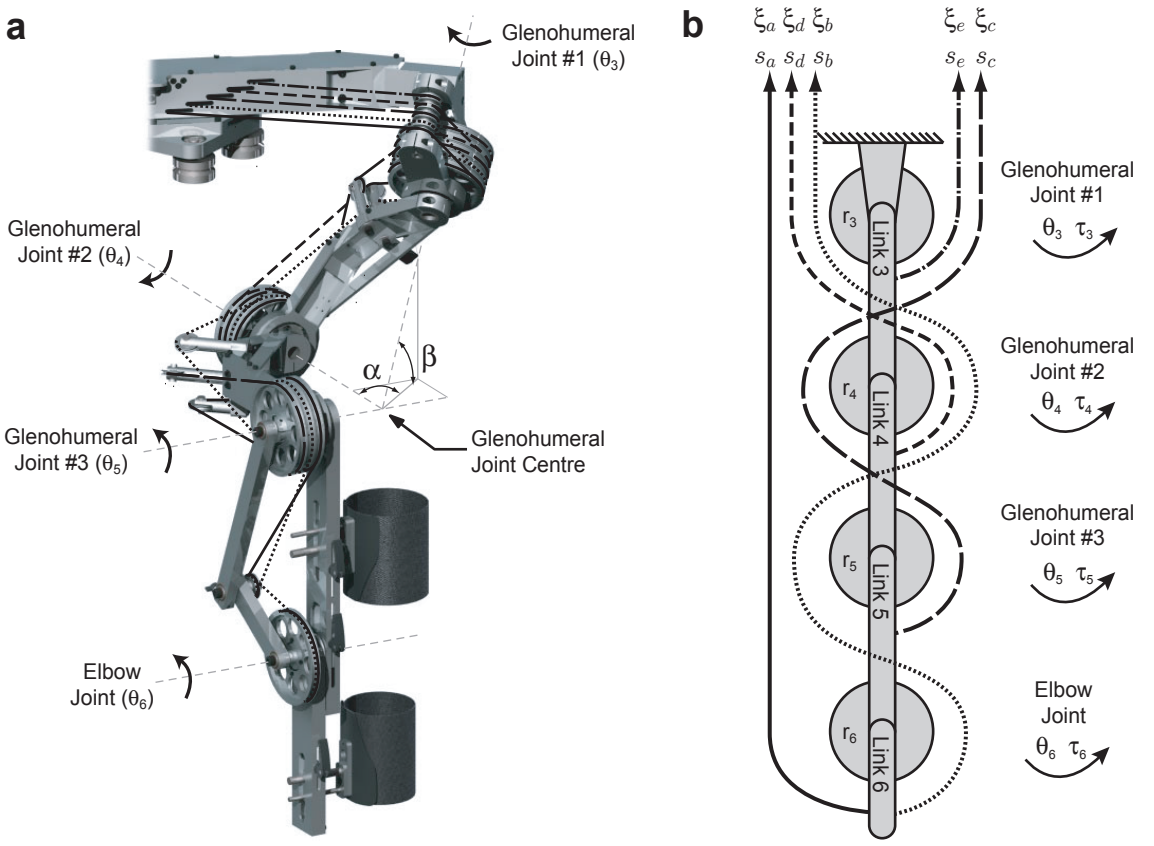

Figure 4.14: The shoulder/elbow mechanism is cable-driven. (a) A CAD drawing of the mechanism showing the selected mechanism with cables included. (b) A simplified planar schematic representation of the selected cable routing structure. Each of the five cables is denoted by a different line type. Each joint has a separate pulley for each cable that passes by the joint. Symbols s, ξ, r, τ and θ represent cable displacement, cable force, pulley radius, joint torque and joint angle respectively.

shoulder girdle angles θ_1 and θ_2 change. Additional terms, $\Delta\theta_{sg1}$ and $\Delta\theta_{sg2}$, must be added to the cable length calculations to account for joints 1 and 2 of the shoulder girdle mechanism, respectively. The following equations were derived for MEDARM.

$$\begin{bmatrix} s_a \\ s_b \\ s_c \\ s_d \\ s_e \end{bmatrix} = \begin{bmatrix} -r_3 & -r_4 & -r_5 & -r_6 \\ -r_3 & r_4 & -r_5 & r_6 \\ r_3 & -r_4 & r_5 & 0 \\ -r_3 & r_4 & 0 & 0 \\ r_3 & 0 & 0 & 0 \end{bmatrix} \begin{bmatrix} \Delta\theta_3 \\ \Delta\theta_4 \\ \Delta\theta_5 \\ \Delta\theta_6 \end{bmatrix} + \begin{bmatrix} -1 & 1 \\ -1 & 1 \\ -1 & -1 \\ -1 & 1 \\ -1 & -1 \end{bmatrix} \begin{bmatrix} \Delta\theta_{sg1} \\ \Delta\theta_{sg2} \end{bmatrix} \tag{4.6}$$

$$\Delta\theta_{sg1} = r_{g1}\Delta\theta_1 \tag{4.7}$$

$$\Delta\theta_{sg2} = r_{g2b}(\Delta\theta_g - \Delta\theta_2) + r_{g2a}(\Delta\theta_{2d} - \Delta\theta_g) - r_{2d}\Delta\theta_{2d} \tag{4.8}$$

Table 4.2: A summary of the antagonism ratio and maximum force ratio for the 11 unique cable routing schemes for a 4DOF cable-drive system. The structures of each system are illustrated in previous work [102].

Scheme	$\boldsymbol{H}$	**Antagonism Ratio**	**Maximum Force Parameter**	**Force Ratio**
i	$[1,1,2,2,2]^T$	2	$[\sqrt{3/2},\sqrt{3/2},2,\sqrt{10},\sqrt{10}]^T$	2.58
ii	$[1,1,2,2,2]^T$	2	$[1,\sqrt{3/2},2,\sqrt{6},\sqrt{6}]^T$	2.45
iii	$[1,1,2,2,2]^T$	2	$[\sqrt{3/2},\sqrt{3},2,\sqrt{6},\sqrt{10}]^T$	2.58
iv	$[1,1,2,2,4]^T$	4	$[1,\sqrt{3/2},2,\sqrt{6},\sqrt{22}]^T$	4.69
v	$[1,1,2,2,4]^T$	4	$[1,\sqrt{3/2},\sqrt{2},\sqrt{6},\sqrt{10}]^T$	3.16
vi	$[1,1,2,2,6]^T$	6	$[1,\sqrt{3/2},\sqrt{2},\sqrt{6},\sqrt{22}]^T$	4.69
vii	$[1,1,2,4,2]^T$	4	$[1,\sqrt{3/2},2,\sqrt{10},\sqrt{6}]^T$	2.45
viii	$[1,1,2,4,4]^T$	4	$[1,1,\sqrt{2},\sqrt{6},\sqrt{6}]^T$	2.45
ix	$[1,1,2,4,4]^T$	4	$[1,1,\sqrt{2},\sqrt{6},\sqrt{10}]^T$	3.16
x	$[1,1,2,4,6]^T$	6	$[1,1,\sqrt{2},\sqrt{6},\sqrt{22}]^T$	4.69
xi	$[1,1,2,4,8]^T$	8	$[1,1,\sqrt{2},\sqrt{6},\sqrt{22}]^T$	4.69

where the signs depend on the direction of cable routing (see Section 4.4.2).

Applied cable forces can be related to applied joint torques using the following equations as described in Section 3.1.2. No modifications are needed in this case.

$$\begin{bmatrix} \tau_3 \\ \tau_4 \\ \tau_5 \\ \tau_6 \end{bmatrix} = \begin{bmatrix} r_3 & 0 & 0 & 0 \\ 0 & r_4 & 0 & 0 \\ 0 & 0 & r_5 & 0 \\ 0 & 0 & 0 & r_6 \end{bmatrix} \begin{bmatrix} -1 & -1 & 1 & -1 & 1 \\ -1 & 1 & -1 & 1 & 0 \\ -1 & -1 & 1 & 0 & 0 \\ -1 & 1 & 0 & 0 & 0 \end{bmatrix} \begin{bmatrix} \xi_a \\ \xi_b \\ \xi_c \\ \xi_d \\ \xi_e \end{bmatrix} \tag{4.9}$$

As will be discussed in Section 4.4.2, forces applied to these cables also create torques at the shoulder girdle joints. However, torques applied to the shoulder girdle joints do not contribute to the applied joint torques of the cable drive system.

Implementation

This system can be implemented using rotary motors to wind up or unwind the cable around a pulley. Encoders measure the rotation of the windup pulley, and thus

a simple calculation provides the length of cable that has been wound up or unwound.

$$s_i = r_{wi}\left(\frac{\theta_{mi}}{\eta_{mi}}\right) \tag{4.10}$$

where for the i^{th} cable, s_i is the cable length change, r_{wi} is the windup pulley radius, η_{mi} is the gear ratio between the motor and the windup pulley, and θ_{mi} is the rotation angle of the corresponding motor.

To determine how much torque to apply at each motor, (4.9) must be solved for the five cable forces. Using the torque resolver technique [102] as described in Section 3.1.2, the cable forces can be expressed by (4.11a)-(4.11e).

$$\begin{aligned}\xi_a = {} & O^-\left(\frac{\tau_6}{r_6}\right) + \frac{1}{2}O^-\left(\frac{\tau_5}{r_5} + \left|\frac{\tau_6}{r_6}\right|\right) + \frac{1}{2}O^-\left(\frac{\tau_4}{r_4} - \frac{\tau_6}{r_6} + O^+\left(\frac{\tau_5}{r_5} + \left|\frac{\tau_6}{r_6}\right|\right)\right) \\ & + \frac{1}{2}O^-\left(\frac{\tau_3}{r_3} - \frac{\tau_5}{r_5} + O^+\left(\frac{\tau_4}{r_4} - \frac{\tau_6}{r_6} + O^+\left(\frac{\tau_5}{r_5} + \left|\frac{\tau_6}{r_6}\right|\right)\right)\right) + \frac{1}{2}\delta \end{aligned} \tag{4.11a}$$

$$\begin{aligned}\xi_b = {} & O^+\left(\frac{\tau_6}{r_6}\right) + \frac{1}{2}O^-\left(\frac{\tau_5}{r_5} + \left|\frac{\tau_6}{r_6}\right|\right) + \frac{1}{2}O^-\left(\frac{\tau_4}{r_4} - \frac{\tau_6}{r_6} + O^+\left(\frac{\tau_5}{r_5} + \left|\frac{\tau_6}{r_6}\right|\right)\right) \\ & + \frac{1}{2}O^-\left(\frac{\tau_3}{r_3} - \frac{\tau_5}{r_5} + O^+\left(\frac{\tau_4}{r_4} - \frac{\tau_6}{r_6} + O^+\left(\frac{\tau_5}{r_5} + \left|\frac{\tau_6}{r_6}\right|\right)\right)\right) + \frac{1}{2}\delta \end{aligned} \tag{4.11b}$$

$$\begin{aligned}\xi_c = {} & O^+\left(\frac{\tau_5}{r_5} + \left|\frac{\tau_6}{r_6}\right|\right) + O^-\left(\frac{\tau_4}{r_4} - \frac{\tau_6}{r_6} + O^+\left(\frac{\tau_5}{r_5} + \left|\frac{\tau_6}{r_6}\right|\right)\right) \\ & + O^-\left(\frac{\tau_3}{r_3} - \frac{\tau_5}{r_5} + O^+\left(\frac{\tau_4}{r_4} - \frac{\tau_6}{r_6} + O^+\left(\frac{\tau_5}{r_5} + \left|\frac{\tau_6}{r_6}\right|\right)\right)\right) + \delta \end{aligned} \tag{4.11c}$$

$$\begin{aligned}\xi_d = {} & O^+\left(\frac{\tau_4}{r_4} - \frac{\tau_6}{r_6} + O^+\left(\frac{\tau_5}{r_5} + \left|\frac{\tau_6}{r_6}\right|\right)\right) \\ & + O^-\left(\frac{\tau_3}{r_3} - \frac{\tau_5}{r_5} + O^+\left(\frac{\tau_4}{r_4} - \frac{\tau_6}{r_6} + O^+\left(\frac{\tau_5}{r_5} + \left|\frac{\tau_6}{r_6}\right|\right)\right)\right) + \delta \end{aligned} \tag{4.11d}$$

$$\xi_e = O^+\left(\frac{\tau_3}{r_3} - \frac{\tau_5}{r_5} + O^+\left(\frac{\tau_4}{r_4} - \frac{\tau_6}{r_6} + O^+\left(\frac{\tau_5}{r_5} + \left|\frac{\tau_6}{r_6}\right|\right)\right)\right) + \delta \tag{4.11e}$$

It is then a simple matter to calculate the torque the motors must produce to generate a given force in the cable.

$$\tau_{mi} = r_{wi}\left(\frac{\xi_i}{\eta_{mi}}\right) \tag{4.12}$$

where for the i^{th} cable, τ_{mi} is the motor torque, r_{wi} is the windup pulley radius, and ξ_i is the cable force as calculated by (4.11).

4.4.2 Shoulder Girdle Drive System

The first joint is a conventional rotary joint, that is driven by an electric motor with a timing belt. The second joint is actuated using the virtual 4-bar linkage. An electric motor with a timing belt drives the driving joint (offset backwards from the sternoclavicular joint) using a timing belt. Motion at the driving joint must be related to motion of the sternoclavicular joint using the techniques described in Section 3.3, where the variables are as defined in Fig. 4.4b.

The weight of the mechanism is substantial because it supports the entire weight of the shoulder/elbow system, the curved track and carriage, as well as the limb itself. The first joint is nearly always under heavy static load conditions because the centre of mass of the exoskeleton is well away from the joint axis (i.e. a large moment arm). Only in the case of large shoulder girdle elevation does the centre of mass cross above the joint axis, relieving the static torque requirements. The second joint needs to provide gravitational support only when the first joint is elevated or depressed, and for typical movements, this effect is small. So, unless the elevation is large, the static torque requirements are much smaller than for the first joint. For both joints, there is a need to be able to provide large static torques, so both motors should be powerful.

As mentioned previously, the cables driving the shoulder/elbow system are routed across both joints of the shoulder girdle mechanism from the base of the system as shown in Fig. 4.15. The cables increase the complexity of the system because each cable must be guided around all the joints by several pulleys. Forces applied in the cables to drive the shoulder/elbow mechanism create unwanted torques at the joints of the shoulder girdle mechanism. Fortunately, this problem can easily be turned into a tremendous benefit. With specially chosen cable routing, the unwanted torques can

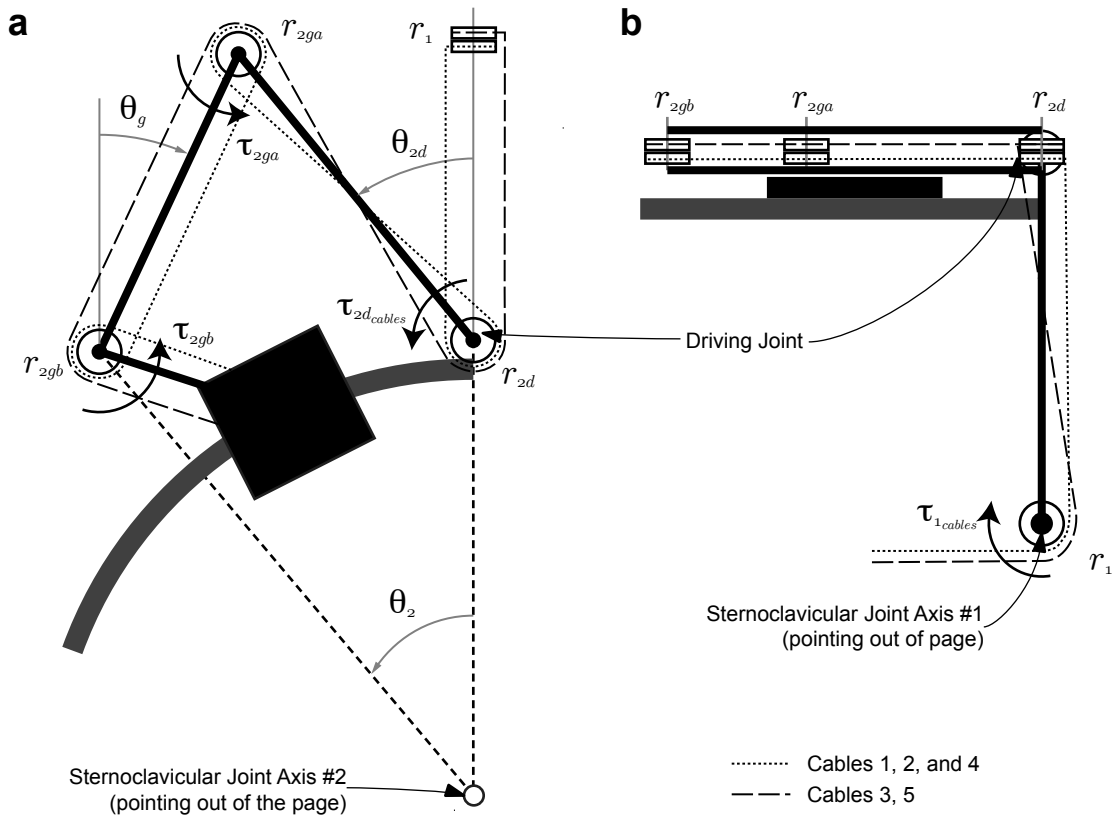

Figure 4.15: A schematic of the cables routed along the shoulder girdle mechanism to the base. (**a**) Top view and (**b**) front view. The cables maintain the same relative routing scheme across all joints of the 4-bar linkage, but all cables are routed the same direction around the first joint axis so that a positive torque is always created.

be used to cancel out some gravitational forces on the shoulder girdle system, and reduce the load on the shoulder girdle motors. At the very least, the cables apply a pretension force to keep the cables under tension. This means that the cables will always apply constant static torques at the joint 1 axis and the joint 2 driving joint axis. In addition to the pretension force, the cables apply a larger variable force (that depends on the torques applied to joints 3-6), which creates variable torques about the shoulder girdle joints. The total torque created by the cables about the shoulder girdle joints can be defined as follows:

$$\tau_{1_{cables}} = r_1(\xi_a + \xi_b + \xi_c + \xi_d + \xi_e) \tag{4.13}$$

$$\tau_{2d_{cables}} = r_{2d}(-\xi_a - \xi_b + \xi_c - \xi_d + \xi_e) \tag{4.14}$$

where $\tau_{1_{cables}}$ and $\tau_{2d_{cables}}$ are the torques created at joint axis 1 and joint 2 driving joint axis, ξ_i is the force provided by the i^{th} cable, and r_1 and r_{2d} are the radii of the pulleys guiding the cables around joint 1 and driving joint 2d, respectively. This formulation assumes that the pulleys at each joint axis are the same size, which need not be the case. The signs indicate the direction of cable routing around the pulleys. For joint 1, the cables are routed all in the same direction so as to provide a constant positive torque to counteract gravity. For joint 2, the gravitational constraints are less of a burden, thus routing the cables all in the same direction provides too much assistance. The combination shown in (4.14) keeps the relative routing form that comes out of the shoulder/elbow system.

The cables are routed around three joints of the virtual 4-bar linkage, so in actual fact, a torque is created about each of these three joints: $\tau_{2d_{cables}}$, τ_{2ga} and τ_{2gb} (see Fig. 4.15a). However, with the proposed cable routing scheme, τ_{2ga} and τ_{2gb} cancel each other out. The net torque is simply the $\tau_{2d_{cables}}$, which is the torque provided to the driving joint of the 4-bar linkage.

Pulley size affects the amount of torque that the cables provide to the shoulder girdle joints. Even with the extra "assistance" from the cables, the weight of the system may be too much for a single motor at joint 1. To assist the motor at this joint with the static torque requirements, an external gravity compensation system is employed. A vertical motorized cable is mounted directly above the end of the curved track (see Fig. 4.1), and applies a vertical force on the track to offset the gravitational forces on the MEDARM.

Implementation

The angular position of joint 1, θ_1, is measured directly from the encoder position of the motor, θ_{m1}.

$$\theta_1 = \frac{\theta_{m1}}{\eta_{m1}} \tag{4.15}$$

where η_{m1} is the gear ratio for joint 1. The angular position of sternoclavicular

joint 2, θ_2, must be calculated from the driving joint motor encoders, θ_{m2d}, using the techniques described in Section 3.3.1 which are updated to include the variables as defined in Fig. 4.4.

$$\theta_2 = \arctan\left(\frac{P_y - l_3 \sin\theta_g}{P_x - l_3 \cos\theta_g}\right) \tag{4.16}$$

where,

$$\theta_g = \arctan\left(\frac{P_y}{P_x}\right) + \arccos\left(\frac{{P_x}^2 + {P_y}^2 + {l_3}^2 - {l_2}^2}{2l_3\sqrt{{P_x}^2 + {P_y}^2}}\right) \tag{4.17}$$

$$P_x = l_1 + l_4 \cos\left(\frac{\theta_{m2d}}{\eta_{m2}}\right) \tag{4.18}$$

$$P_y = l_4 \sin\left(\frac{\theta_{m2d}}{\eta_{m2}}\right) \tag{4.19}$$

and η_{m2} is the gear ratio for the driving joint of joint 2.

The torque required at the driving joint axis to produce a torque at the second sternoclavicular joint axis is given by (3.59), where the variables are as defined in Fig. 4.4b. However, the contributions from the cables must also be included for the torques at both joints. The required motor torques, τ_{mi}, to create a total torque, τ_i, about the sternoclavicular joint axis given the contribution from the cables, $\tau_{i_{cables}}$ (Equations (4.13) and (4.14)), are given by the following equations:

$$\tau_{m1} = \frac{\tau_1 - \tau_{1_{cables}}}{\eta_{m1}} \tag{4.20}$$

$$\tau_{m2} = \frac{\left(\frac{l_4 \sin(\theta_g - \theta_{2d})}{l_2 \sin(\theta_g - \theta_2)}\right)\tau_2 - \tau_{2d_{cables}}}{\eta_{m2}} \tag{4.21}$$

4.4.3 Dynamic Model and Simulation

To make appropriate choices for the eight electric motors required to actuate MEDARM, a dynamic model of the exoskeleton and the human limb has been created in MATLAB based on the robot toolbox [108]. The model was also used to specify a number of other design parameters including bearing strength, joint gear ratios, and cable load capacity.

The model takes the form of a rigid-body manipulator, and assumes that the cable dynamics are not significant. Dynamic parameters of the exoskeleton including lengths, masses and inertial properties are estimates from CAD drawings. The same properties of the human upper-limb were calculated from anthropometric data tables based on user height and weight [15] and are integrated into the model. The model was adapted to account for the external gravity compensation system, and includes CAD estimates of viscous and static friction. Given a trajectory for each joint, the model calculates the joint torques required to achieve that motion. The cable forces required to generate these joint torques are then calculated using the cable force equations (4.11a)-(4.11e). The final output is the torque outputs for all eight motors, the force in each cable, and all forces and non-axial moments at each joint.

To obtain an estimate of the peak dynamic motor torques for non-contact applications, the model was used to simulate various reaching movements with a peak end-point velocity of 1.0 m/s. Anthropometric limb measurements were chosen to meet the maximum design requirements (Te.4). Movements included single joint motions through the full range of each joint, and a range of typical multi-joint reaching movements such as reaching towards the face or chest from a relaxed position. The most demanding positions for the exoskeleton system in terms of static torque requirements are those in which the arm is raised to the horizontal plane with the elbow fully extended. The gravitational component of the joint torques is the most significant contribution, and produces the largest stresses on the motors in static situations, therefore each position was held for one second to facilitate measurements of peak static torque.

To give an idea of the information that can be gleaned from this model, a small selection of possible outputs for a sample of movements is shown in Fig. 4.16. From this type of data, it was possible to make informed design decisions about many aspects of the robot. In all of the plots, the peaks occur during the movement

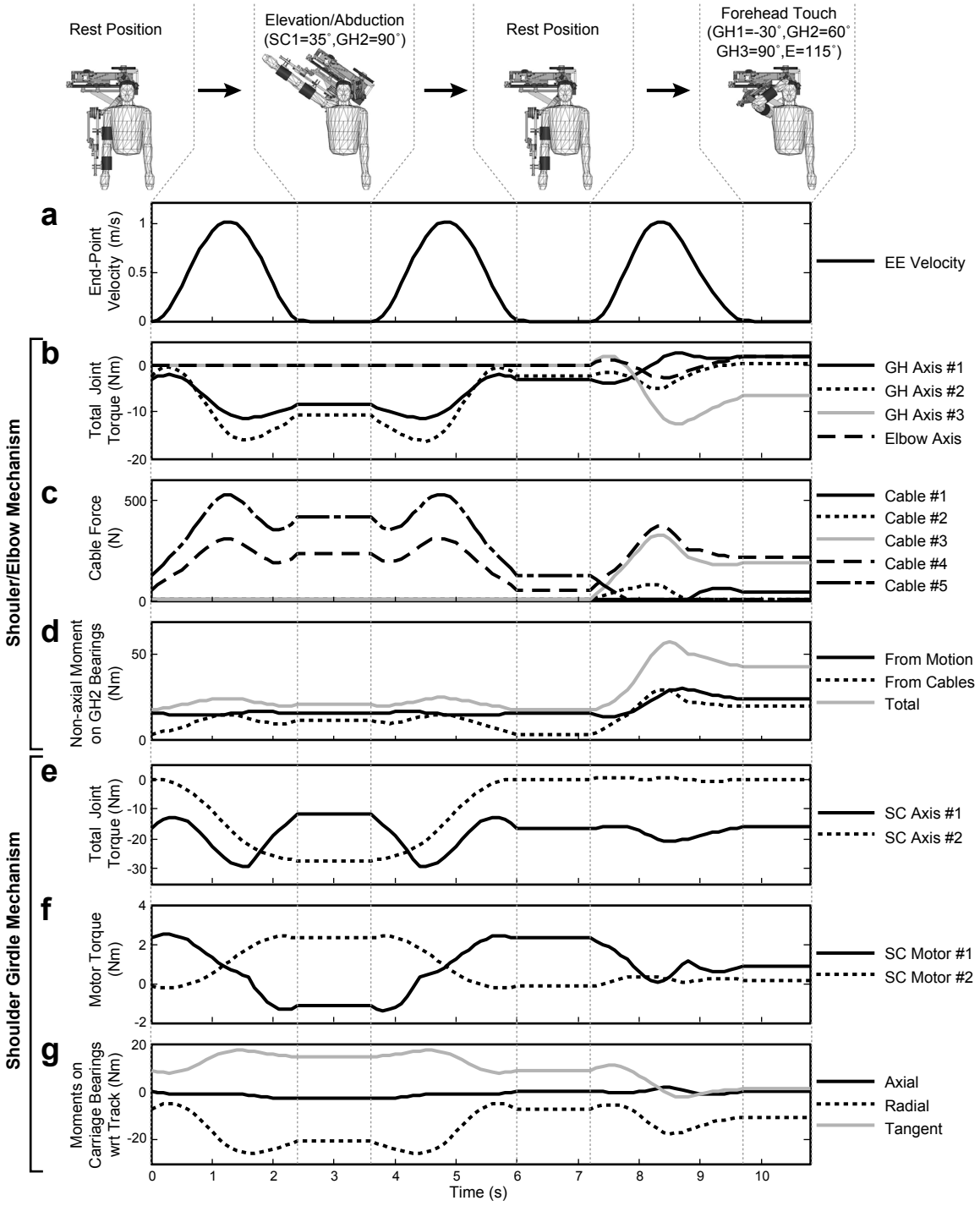

Figure 4.16: A selection of simulation results for some movements with a 50^{th} percentile person. The images at the top show the movements that were selected for this sample (GH = glenohumeral joint, SC = sternoclavicular joint). (a) confirms the peak end-point velocity of 1.0m/s. (b)-(d) illustrate the corresponding total joint torques and cable forces for the shoulder/elbow mechanism, as well as the non-axial moments at the GH2 joint bearing, respectively. (e) and (f) show the joint and motor torques for the shoulder girdle mechanism, respectively. (g) shows the moments encountered by the carriage on the track during the movements.

Table 4.3: Maximum torque output for each joint.

Joint	Static Torque (Nm)	Peak Torque (Nm)
Shoulder Girdle #1	±24	±73
Shoulder Girdle #2	±30	±91
Glenohumeral #1	+39, −26	±60
Glenohumeral #2	+39, −26	±60
Glenohumeral #3	+39, −26	±60
Elbow	±13	+40, −30

periods, and the constant values occur during static postures. Therefore, motors and gear ratios were selected using this data. The simulations also enabled selection of braided stainless steel cable of appropriate size, and also joint bearings with sufficient load capabilities. From Fig. 4.16c, it is clear that different cables are recruited for different motions, and peak load limits can be obtained from the results. The overall torque capabilities of each joint of the exoskeleton are shown in Table 4.3, and are a result of the limits of both the motors and the cable strength.

4.4.4 Motor Details

Motors should operate very smoothly in order to provide the most natural motion for the user. Brushless, slotless electric motors are an ideal choice because there is zero cogging torque. Each motor has a built-in optical encoder that is used to provide motor angle measurements. For the cable-drive system, these measurements provide the cable length changes needed to calculate the corresponding joint angles. Each motor incorporates an electric brake which serves two important functions. First, the brakes engage any time there might be a fault in the drive system or if there is a power outage. This will guarantee that the mechanism will not collapse during an emergency. Second, the brakes provide a means to ensure that cable tension is maintained when the power is turned off and the robot is not in use. If the brakes did not engage when the power was turned off, the motors would be able to move freely, allowing the cables to unwind and fall off the pulleys.

4.5 Estimated Cost

Estimates for the cost of parts for MEDARM are summarized in Table 4.4. The parts have been categorized into three main categories: motion control, electrical, and mechanical. The motion control category involves all motors, encoders, drives, and control cards necessary to actuate and control the system. The electronics section includes all wiring, connectors, power supplies and housings required to connect all of the system together. The mechanical section includes all other components. It is clear that the motor and electronics systems dominate the expense of the robot, accounting for about 65% of the total cost. Much of this cost arises from the need for large motors and the associated drives.

Table 4.4: A summary of the estimated cost for parts for MEDARM.

Part	**Cost**
Motion Control	
Motors, Drives, and Cables	$33,000
Motion Control Card	$9,000
Secondary Encoders	$4,000
Sub-Total	**$46,000**
Electrical	
Electronic Components	$1,500
PCBs	$3,000
Sub-Total	**$4,500**
Mechanical	
Shafts, Washers, Screws, Clamps, etc...	$3,500
Bearings	$1,500
Pulleys	$5,000
Timing Belts	$200
Curved Track and Carriage	$3,500
Cable and Fittings	$500
Material and Tooling for Machining	$8,000
Frame and Chair	$4,000
Arm Cuffs	$2,000
Sub-Total	**$28,200**
Total	**$78,700**

Chapter 5: Planar MEDARM

MEDARM is based on a new cable-driven virtual 4-bar linkage. This new design requires testing before continuing the development process. It was decided that the best way to test the design would be to build a simpler robot based on the same design concepts. This way, any unanticipated issues could be more easily addressed.

It was immediately apparent that the new design could benefit the evolution of KINARM, which is used in this research lab to assess and manipulate the mechanics of multi-joint motion [5]. As introduced in Table 2.4, and as shown in Fig. 5.1, KINARM is a robotic exoskeleton (produced by BKIN Technologies, Kingston, ON, Canada) that attaches to the upper-limb, allowing movements of the shoulder and elbow in the horizontal plane. KINARM is backdriveable, lightweight, and has low friction. Its primary use has been to study motor function of the upper-limb, but it is also being used to examine sensorimotor impairments of subjects with stroke [24, 25].

While KINARM is already a valuable tool, there are many questions it cannot answer. For example, because it provides only two degrees of freedom (2DOF: 1 shoulder and 1 elbow), it cannot answer questions about redundancy. To help answer these questions, it would be useful to add a third joint for wrist motion. In a clinical setting, a wrist joint might allow a more complete functional assessment of the limb, as the distal limb typically exhibits more functional deficits than the proximal limb. Presently, KINARM is driven by equipment placed above the shoulder joint (see Fig. 5.1) because the torso prevents equipment from being placed underneath. The mechanism then wraps around the arm to provide support for the limb from the underside. A consequence of this design is that the equipment must be placed beside the user's head. While this may not be a problem for many users, others may find it confining, particularly for bilateral systems because there is equipment on both sides

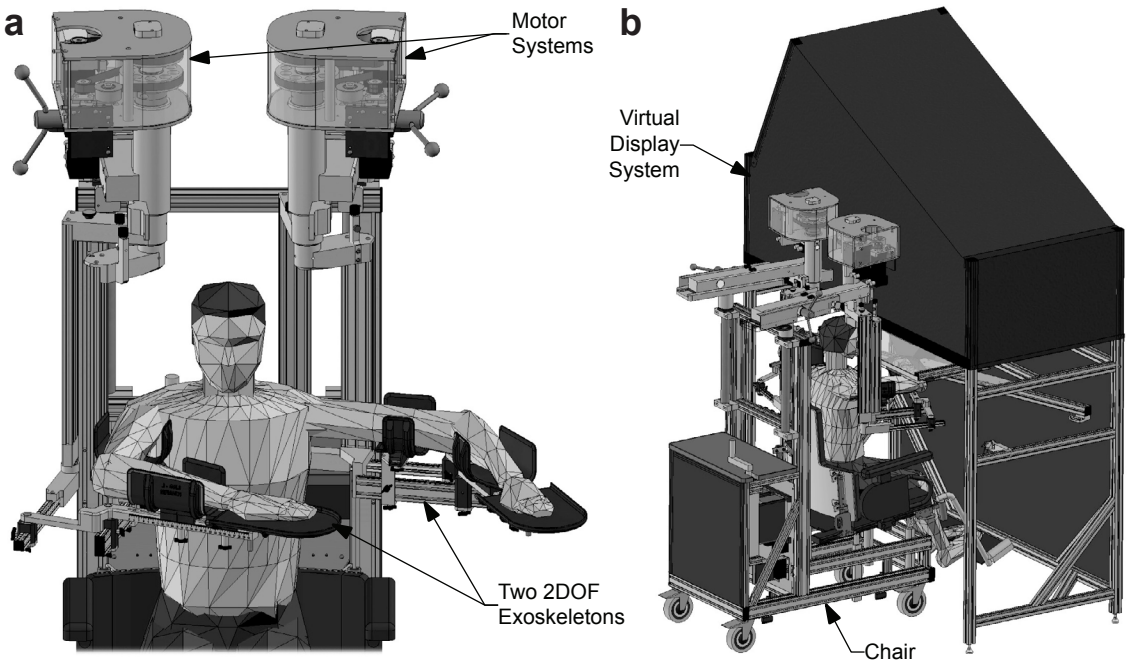

Figure 5.1: CAD drawings of KINARM: (a) a close up view of the exoskeleton mechanism, and (b) a view of the KINARM with the virtual display workstation.

of the head. In terms of user comfort and clinical appeal, it would be beneficial to move all of the equipment away from the user's head. A third issue is that the entire weight of the exoskeleton and the user's limb is supported at the shoulder joint axis, and thus a large bending moment causes substantial vertical out-of-plane compliance. Such compliance can cause problems with position control stability.

With this in mind, a simpler version of MEDARM was designed to act as a prototype for MEDARM and as a revision to KINARM. MEDARM's virtual 4-bar linkage design has the potential to extend KINARM's capabilities in a way that would be difficult with KINARM's present design. The design of this new robot, called Planar MEDARM, will be described in this chapter.

5.1 Planar MEDARM Design Objectives

The fundamental goal for Planar MEDARM is to develop a planar version of MEDARM that uses the same curved track design and that uses the same type of

cable-drive transmission. The simplified design shares the same overall purpose with MEDARM, therefore many of the design objectives outlined for MEDARM in Section 4.1 apply equally well for Planar MEDARM. However, it is useful to reiterate the main objectives, and describe the new objectives that relate to KINARM.

As a minimum, the design must incorporate MEDARM's virtual 4-bar linkage and must be driven by an open-ended cable-drive actuation system. It is appreciated that there are several other good choices for actuating this type of planar device, but as it is intended as a proof-of-concept design for MEDARM, a similar open-ended cable system must be used. The planar nature of the device significantly simplifies the initial implementation and testing of the new mechanism. The cable-drive system will be smaller, requiring fewer motors, and because the device operates in the horizontal plane, cable routing will be much simpler. Moreover, the motor system does not need to provide any type of gravity compensation. All ideas relating to the actuation system including pulley design, joint design and adjustment are simplified because only two dimensions need to be considered.

Another important goal of this planar design is to determine whether the new mechanism can be used as a revision for KINARM. Thus, the design must include three fully actuated planar DOF: one at the shoulder, one at the elbow, and a third at the wrist. The design should move all equipment away from the user's head, and reduce vertical out-of-plane compliance. In addition, Planar MEDARM should be able to achieve these new design features without a significant compromise in performance relative to KINARM. In particular, Planar MEDARM should feel transparent to its users. Therefore the new robot should be backdriveable, and the friction should be as low as possible. The inertia of the exoskeleton should be low and proportional to the upper-limb itself so that the user can adapt more easily when moving with the device. Furthermore, a subject should be able to perform the same types of reaching tasks using Planar MEDARM as they can with KINARM. Finally, Planar MEDARM should

be able to accommodate users of a wide range of size. To fit the majority of users, the length of the mechanism should have a range of approximately 0.26-0.37m and 0.20-0.29m for the upper-arm and forearm limb segments, respectively. The handle position should also be adjustable.

5.2 Planar MEDARM Design Overview

Planar MEDARM (Fig. 5.2) is a 3DOF exoskeleton robot that provides independent measurement and control of motion at the shoulder, elbow and wrist in the horizontal plane. No shoulder girdle actuation is provided in this prototype. The

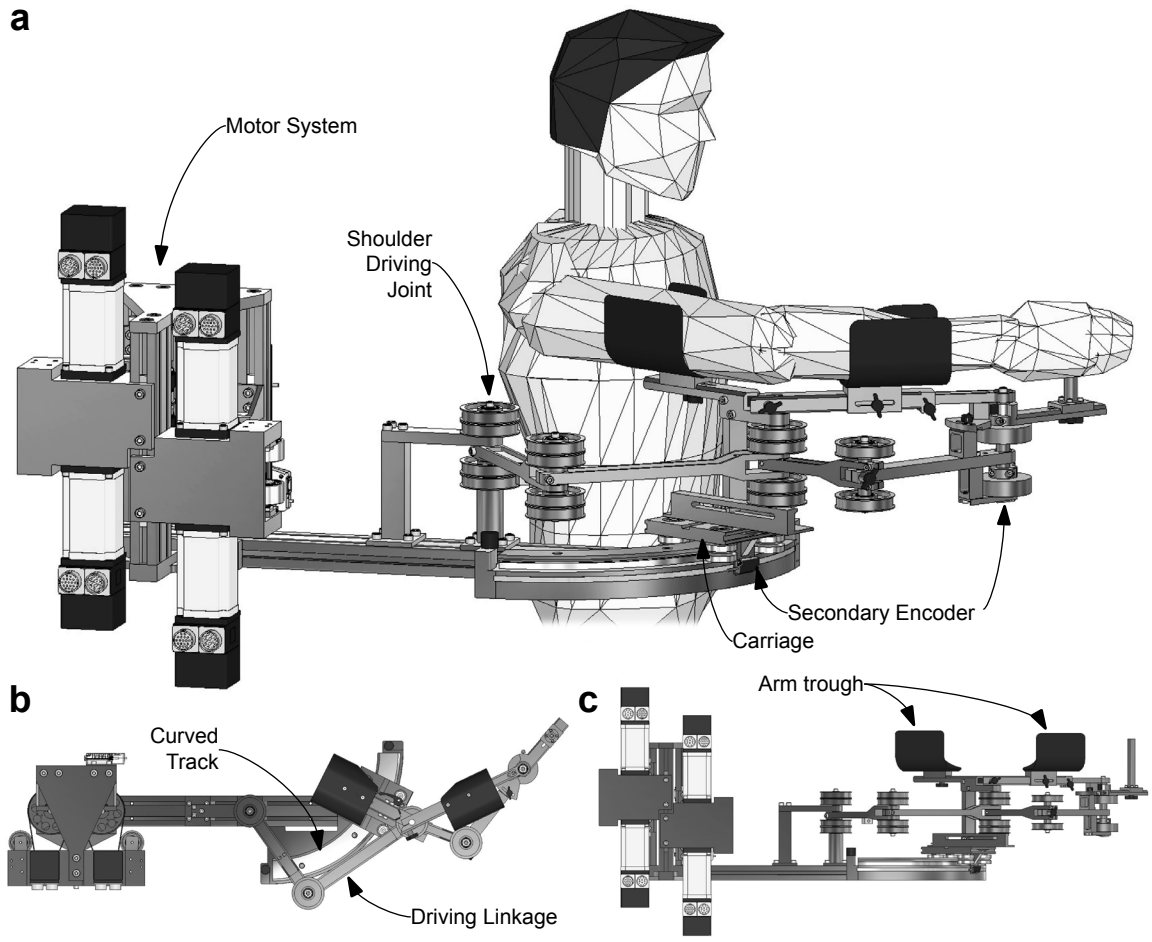

Figure 5.2: CAD drawings of Planar MEDARM: (a) set up with a user, (b) top view and (c) side view. The mechanism provides actuation of 3DOF in the horizontal plane using a cable-drive system (cables not shown here). The mechanism is located entirely underneath the user's arm, and the motors are mounted behind the user.

shoulder mechanism takes advantage of MEDARM's curved track mechanism, enabling the entire mechanism to be located underneath the user's arm. All joints are actuated by an open-ended cable-drive system. All three joint axes are parallel, and the distances between the axes are adjustable to accommodate users of different size.

A virtual display system was built for Planar MEDARM so that reaching performance could be tested. The system is based on the same principle of KINARM's

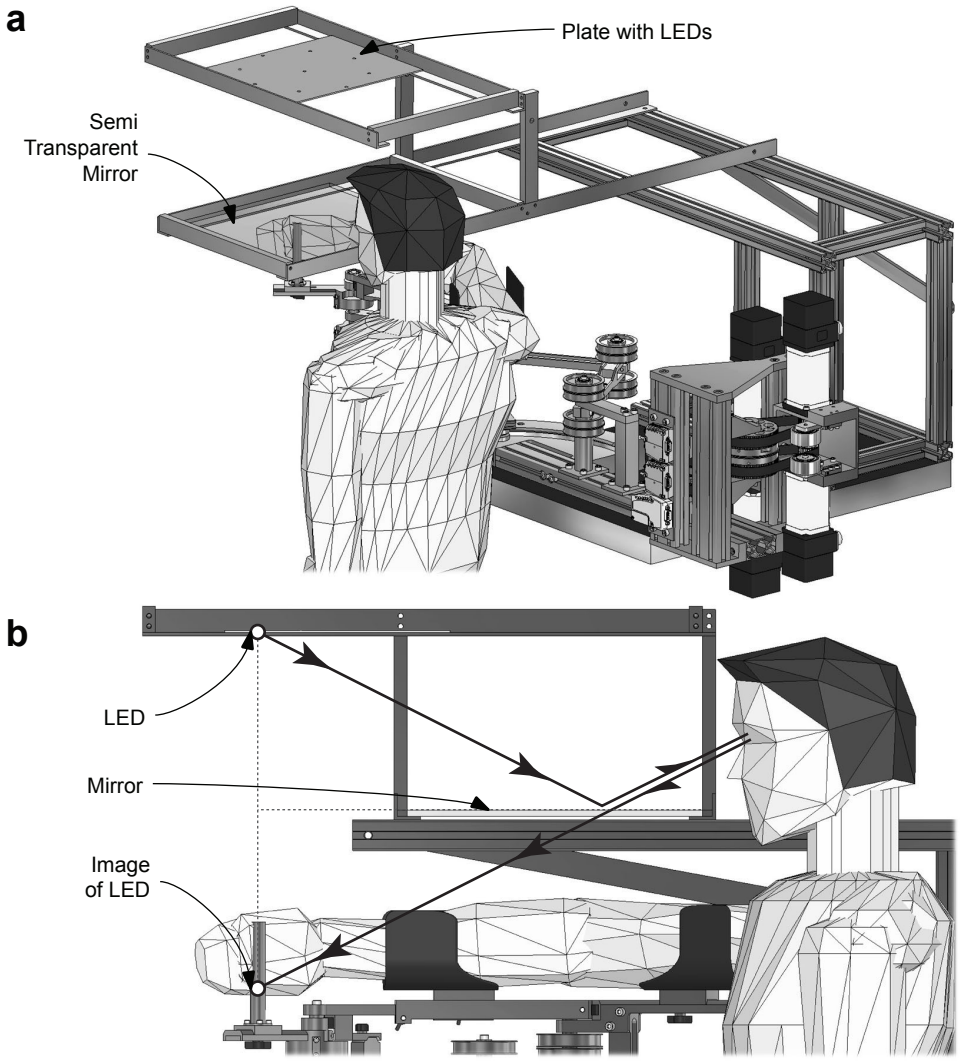

Figure 5.3: (a) Planar MEDARM's virtual display is a smaller, simplified version of the system used by KINARM. A basic structure holds a semi-transparent mirror equidistant from a set of LED lights above the workspace and the working plane of the robot. (b) The user looks through the mirror to see his/her limb, while light from the LEDs is reflected from the mirror so that they appear to be in the same plane as the limb.

display system (see Fig. 5.1b) [5]. This type of system allows unrestricted access to the workspace and significant flexibility in the type of visual information presented to the user. For Planar MEDARM, a basic structure holds a semi-transparent mirror and a set of LED lights above the workspace (see Fig. 5.3a). The mirror is placed equidistant from the working plane of the robot and the LEDs. When the user looks through the mirror to see his/her limb, the LEDs are reflected from the mirror so that they appear to be in the same plane as the limb, as shown in Fig. 5.3b.

5.3 Planar MEDARM Mechanical Design

5.3.1 Mechanism Design

The obvious choice for testing the curved track mechanism was the shoulder joint, because it is difficult to access the vertical shoulder joint axis due to interference with the user's body. The curved track mechanism was designed to overcome this same problem for the sternoclavicular joint in MEDARM, therefore this was a natural choice. An additional benefit is that the curved track can be fixed to the base.

Incorporating the curved track mechanism into the shoulder joint provides a simple solution for multiple mechanical design issues. Fig. 5.4 takes a step-by-step approach to describe the logic behind the final design (Fig. 5.4d), and begins by considering the three-joint system that the exoskeleton aims to mimic (the upper-limb). The simplest cable-drive system that can mimic the upper-limb is a standard serial linkage as shown in Fig. 5.4a. Different people have different limb lengths, therefore the links of the mechanism must be adjustable (as shown by the gray arrows). However, the mechanism in Fig. 5.4a would run into three problems, as follows.

Cable Tension: A concern with the design of Fig. 5.4a is that the cables do not permit free link-length adjustments when the actuators are not applying tension. The cables are routed along the links from joint to joint, thus changing the length of the links will change the distance between the joints and hence length of cable required to

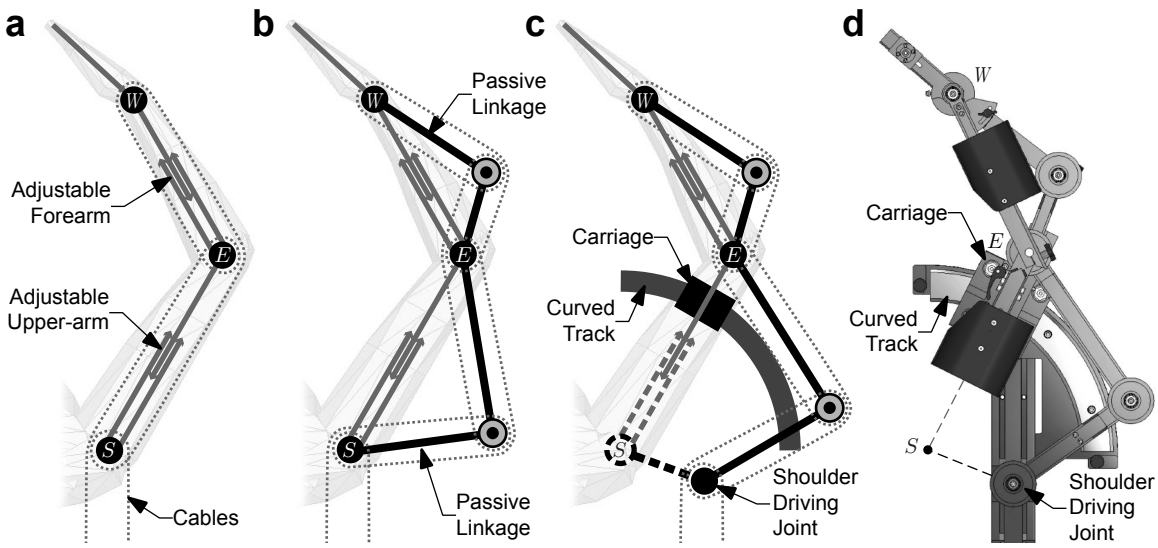

Figure 5.4: The final mechanism design overcomes three problems by incorporating MEDARM's curved track mechanism. S, E, and W represent the shoulder, elbow and wrist joints, respectively. As shown in (a), simply connecting the three cable-driven joints by standard serial linkages offers no way to maintain cable length when adjusting the link lengths, provides support only at the shoulder joint axis, and interferes with the user's body. (b) By routing the cables along passive triangular linkages, the limb segment lengths (in gray with arrows) can be adjusted without the cables falling off. (c) By placing a curved track and carriage underneath the arm and centred about the shoulder joint, the exoskeleton and the user's limb are well-supported. Moving the driving joint away from the shoulder joint axis creates a virtual 4-bar linkage like MEDARM (dashed lines) that allows all equipment to be moved away from the user. (d) The final mechanism design incorporates all of these ideas, and is shown without cables for clarity.

pass along the link. A single link length change can be up to ~ 10 cm, thus the cable will be as much as ~ 20 cm too short or too long. This is more than sufficient for all of the cables to fall off the pulleys entirely if one or both links are shortened. The solution is to guide the cables along passive triangular linkages between each joint as shown in Fig. 5.4b. Now, if the limb segment lengths are adjusted to accommodate different size users, the total distance between joint axes does not change.

Gravity Support and Body Interference: There are two additional drawbacks for both Fig. 5.4a and 5.4b. The first is that the weight of both the exoskeleton and the limb must be supported at the shoulder joint axis. Providing support only at this point means that a significant bending moment would be applied to the shoulder

joint axis. Not only does this put significant force on the shoulder joint bearings, but also, it invariably leads to out-of-plane compliance. The second problem is that all equipment must be attached to or passed across the shoulder joint axis. The torso prevents equipment from being placed directly under the shoulder joint, therefore all equipment must be placed above the shoulder, resulting in a substantial amount of equipment directly beside the user's head. Not only can this be uncomfortable for the user, but also it limits the amount and kind of equipment that can be used.

The solution to both of these problems is to incorporate MEDARM's virtual 4-bar linkage into the design. A circular track on which a low-friction carriage can freely move is placed underneath the upper-arm so that it is centred on the shoulder joint (Fig. 5.4c). Also, all equipment on the shoulder joint axis is moved back and away from the shoulder joint axis. The passive linkage of the upper-arm becomes an active linkage that drives the carriage along the track. In this configuration, the combined weight of the exoskeleton and limb is supported by the carriage, and all equipment is moved away from the user. The resulting motion is identical to a 4-bar linkage, but there are no physical structures near the shoulder joint axis as indicated by the dashed lines in Fig. 5.4c. A CAD view of the final mechanism is shown in Fig. 5.4d.

Planar MEDARM's structure is similar to KINARM in that both can be described as a 4-bar linkage (see Fig. 5.5). The difference is that Planar MEDARM does not require any physical structures on the shoulder joint axis, whereas KINARM is supported entirely at the shoulder joint axis. An advantage of this new design is that all equipment is moved away from the user, and because there is no longer any interference with the user's body, the equipment can be placed underneath the arm entirely. Planar MEDARM's design also allows an actuated DOF at the wrist, which would be a challenge to incorporate into the current KINARM design. An additional benefit of the new design is reduced vertical compliance because the weight of the arm will be directly supported by the carriage near the elbow joint axis.

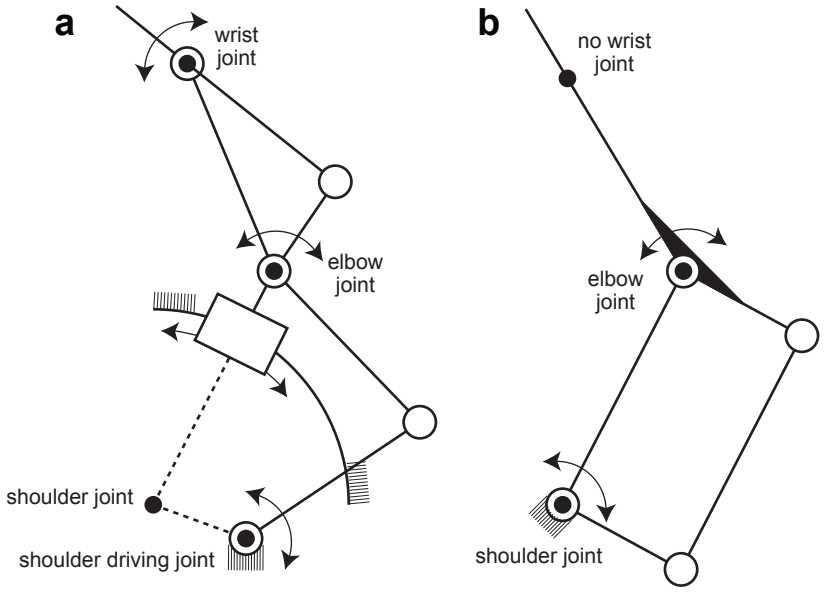

Figure 5.5: Top view schematics of (a) Planar MEDARM and (b) KINARM. Planar MEDARM has 3DOF (shoulder, elbow, and wrist), and is driven by a joint that is offset from the shoulder joint axis and that is part of a virtual 4-bar linkage. KINARM has 2DOF (shoulder and elbow) and is driven directly through the shoulder joint axis, where the elbow is driven by a 4-bar linkage (parallelogram). The shoulder joint axis is the only support point for KINARM, while Planar MEDARM is supported by its curved track.

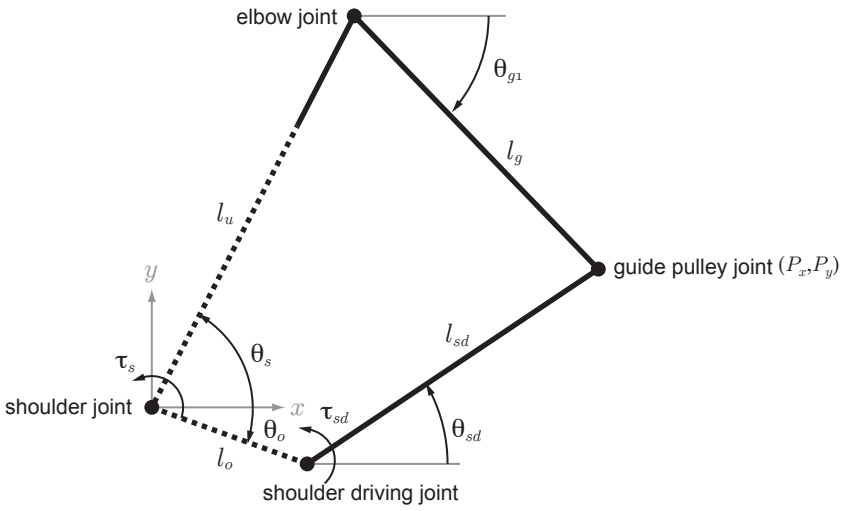

Figure 5.6: A schematic of Planar MEDARM's virtual 4-bar linkage. The links and angles are related to Fig. 3.6: $\theta_o = -20°(= \alpha_1)$, $l_o = 0.125$m $(= r_1)$, $l_g = 0.25$m $(= r_3)$, and $l_{sd} = 0.20$m $(= r_4)$. $l_u(= r_2)$ is the upper-arm length (0.26m and 0.37m). $\theta_s(= \alpha_2)$ is the shoulder joint angle, and $\theta_{sd}(= \alpha_4)$ is the shoulder driving joint angle. Knowing θ_{sd}, both θ_s and θ_{g1} can be determined. Likewise, it is possible to determine how much torque to apply at the shoulder driving joint, τ_{sd}, to produce a torque at the shoulder joint, τ_s.

A schematic view of the 4-bar linkage is shown in Fig. 5.6. The kinematics of this 4-bar linkage are described in Section 3.3. Using these kinematic relations, knowledge of the motion of the shoulder joint can be obtained from knowledge of the motion about the shoulder driving joint. An important note to make is that although the mechanical structure of Planar MEDARM's 4-bar linkage is the same as MEDARM, the driving mechanism is different. For Planar MEDARM, the 4-bar linkage is an integral part of the open-ended cable drive system, rather than just a means to guide cables to the base of the system. The effect on the cable-drive calculations will be addressed in Section 5.4.1.

5.3.2 Joint Design

The joints of Planar MEDARM are simpler than MEDARM due to the planar nature of the device. Each joint shaft is held in place by a pair of bearings, and thus the shaft is free to rotate. All pulleys are similar to the MEDARM pulleys in that each one is mounted to the shaft by a pair of bearings. The driving pulleys (with cable terminations) are clamped directly to the joint shafts. All five joints follow this design; the wrist, the elbow, the two guiding joints, and the shoulder driving joint.

The wrist and elbow joints are very similar in other respects. Each incorporates a secondary high resolution optical encoder which provides a direct measurement of the joint angle. A glass scale is glued to the base of the joint shaft, and the sensor is mounted such that it is pointing upwards towards the scale. In both joints, mechanical joint limits are machined directly into the linkages. The links simply touch each other at the limits of the motion. Rubber pads soften the contact. There are no adjustments built into these joint limits in this prototype.

The shoulder joint is different because there is no equipment on its axis. Instead, the carriage and curved track define the shoulder joint axis, thus the secondary encoder must employ a different design. In this case, a tape scale is mounted to the

base of the system, concentric with the track. The sensor is mounted to the underside of the carriage so that it runs along the tape scale as the carriage moves along the track. Knowing the spacing of the tape scale grating and the radius onto which the scale is mounted allows direct knowledge of the shoulder joint angle. Joint limits are of the same style as for the curved track in MEDARM. Rubber bumpers are mounted to the end of the track, and the carriage simply contacts these bumpers at the joint limits. All of the joint limits are fixed and thus are not adjustable.

Secondary encoders offer several benefits to this design. Most importantly, they provide direct measurements of the joint angle, bypassing any flexibility and friction in the mechanism. Therefore, it is not necessary to rely on calculations based on measurements of several motor angle rotations. Using such high resolution encoders helps to provide more smooth velocity and acceleration measurements.

5.3.3 User Attachment and Alignment

The user alignment and attachment design is a mixture of ideas from MEDARM and KINARM, and is illustrated in Fig. 5.7. It is first necessary to align the user's shoulder joint centre (glenohumeral joint) with the robot. Currently, this is achieved simply through adjustment of the chair position. The upper-arm and forearm lengths can be independently adjusted to accommodate users of different size. Upper-arm length can be adjusted by sliding the elbow joint relative to the carriage. A single quick-release clamp is used to lock the joint in place as shown in Fig. 5.7b. Forearm length can be adjusted by positioning the wrist joint using a telescopic linkage, which is then clamped using thumbscrews (see Fig. 5.7a).

The user is aligned with the mechanism at the upper-arm and forearm using fiberglass arm troughs which can be adjusted along the linkages (see Fig. 5.7a). There is no need to adjust perpendicular to the plane, so there is no need to strap the limb in place using a cuff as is required for MEDARM. The system is designed to allow the

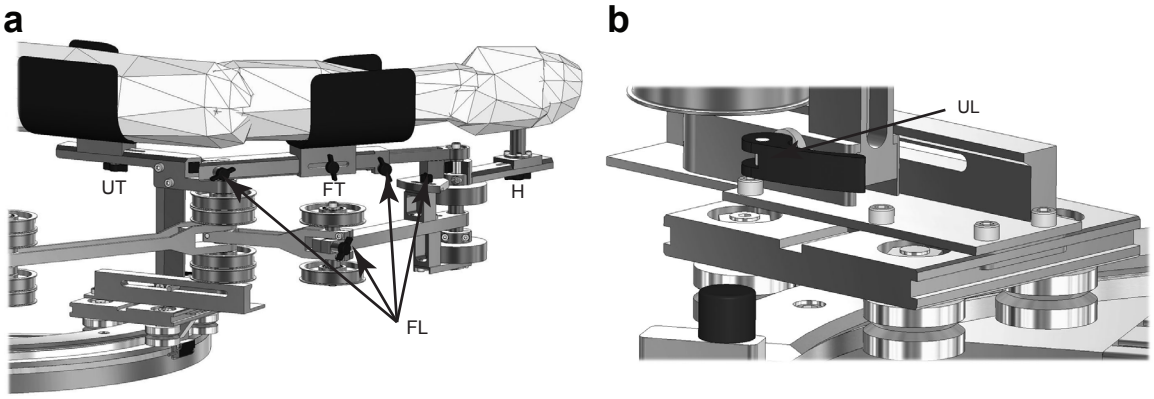

Figure 5.7: Close-up views of the adjustment system. (a) A side view of the exoskeleton showing all thumbscrews needed to adjust the exoskeleton for different size users. (b) A close-up view of the carriage (opposite side view of (a)), showing the quick-release clamp for the upper-arm length adjustment. The adjustment labels are as follows: UL - upper-arm length, FL - forearm length, UT - upper-arm trough, FT - forearm trough, H - handle.

arm troughs to be easily swapped for different sizes to accommodate a wide range of users. Currently, the subject grasps a handle. The location of the arm troughs and the handle can be fixed with a single thumbscrew clamp as shown in Fig. 5.7a.

All links are custom machined aluminum to keep the mass and inertial properties low in order to minimize the exoskeleton's influence on natural limb motion. Each joint has built-in mechanical joint limits to ensure that the robot does not extend the user's arm beyond physiological limits.

5.4 Planar MEDARM Actuation System

Planar MEDARM is actuated entirely by an open-ended cable-drive system that is very similar to the one proposed for MEDARM. However, there are only three joints to actuate, rather than four. There are no motors located directly on any of the joint axes, and all motors are located behind the user, out of the way. Fig. 5.8 illustrates the system.

Planar MEDARM's design would perhaps be better suited to using another type of drive system, but because this was meant to be a prototype for MEDARM, Planar

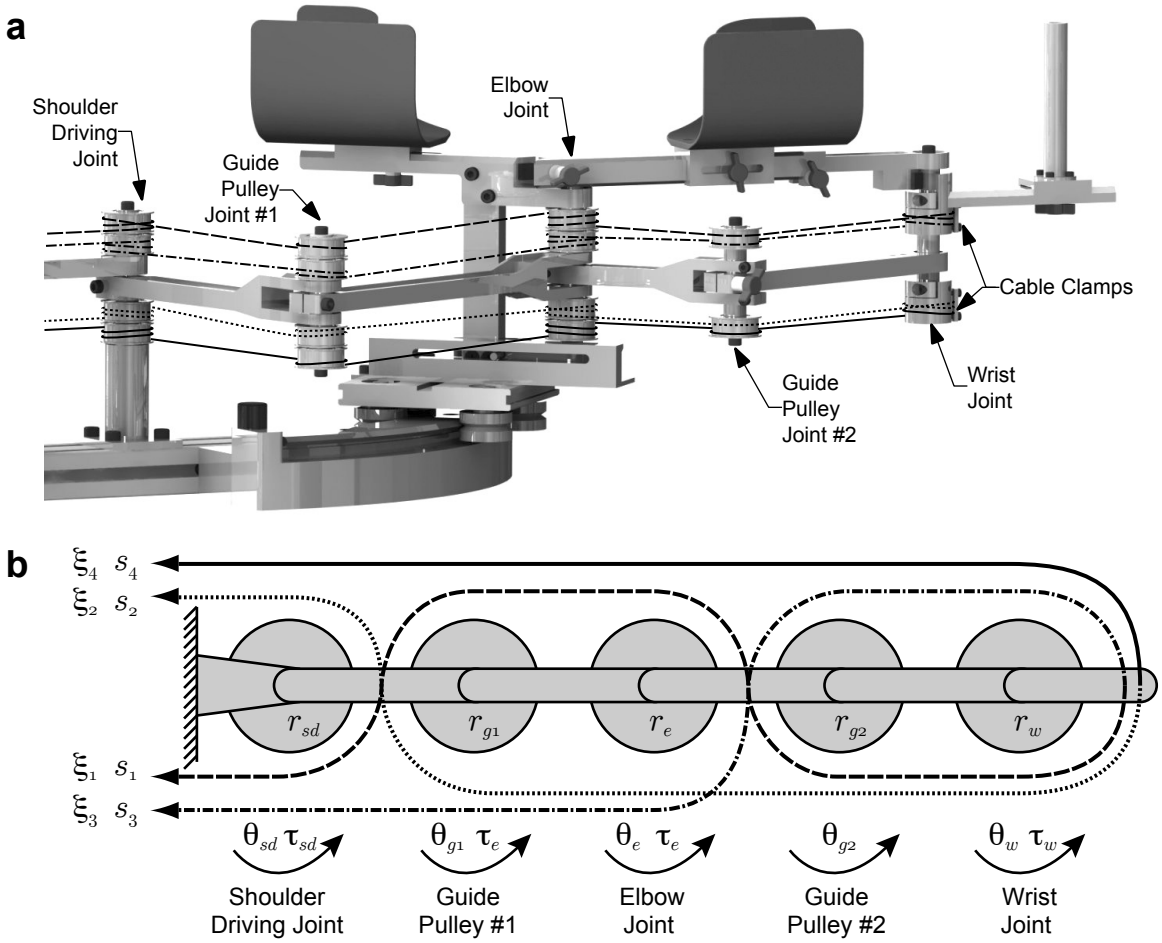

Figure 5.8: (a) A CAD drawing illustrating the cable routing scheme used in the original configuration. (b) A simplified planar schematic representation of the original cable routing structure. Each of the four cables is denoted by a different line type. Symbols s, ξ, r, τ and θ represent cable displacement, cable force, pulley radius, joint torque and joint angle respectively.

MEDARM was designed specifically to use the same type of routing scheme. This section will describe the cable-drive system, and its differences from the one proposed for MEDARM. Also, there will be a brief description of the electronics and control system used to communicate with the robot.

5.4.1 Cable-Drive System

As mentioned in Sections 3.2 and 4.4.1, there are several ways to route the cables around the joints, and this has a significant effect on performance. There are five

Table 5.1: A summary of the antagonism ratio and maximum force ratio for the 5 unique cable routing schemes for a 3DOF cable-drive system. The structures of each system are illustrated in previous work [102].

Scheme	$\boldsymbol{H}$	**Antagonism Ratio**	**Maximum Force Parameter**	**Maximum Force Ratio**
i	$[1,1,2,2]^T$	2	$[1,\sqrt{3/2},\sqrt{2},\sqrt{6}]^T$	2.45
ii	$[1,1,2,4]^T$	4	$[1,1,\sqrt{2},\sqrt{6}]^T$	2.45
iii	$[1,1,1,1]^T$	1	$[\sqrt{3/2},\sqrt{3/2},\sqrt{2},\sqrt{2}]^T$	1.15
iv	$[1,1,1,1]^T$	1	$[1/\sqrt{2},1/\sqrt{2},1/\sqrt{2},1/\sqrt{2}]^T$	1
v	$[1,1,2,2]^T$	2	$[1/\sqrt{2},1/\sqrt{2},\sqrt{3/2},\sqrt{2}]^T$	1.61

unique cable routing schemes for a 3DOF system [102]. The schemes were analyzed as described in Section 3.2 to find the choice which has the best compromise between having both minimal antagonism between cables (and hence the most even distribution of forces across the cables), and minimal peak forces. The results are summarized in Table 5.1. Scheme "iv" was chosen (see Fig. 5.8b) because both the antagonism ratio and the maximum force ratio are 1 (best choices).

The relationship between joint motion and cable motion follows the same formulation as shown in Section 3.1. However, Planar MEDARM's novel virtual 4-bar mechanism requires special modifications to account for the fact that the cables are routed along one edge of the 4-bar linkage. In fact, the 4 cables are routed across 4 joints (shoulder driving joint, guide pulley joint #1, elbow joint, and wrist joint, as indicated in Fig. 5.8) rather than 3, because the guide pulley on the 4-bar linkage that drives the shoulder also contributes to the motion. The result is that the cables that reach the elbow and wrist joints change length as the shoulder moves. Fortunately, the guide pulley angle is not independent because it is a function of the other angles of the 4-bar linkage. The cables also pass around a second guide pulley on the forearm linkage, but this linkage is fixed and thus does not affect the system. Therefore, after some modifications to account for the 4-bar linkage, the cable displacement, s, and

the change in joint angle, $\Delta\theta$, can be related using (5.1) and (5.2).

$$\begin{bmatrix} s_1 \\ s_2 \\ s_3 \\ s_4 \end{bmatrix} = \begin{bmatrix} -r_{sd} & r_e & -r_w & -1 \\ r_{sd} & -r_e & -r_w & 1 \\ -r_{sd} & -r_e & r_w & 1 \\ r_{sd} & r_e & r_w & -1 \end{bmatrix} \begin{bmatrix} \Delta\theta_{sd} \\ \Delta\theta_e \\ \Delta\theta_w \\ \Delta\theta_{4bar} \end{bmatrix} \tag{5.1}$$

where $\Delta\theta_{4bar}$ is the added term:

$$\Delta\theta_{4bar} = r_{g1}\Delta\theta_{sd} - r_e\Delta\theta_s + (r_e - r_g)\Delta\theta_{g1} \tag{5.2}$$

These relationships are illustrated in Fig. 5.8b. Note that θ_s refers to the actual shoulder joint, and that θ_{sd} refers to the shoulder driving joint.

Likewise, to relate cable force to joint torque, some modifications must be made to the formulation described in Section 3.1 to account for the contributions from the 4-bar linkage. The reason for the modification is that when a torque is applied to the elbow joint, a torque of the same magnitude is also applied at the guide pulley joint. This occurs because the cables are routed around the guide pulley in the same manner as the elbow joint, and therefore a torque is simultaneously applied to the 4-bar mechanism. The result is an unwanted torque about the shoulder joint. To correct this problem, an additional torque, τ_{4bar}, must be applied to the shoulder driving joint whenever an elbow torque is applied, in addition to the properly scaled shoulder torque, τ_s. This relation is defined by (5.3).

$$\tau_{sd} = \left(\frac{l_{sd}\sin(\theta_{g1} - \theta_{sd})}{l_u \sin(\theta_{g1} - \theta_s)} \right) \tau_s + \tau_{4bar} \tag{5.3}$$

where τ_{4bar} is given by:

$$\tau_{4bar} = \left(1 - \frac{l_{sd}\sin(\theta_{g1} - \theta_{sd})}{l_u \sin(\theta_{g1} - \theta_s)} \right) \tau_e \tag{5.4}$$

Using the same formulation as (3.9) from Section 3.1.2, cable force, ξ, and joint torque, τ, can be related using (5.5):

$$\begin{bmatrix} \tau_{sd} \\ \tau_e \\ \tau_w \end{bmatrix} = \begin{bmatrix} -r_{sd} & r_{sd} & -r_{sd} & r_{sd} \\ r_e & -r_e & -r_e & r_e \\ -r_w & -r_w & r_w & r_w \end{bmatrix} \begin{bmatrix} \xi_1 \\ \xi_2 \\ \xi_3 \\ \xi_4 \end{bmatrix} \tag{5.5}$$

where τ_{sd} is the total torque to be commanded to the shoulder driving joint, as defined by (5.3). The scaling factor in (5.3) is determined from (3.59) in Section 3.3. It should be noted that with an elbow torque command of zero, τ_{4bar} becomes zero, and therefore τ_{sd} reduces to a single term that describes the applied shoulder torque.

Implementation

Changes in cable length are achieved by winding up or unwinding cable from driving pulleys. A cable is clamped to each driving pulley, which is driven by a slotless brushless DC motor (Compumotor SM Series, Parker Hannifin Corporation, Rohnert Park, CA, U.S.A.) using a timing belt. Thus, a rotation of the motor either winds up or unwinds the cable from the driving pulley. Each motor has a built-in optical encoder, which measures the rotation of the windup pulley, and thus a simple calculation provides the length of cable that has been wound up or unwound.

$$s_i = r_{wi}\left(\frac{\theta_{mi}}{\eta_{mi}}\right) \tag{5.6}$$

where for the i^{th} cable, s_i is the cable length change, r_{wi} is the windup pulley radius, η_{mi} is the gear ratio between the motor and the windup pulley and θ_{mi} is the rotation angle of the motor.

Using these cable length changes, it is possible to use (5.1) to obtain the changes in joint angles that are associated with the cable system. The angles of the four-bar linkage can be found as needed using the techniques described in Section 3.3.1, and with variables defined as in Fig. 5.6.

$$\theta_s = \arctan\left(\frac{P_y - l_g\sin\theta_{g1}}{P_x - l_g\cos\theta_{g1}}\right) \tag{5.7}$$

where,

$$\theta_{g1} = \arctan\left(\frac{P_y}{P_x}\right) - \arccos\left(\frac{{P_x}^2 + {P_y}^2 + {l_g}^2 - {l_u}^2}{2l_g\sqrt{{P_x}^2 + {P_y}^2}}\right) \tag{5.8}$$

$$P_x = l_o\cos\theta_o + l_{sd}\cos\theta_{sd} \tag{5.9}$$

$$P_y = l_o\sin\theta_o + l_{sd}\sin\theta_{sd} \tag{5.10}$$

To determine how much torque to apply at each motor, (5.5) must be solved for the four cable forces. Using the torque resolver technique [102] as described in Section 3.1.2, the cable forces can be expressed as (5.11a)-(5.11d).

$$\xi_1 = \frac{1}{2}O^+\left(\frac{\tau_e}{r_e} - \frac{\tau_w}{r_w}\right) + \frac{1}{2}O^-\left(\frac{\tau_{sd}}{r_{sd}} + \frac{1}{2}\left|\frac{\tau_e}{r_e} - \frac{\tau_w}{r_w}\right| - \frac{1}{2}\left|\frac{\tau_e}{r_e} + \frac{\tau_w}{r_w}\right|\right) + \delta \quad (5.11a)$$

$$\xi_2 = \frac{1}{2}O^-\left(\frac{\tau_e}{r_e} + \frac{\tau_w}{r_w}\right) + \frac{1}{2}O^+\left(\frac{\tau_{sd}}{r_{sd}} + \frac{1}{2}\left|\frac{\tau_e}{r_e} - \frac{\tau_w}{r_w}\right| - \frac{1}{2}\left|\frac{\tau_e}{r_e} + \frac{\tau_w}{r_w}\right|\right) + \delta \quad (5.11b)$$

$$\xi_3 = \frac{1}{2}O^-\left(\frac{\tau_e}{r_e} - \frac{\tau_w}{r_w}\right) + \frac{1}{2}O^-\left(\frac{\tau_{sd}}{r_{sd}} + \frac{1}{2}\left|\frac{\tau_e}{r_e} - \frac{\tau_w}{r_w}\right| - \frac{1}{2}\left|\frac{\tau_e}{r_e} + \frac{\tau_w}{r_w}\right|\right) + \delta \quad (5.11c)$$

$$\xi_4 = \frac{1}{2}O^+\left(\frac{\tau_e}{r_e} + \frac{\tau_w}{r_w}\right) + \frac{1}{2}O^+\left(\frac{\tau_{sd}}{r_{sd}} + \frac{1}{2}\left|\frac{\tau_e}{r_e} - \frac{\tau_w}{r_w}\right| - \frac{1}{2}\left|\frac{\tau_e}{r_e} + \frac{\tau_w}{r_w}\right|\right) + \delta \quad (5.11d)$$

It is then a simple matter to calculate the torque that motor i must produce to generate a given force in cable i.

$$\tau_{mi} = r_{wi}\left(\frac{\xi_i}{\eta_{mi}}\right) \quad (5.12)$$

where τ_{mi} is the motor torque, r_{wi} is the windup pulley radius, and ξ_i is the cable force as calculated by (5.11).

5.4.2 Electronics and Control

Overall, the motor encoders are capable of measuring joint angle in increments of 0.006° (±0.02° accuracy). To prevent the cables from becoming slack when the system is turned off or during a power failure, each motor is equipped with an electric brake. All motors are located behind the user, as shown in Fig. 5.2. In addition, secondary optical encoders (Mercury I and II Series, Micro-E Systems, Natick, MA, U.S.A.) are mounted directly to each joint. The elbow and wrist joint encoders each employ a high-resolution rotary glass scale, and the angles can be measured in increments of 0.0001° and 0.0002°, respectively with an accuracy of ±0.005°. The

shoulder joint encoder measures shoulder angle in increments of 0.00004° (±0.00002° accuracy) using a tape scale mounted to the outer diameter of the curved track. Using such high resolution secondary encoders permits a much smoother calculation of joint velocity and acceleration.

The present motion control system used for this prototype is basic, and a schematic of the hardware is shown in Fig. 5.9. Each motor is powered by a servo drive amplifier (Compumotor Gemini GV Series, Parker Hannifin Corp., Rohnert Park, CA, U.S.A.) operating in torque mode such that the motors provide a torque proportional to

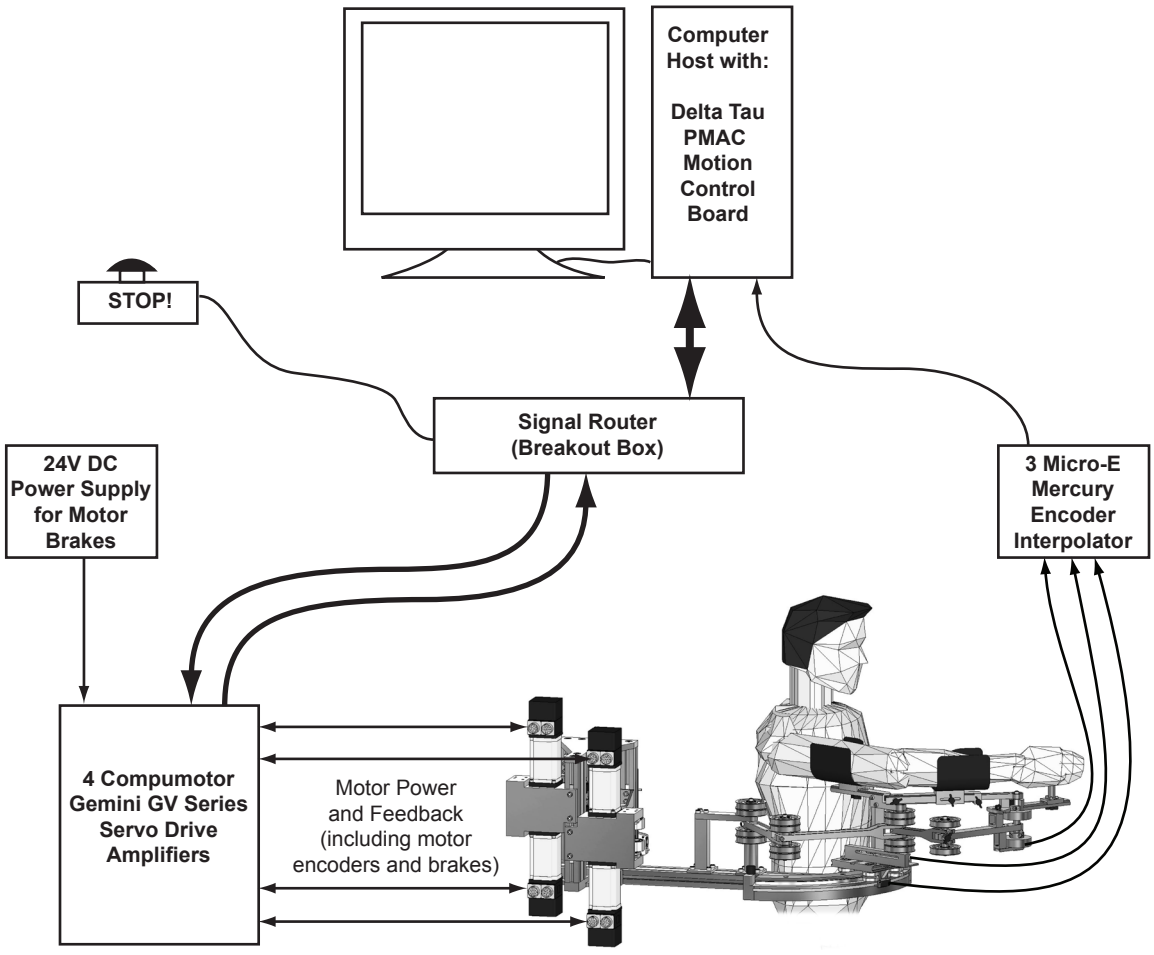

Figure 5.9: A schematic of the hardware used to operate Planar MEDARM. The PMAC motion control card is the central component, performing all calculations relating to the robot motion. A breakout box is used to route all signals between the PMAC and the motor drives. A separate power supply is used to provide power tot he motor brakes.

a ±10 V command. In contrast with other robots (i.e. KINARM), which do not consume significant power when operating with zero joint torques, Planar MEDARM's motors consume power continuously in order to maintain a cable pretension. The peak power of each drive is 1.1 kW, and the maximum continuous power is 0.44 kW [109]. The drives are wired with a single emergency disable switch. Additionally, the drives route the power to the motor brakes so that the brakes engage when the drives are disabled or a fault is detected.

The heart of the system is a motion control card (PMAC, Delta Tau Data Systems Inc., Chatsworth, CA, U.S.A.). The motion control card receives the quadrature encoder signals from the four motor encoders and three secondary encoders as input. The output is simply four ±10 V analog torque command signals which are sent to the four servo drives. Presently, the motion control card is programmed directly with all instructions necessary to calculate joint kinematics and apply joint torques. While basic control algorithms have been hard-coded into the motion control card, a custom software package is required to apply more advanced control and data handling. The Dexterit-E software package (BKIN Technologies, Kingston, ON, Canada) was adapted to allow very simple data collection from Planar MEDARM.

5.4.3 Dynamic Model and Simulation

A dynamic model was created for Planar MEDARM based on the model created for MEDARM (Section 4.4.3). The model is defined as a standard rigid-body manipulator with negligible cable dynamics. Once again, dynamic parameters of the exoskeleton are estimates from CAD drawings, and upper-limb parameters were calculated from anthropometric data tables based on user height and weight [15].

Simulations were performed for various reaching movements with a peak end-point velocity of 1.0m/s [8]. Movements included single-joint motion through each joint's full range, and a variety of multi-joint reaching movements. The simulations were used

to determine the range of forces/torques that would occur during these movements, which were in turn used to select motors, gear ratios, cables and bearings.

Dynamic Manipulability

An additional step taken with Planar MEDARM's dynamic model was to map out the dynamic manipulability across the workspace. This allows the dynamic effects of the exoskeleton on the user's limb to be visualized.

Dynamic manipulability refers to the ability of a manipulator (robot or human limb) to apply forces or to accelerate its end-effector. Like kinematic manipulability (as defined in Section 4.3.2), dynamic manipulability varies depending on the configuration of the mechanism in the workspace. However, dynamic manipulability also takes into account the inertial properties of the mechanism.

It can be shown that the dynamic manipulability for a manipulator is an ellipsoid [104]. If the manipulator is initially at rest, and the the set of joint torques, $\boldsymbol{\tau}$ is restricted to unit norm:

$$\boldsymbol{\tau}^T \cdot \boldsymbol{\tau} = 1 \tag{5.13}$$

the ellipsoid will have the following form:

$$\boldsymbol{a_{ee}}^T J^{\dagger T} M^T M J^{\dagger} \boldsymbol{a_{ee}} = 1 \tag{5.14}$$

where $\boldsymbol{a_{ee}} = [a_x, a_y, a_z]^T$ is the acceleration of the end-effector in Cartesian space, J is the Jacobian matrix for the given configuration, and M is the inertia matrix of the mechanism. Planar MEDARM is redundant, therefore J is not a square matrix, and therefore cannot be inverted. As a result, the pseudo-inverse, $J^{\dagger}$, must be used and is given by:

$$J^{\dagger} = J^T \left(JJ^T\right)^{-1} \tag{5.15}$$

For a planar system such as Planar MEDARM, expanding (5.14) results in a 2D ellipse. If this ellipse is drawn centred on the end-effector of the mechanism, the distance from the end-point of the mechanism to the ellipse is a measure of the

acceleration that can be imposed on the end-effector along the given direction. This is for the case when the set of applied joint torques has unit norm, as in (5.13).

Fig. 5.10 shows the dynamic manipulability ellipse for Planar MEDARM in a variety of configurations. Fig. 5.10a is for 50^{th} percentile user, and Figs. 5.10b and 5.10c are for the smallest and largest configurations of Planar MEDARM, respectively. In all plots, there are two ellipses at each configuration. The black ellipse is for the subject's limb without Planar MEDARM. The gray ellipse is for the case when the limb is attached to Planar MEDARM.

Looking at Fig. 5.10a, it is clear that the manipulability varies according to the configuration. A flat ellipse indicates that the mechanism cannot accelerate in one direction. This occurs at a singular configuration which, for Planar MEDARM, can happen only at the workspace boundary (i.e. the arm cannot be accelerated beyond its workspace). The shape of the black (limb only) and gray (limb with Planar MEDARM) ellipses are comparable, although the gray ellipses are smaller. This is expected because the added mass and inertia of the exoskeleton will reduce the possible acceleration for the set of unit norm joint torques. Also, several of the ellipses exhibit a slight rotation when the exoskeleton is included. This indicates that the presence of the robot changes the mass distribution of the limb. It should be noted that the absolute angle of the shoulder joint does not affect the dynamic manipulability of the system, therefore for clarity, Fig. 5.10 shows the case for just one shoulder angle.

Figs. 5.10b and 5.10c show the smallest and largest possible configurations of Planar MEDARM. For the smallest case, it is expected that the exoskeleton will have a greater effect on the limb, and this is observed. There is a greater size difference between the black and gray ellipses, and the rotation is more apparent. For the largest case, the exoskeleton has a smaller influence on the limb. There is a smaller size difference and a smaller degree of relative rotation. Overall, the effect of Planar

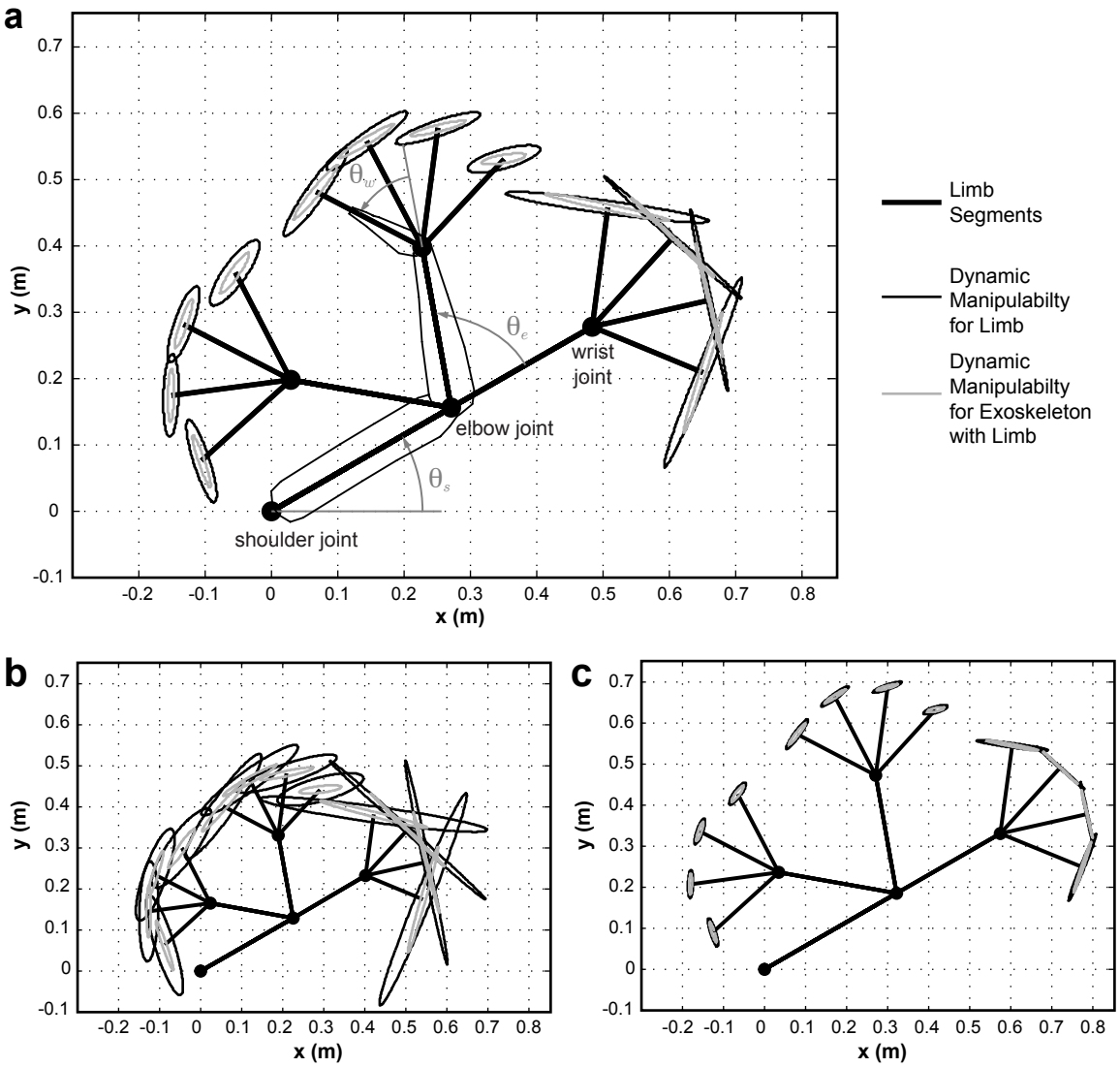

Figure 5.10: (a) Simulated dynamic manipulability of Planar MEDARM with a 50^{th} percentile limb for a variety of configurations across the workspace. (b) Smallest and (c) largest configuration for Planar MEDARM. The distance from the end-point of the robot links to the ellipse is a measure of the acceleration that can be imposed on the end-effector along the given direction for the case when the set of applied joint torque has unit norm. The solid black and light gray ellipses indicate the dynamic manipulability for the limb and Planar MEDARM with the limb, respectively.

MEDARM on the dynamics of the limb is predicted to be minimal.

5.5 Cost

The approximate cost of the components required to build Planar MEDARM is summarized in Table 5.2. Labour costs are not included. As before, the parts have been categorized into three categories: motion control, electrical, and mechanical. The motion control category involves all motors, encoders, drives, and control cards necessary to actuate and control the system. The electronics section includes all wiring, connectors, power supplies and housings required to connect all of the system together. The mechanical section includes all other components. As with MEDARM, the motor and electronics systems dominate the expense of the robot, accounting for more than 75% of the total parts cost.

Table 5.2: A summary of the cost of the parts for Planar MEDARM. Labour is not included.

Part	**Cost**
Motion Control	
Motors, Drives, and Cables	$11,600
Motion Control Card	$4,000
Secondary Encoders	$2,900
Sub-Total	**$18,500**
Electrical	
Electronic Components	$450
PCBs	$1,500
Sub-Total	**$1,950**
Mechanical	
Shafts, Washers, Screws, Clamps, etc...	$1,050
Bearings	$250
Pulleys	$1,750
Timing Belts	$50
Curved Track and Carriage	$550
Cable and Fittings	$500
Material and Tooling for Machining	$2,000
Arm Troughs (one size)	$500
Sub-Total	**$6,650**
Total	**$27,100**

Chapter 6: Planar MEDARM Evaluation

A prototype of Planar MEDARM has been fully assembled (Fig. 6.1). This chapter is devoted to detailing performance evaluation procedures and results for the prototype. Also, a brief description of some rehabilitation control strategy testing performed with Planar MEDARM will be discussed.

6.1 Planar MEDARM Performance Evaluation

One of the main goals of the prototype is to analyze the cable-drive transmission system and also the curved track mechanism. The performance evaluation outlined in this section relates specifically to this goal.

Before any tests were performed, several checks were made to ensure that the robot was providing the correct feedback. First, the secondary encoders at the joints were used to confirm that the joint angle calculations based on the motor encoder readings were correct. Also, the motors and servo amplifiers were calibrated (to account for variations in the windings between the motors) to ensure that the torque output would be as expected for all four motors. Calibration is particularly important in this type of robot as the four cables require constant pretension to be applied by the motors. Small differences between the motors lead to the application of a small torque at one or more of the joints. With the motors calibrated, some measurements were made with a force transducer to confirm that the correct torques were generated.

6.1.1 Measured Parameters

Several fundamental performance parameters of the Planar MEDARM prototype have been measured including: joint friction, inertia as seen at the joints, joint compliance, and vertical (out-of-plane) compliance. Data collection has also been tested by collecting several samples of experimental data using Planar MEDARM. The per-

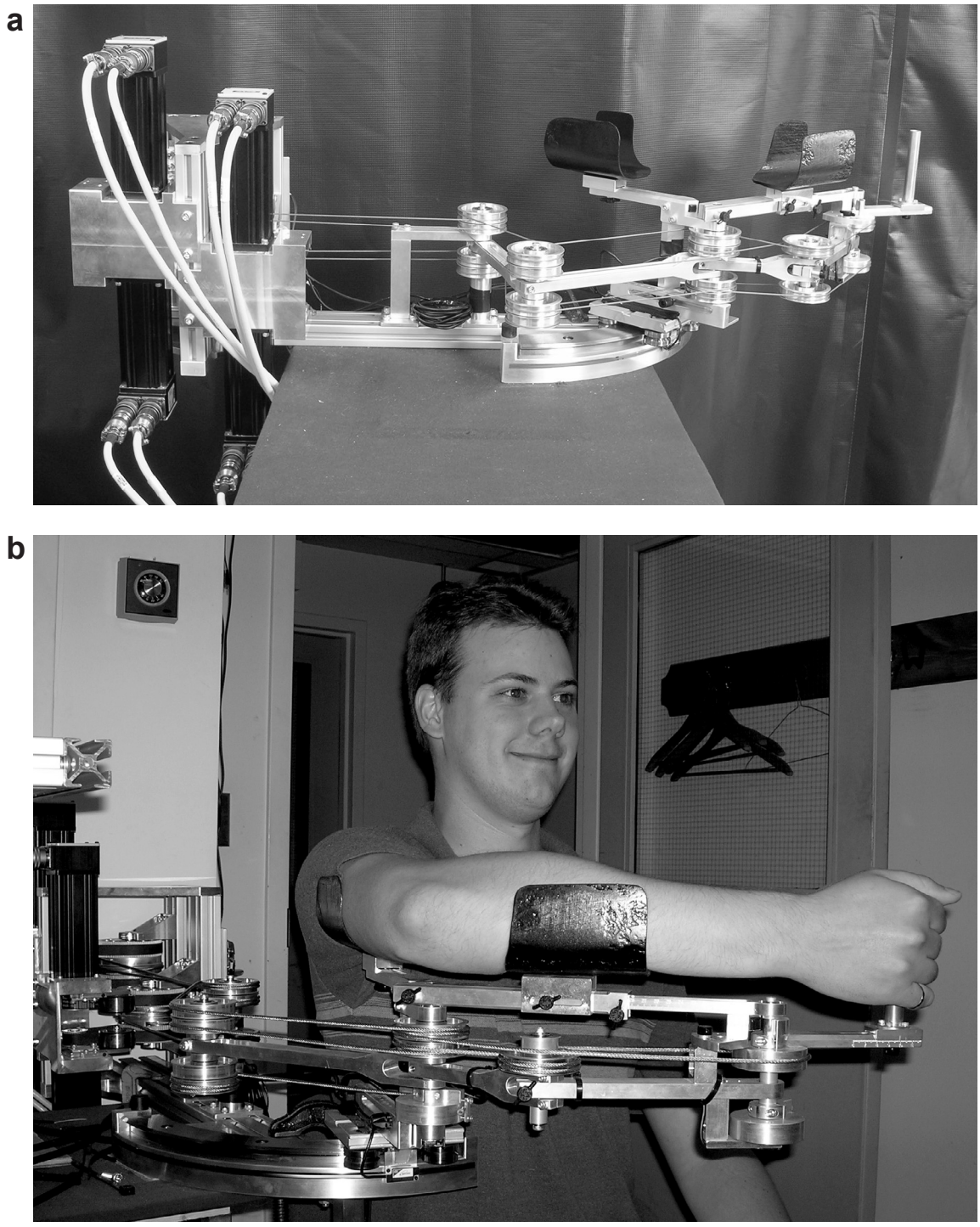

Figure 6.1: (a) A photo of the fully constructed Planar MEDARM prototype in its original configuration. The view was chosen to match the CAD view from Fig. 5.2a. (b) A photo of Planar MEDARM in use.

formance measures are compared directly to those of KINARM where possible. The following is a brief description of the testing parameters and the methods used to obtain measurements.

Joint Friction: Friction in a robotic system can have both beneficial and detrimental effects on performance. Friction can provide a level of damping that helps to stabilize the system under position control. However, high friction affects natural passive motion, which can interfere with measurements of reaching movements. The main application of this robot is measuring motor performance, which demands smooth transparent operation of the device, therefore low friction is desirable.

To obtain an idea of the friction that a user would experience at each joint of the exoskeleton, static friction was measured. Static friction can be measured simply by determining the minimum torque required to create a movement at the joint. Friction is a highly variable parameter which is influenced by many aspects of the system, therefore the friction was measured for several configurations across the range of motion of the joint, and an average friction torque measurement was obtained.

The accuracy was determined by finding the maximum and minimum friction values for the entire joint ROM. It was determined that the static friction measurements are accurate to within ± 0.05 Nm. Torque ripple created by the servo drives is the dominant source of error.

Inertia: The inertia of the exoskeleton as seen by the joints of the user also has a significant impact on the performance of the system. Ideally, from an experimental point of view, the inertia should be zero, but of course this is not possible. More practically, the inertia of the exoskeleton should be kept as low as possible, and should be proportional to the inertia of the human upper-limb. Otherwise, the device will have a significant effect on the natural intersegmental dynamics of the limb.

Section 5.4.3 introduced the estimated dynamic manipulability of Planar MEDARM. Fig. 5.10 showed the difference in dynamic manipulability between the

limb and the limb with Planar MEDARM attached. The difference is due to the inertia of the robot. While dynamic manipulability incorporates the inertia of the exoskeleton, inertia as seen at the joints is not explicitly addressed. This section will investigate the inertia specifically.

The inertia of Planar MEDARM as seen by the joints of the user was estimated from the detailed CAD drawings used to manufacture the prototype. The gear ratio and the number of motors driving the joint were incorporated into the calculations. All calculations specified a shoulder angle of 45°, an elbow angle of 90°, and a wrist angle of 0°, which corresponds to a typical starting point for a reaching task.

Considering that manufacturing processes typically produce parts with a tolerance of ±0.1mm (at most), it is expected that the actual inertia values are within approximately 1% of the CAD estimates. Another source of error arises from neglecting cable mass in the estimates.

Compliance: Compliance has a significant impact on the overall performance of a robot. With high compliance, tight position control is not possible, and it is not possible to accurately measure true joint angles without secondary encoders on the joints. This is a result of the elastic properties within the system. Sources of compliance include elasticity of cables and belts, and bending of shafts and linkages.

In-plane joint compliance was measured by reading the change in position noted by the motor encoders while commanding a joint torque to the system with all joints locked in place. The effective torsional spring constant (i.e. stiffness, and hence compliance) could then be easily calculated from Hooke's Law. The joint torque was applied in 0.5Nm increments up to the maximum output of the motors. Note that for Planar MEDARM, the joint compliance can be different for positive and negative rotations due to the distribution of the cables, but here, the average is presented.

The compliance values presented here are based on measurements of cable length change (motor encoder readings), torque, and pulley radii, each of which have an

associated measurement error. Propagating these errors through the calculations leads to a compliance accuracy of ±9%. The largest source of error comes from the cable displacement measurements which are limited by the accuracy of the motor encoders.

Vertical compliance was measured by placing known masses at the wrist joint and measuring the resulting vertical displacement. The system was configured with a shoulder angle of 45°, an elbow angle of 90°, and a wrist angle of 0°. Accuracy of the vertical compliance measurements is ±1%. The main source of error is the vertical distance measurement.

Reaching Task: To determine its applicability to the real world, Planar MEDARM was set up to perform one of the standard tasks that is performed in motor control research - the centre-out reaching task [110, 111]. The virtual display system shown in Fig. 5.3 of Section 5.2 was assembled and attached to Planar MEDARM. The display is capable of presenting to the user any one of eight peripheral targets equally spaced around a 10 cm radius circle. Several healthy volunteers were recruited to perform this experiment to test out the robot's measuring abilities.

The system was calibrated so that the starting point for the user (central target) was aligned with the handle of the exoskeleton when the shoulder and handle were aligned at $x = 0$ and that the elbow was 90°, and the wrist was 0° (see Fig. 6.2). The subject was directed to move as quickly and as accurately as possible from the central target to the peripheral targets as they appeared one at a time in the display. The subject was not directed to follow a specific trajectory. After reaching the target, the subject moved back to the central target. Planar MEDARM recorded the three joint angles during the outward movement. Each target was displayed a total of 10 times, in random order. Dexterit-E (BKIN Technologies, Kingston, ON) was used to develop the experimental protocol and to collect the data.

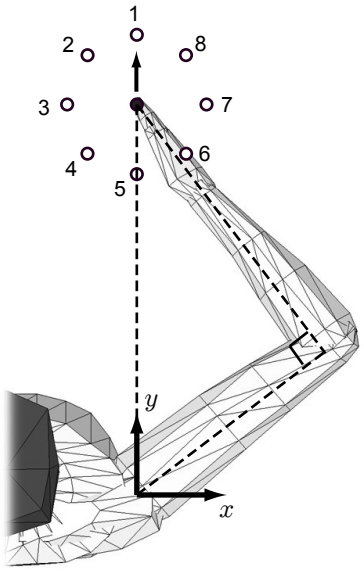

Figure 6.2: The experimental reaching task layout. A set of eight targets (open circles) evenly distributed around a circle of 10cm radius is projected into the plane of Planar MEDARM. A central target lies in the centre of this circle. The central target (closed circle) is positioned to match the location of Planar MEDARM's handle when it is aligned with the shoulder joint axis ($x = 0$) and and when the elbow is 90°, and the wrist is 0°.

6.1.2 Systems Tested

In order to obtain a better idea about how the above performance measures are affected by the components and specific design features of Planar MEDARM's actuation and transmission system, the measures were obtained for several variations of the actuation system. Starting with the original design as described in Section 5.2, changes were made one at a time, but each consecutive variant maintained the changes from the previous systems. In the end, the final system consisted of all changes. Each modification was chosen to upgrade the performance of the system without requiring any structural changes or changes to the prototype's overall mechanism design.

System a - Original: The original design was tested first. The main parameters include a gear ratio of 6 (3 from belts, 2 from cable pulleys), a cable routing structure as in Fig. 5.8b, pulley diameter of 60mm, and cable diameter of 1.19mm.

System b - Gear Ratio: The goal of this first change was to reduce both the friction and inertia of the motor system. The overall gear ratio was reduced to 2

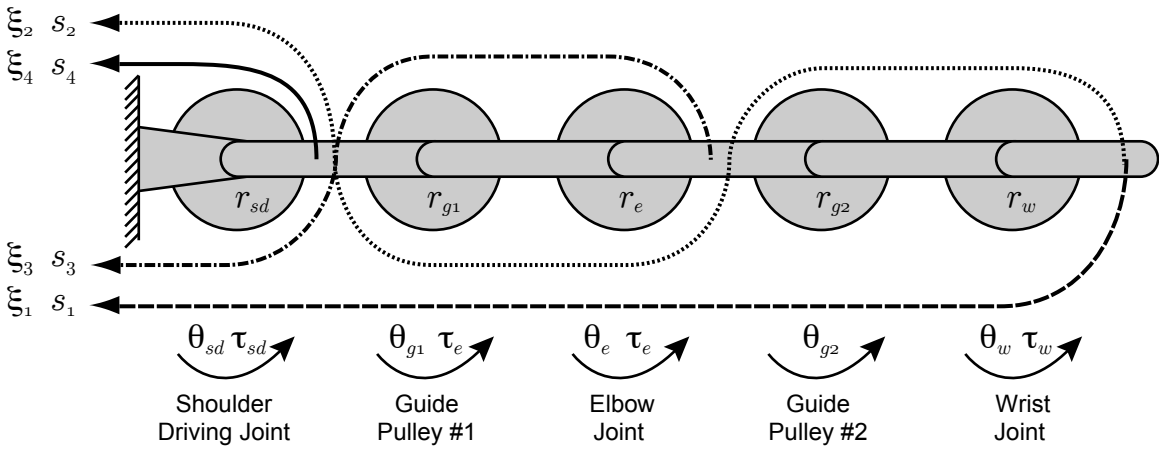

Figure 6.3: Planar schematic representation of the alternate cable routing structure of *system c*. There are 4 cables at the shoulder, 3 at the elbow, and 2 at the wrist.

(3 from belts, 2/3 from cable pulleys) by adding an adapter to the cable-windup system. The adapter provides a 90mm diameter pulley to wind up the cable, whereas the original system used a 30mm diameter pulley. This will result in a substantial reduction of both parameters for the wrist joint, as the motor system is by far the most dominant component (see results in Section 6.1.3).

System c - Cable Routing: The goal of the second change was to further reduce the overall friction and inertia about the wrist and elbow joints. An alternate cable routing structure (scheme "i" from Table 5.1) was implemented to drive the joints (Fig. 6.3). While the original structure has the lowest and most even force distribution, it requires all four cables to span all three joints. In contrast, the new structure needs only two cables for the wrist, three for the elbow and four for the shoulder. Friction and inertia will be reduced at both the wrist and elbow because fewer motors are connected to these joints. However, these reductions will come at the expense of even force distribution and also joint compliance.

System d - Thicker Cable: The primary goal of this third change was to decrease the compliance by increasing the thickness of the cables. Doubling the cable diameter from 1.19mm to 2.38mm, increases the cross-sectional area of the cable by

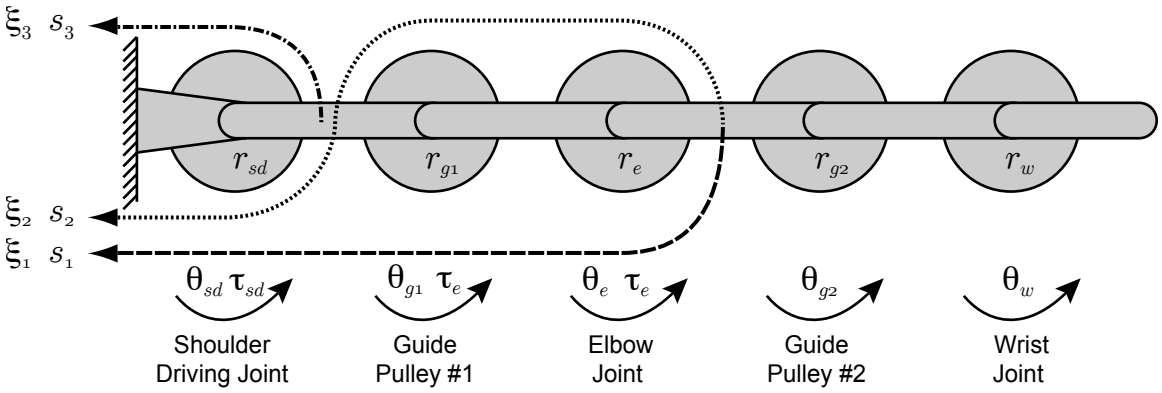

Figure 6.4: Planar schematic representation of the 2DOF structure of *system e*. There are 3 cables at the shoulder, 2 at the elbow, and 0 at the wrist (free to rotate).

a factor of four, and thus reduces compliance of the cable by a factor of four.

System e - 2DOF: The fourth change was to convert the system to a 2DOF robot for a more direct comparison with KINARM. The wrist joint is still present (can be locked), but it is not actuated because the cables were removed from the wrist joint. The secondary encoder at the wrist can still measure wrist position, even though it is not being actuated. The cable drive system now requires only three cables to drive the shoulder and elbow joints, and thus the cable structure was updated. There is only one structure for a 2DOF system with three cables (see Fig. 6.4).

System f - KINARM: As a base of comparison, the same parameters were measured for KINARM. No special changes were made to KINARM, so all testing parameters were measured for both the shoulder and elbow.

6.1.3 Results

Measurements of joint friction are shown in Fig. 6.5a for all systems. Friction was initially several times larger than KINARM, but it is clear that the changes provided a substantial reduction of friction. The biggest improvement occurred for *system b* when the gear ratio was changed. The friction was nearly halved for all three joints. This makes intuitive sense because reducing the gear ratio by a factor of three, reduces the

friction of the motor system (the motors, the timing belts and the associated pulleys) as seen by the joints by a factor of three. Since all four motors are connected to all three joints, this is a substantial reduction. Another substantial reduction in friction occurred for the elbow and wrist when switching the cable routing structure (*system c*). This reduction cut the friction at the wrist in half simply by removing two cables (including pulleys, belts and motors) entirely from the wrist drive system. Similarly, the elbow friction was reduced by a quarter because the one of the four cables was removed. For *system e*, the wrist joint friction was not measurable using our approach as the only possible source of friction is a pair of bearings on the wrist joint shaft.

The friction at the elbow was reduced to a magnitude comparable with KINARM. Similarly, the wrist exhibited low friction. In contrast, the shoulder joint has substantially higher friction. An estimate of the friction in the curved track system indicates that about half of the measured friction (in *systems b-e*) comes from the curved track and carriage. It should be noted that moving from *system a* to *system c*, the friction was reduced by similar magnitudes at each joint. However, the reduction in friction of the wrist joint is most perceptible by the user.

Fig. 6.5b shows the estimates of the inertia as seen by the joints. The length of the bars for each system show the estimated range of inertia for the robot. The bottom of the bar indicates the inertia for the exoskeleton when set up for the smallest arm, and the top of the bar is for the largest arm. The exoskeleton can be adjusted anywhere in between this range. The dashed lines in the plots indicate the estimated inertia of a limb size-matched to the minimum and maximum size of Planar MEDARM.

It is clear that except for the wrist joint in *system a*, the inertia of the robot is similar to the inertia of the human limb. After reducing the gear ratio of the system and changing the cable routing structure, the apparent wrist inertia dropped dramatically. In *systems c and d*, both the elbow and wrist joint inertias lie within the lowest range of the human limb. In the worst case, for the smallest person,

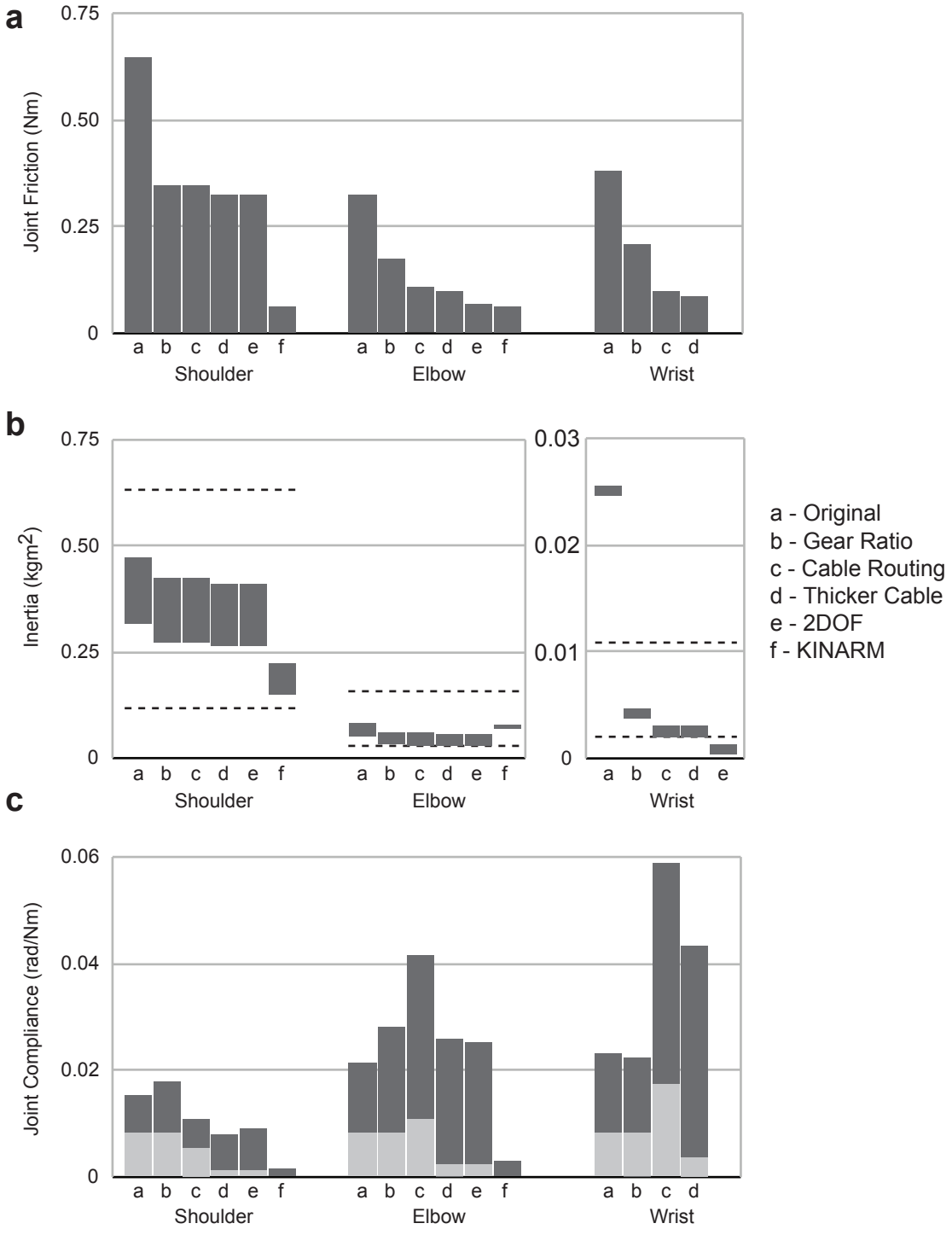

Figure 6.5: Overall (a) joint friction (±0.05 Nm), (b) inertia as seen by the joints (±1%), and (c) compliance at the joints (±9%) for all variants of the prototype. In (b), the dashed lines represent the minimum and maximum inertia of the human arm. The bottom and top of the bars indicate the estimated inertia of the exoskeleton when set up for the smallest and largest arms, respectively. In (c), the total height of the bars indicate the total measured compliance of the exoskeleton. The light portion of the bars indicate the estimated contribution of the cables to the measured compliance.

the inertia of the robot is roughly equal to the inertia of their limb at the elbow and wrist. However, the shoulder joint inertia is relatively higher than the elbow and wrist compared with the human limb, and the changes had little effect. This is a result of the heavy carriage used in the curved track mechanism. The shoulder inertia of Planar MEDARM is higher than KINARM, while its elbow inertia is marginally less.

In-plane joint compliance is shown in Fig. 6.5c. The total height of the bars is the measured compliance, while the light gray portion indicates the estimated contribution of the cables to the measured compliance. It is clear that changing the gear ratio and cable routing scheme both increased the compliance of Planar MEDARM overall. This occurred because the larger pulley winding up the cables causes more cable length change for a given rotation, and there are fewer cables attached to the elbow and wrist joints.

In *system d*, upgrading to the thicker (and stiffer) cable helped to reduce the compliance, but this reduced only the compliance contributed by the cables themselves. The large proportion of dark gray in the bars for *system d* indicates that the majority of the compliance ($\sim 90\%$) comes from a source other than the cables. One source of compliance is the timing belts, but the major source is the structure of the mechanism itself. There are several points in the system that visibly bend when loads are applied. These structural elements include the main support beam, the wrist joint axis, and the elbow joint axis. The cable compliance in *system d* is less than KINARM's total compliance, so there is potential to reduce the compliance to comparable levels.

One of the advantages of Planar MEDARM's design over KINARM is the support against gravity that the curved track provides. Indeed, the vertical compliance measured for Planar MEDARM is 0.047mm/N whereas for KINARM it is 0.132mm/N. Planar MEDARM is nearly 3 times stiffer than KINARM for out-of-plane motion, despite the fact that Planar MEDARM was measured in its worst configuration (90° elbow), where most of the measured compliance is a result of the elbow axis bending.

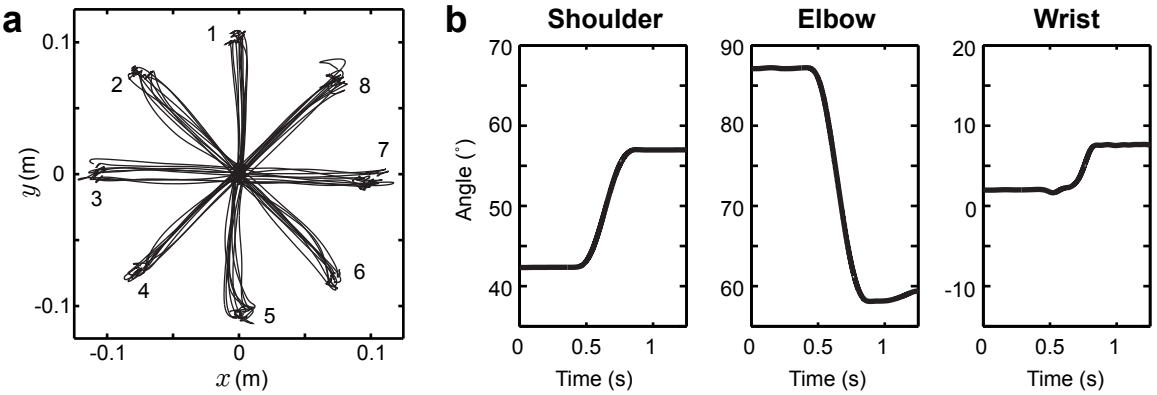

Figure 6.6: Results of a basic reaching experiment using the Planar MEDARM. (a) The hand path traces for all trials are plotted. (b) The joint angle profile for one of the trials to target 1 (see Fig. 6.2).

The reaching task tests were run as a qualitative test (no numerical analysis was performed) to see how users perceived Planar MEDARM during use. It is important that the exoskeleton feel comfortable and natural for the user. The test was performed to make sure that users were able to make smooth reaching movements, which is an indication of whether or not the exoskeleton is unduly influencing motion. When asked about how it feels to use the robot, subjects noted that it was comfortable, but some subjects pointed out that there is an audible noise while moving the shoulder. This noise is generated by the friction between the carriage and the track.

Fig. 6.6a shows the hand path recorded by Planar MEDARM for all ten trials to each of the eight targets for a single subject. As expected from previous reaching experiments, the results exhibit relatively straight trajectories with a certain amount of trial-to-trial variability depending on movement direction [111]. In this context, variability simply refers to the fact that the reaching movements do not follow the same trajectory for each trial. An important concept is that the variability changes with movement direction. Looking at Fig. 6.6a, it is clear that some reaching directions exhibit more variability than others (for example, target 2 exhibits more variability than target 1). Fig. 6.6b shows a sample of the recorded joint motion for a single trial reaching to target 1 (see Fig. 6.2). This confirms that all three joints are indeed

contributing to limb motion.

6.1.4 Suggested Upgrades and Improvements

Planar MEDARM's performance testing has highlighted several areas for improvement. This section explains several suggested upgrades and improvements based on this testing and also based on some general observations from working with the prototype. The majority of ideas relate to the structural design and the actuation system.

Curved Track: The main area for improvement is the curved track itself, which is the main source of friction, inertia and audible noise for the shoulder joint. With an improved implementation, these shortcomings should not be insurmountable. Inertia at the shoulder is a direct result of the mass of both the carriage and the guide pulleys on the driving linkage. With all of this weight displaced far from the centre of rotation, it is not surprising that the inertia is high. Removing one of the carriage's four wheels (the most massive components), using smaller wheels for the remaining three wheels, designing a custom carriage, and using smaller guide pulleys could reduce the shoulder inertia by at least 25% bringing the inertia much closer to proportion with the other joints and with KINARM. This reduction would not affect the other joints. Also, it is important to note that about 40% of the inertia as seen at the shoulder comes from all of the structures and pulleys needed to attach and actuate the wrist joint. Considering that Planar MEDARM was designed specifically to add a wrist joint and to place the support point for the mechanism away from the joint axis, it is a substantial achievement to maintain joint inertia on the same level as KINARM.

While the inertia can easily be reduced, friction at the curved track may be more challenging. Removing one wheel from the carriage will reduce the bearing friction by 25%, but this would reduce the friction at the shoulder by only about 10-15% overall. As indicated by the audible noise, the curved track system does not roll as smoothly as it perhaps could. The track system was designed for heavy-duty industrial use

and the wheel surfaces are flat to help distribute the forces on the track. It may be possible that a custom wheel system with specially contoured wheels would focus the force onto a smaller surface, reducing the friction at the expense of strength. The strength of the present carriage is far above the needs for this application, so this is a realistic compromise.

Elbow Joint: The elbow joint is a significant source of both in-plane and vertical compliance. The elbow joint shaft is clamped to the system only at the base (see Fig. 5.7b in Section 5.3.3). There is little to prevent the entire shaft from bending. It is possible to see the joint bend when forces are applied to the forearm. In fact, the lack of stiffness at the elbow joint also causes up-and-down flexing of the driving linkage. If the elbow joint can be made more stiff, there would be no flexion in the driving linkage. Possible solutions might involve making a wider clamping base mated with a more rigid clamping surface. Also, reducing the overall length of the shaft would be a significant benefit in terms of stiffness as well as inertia. Overall, a stiffened joint and improved sliding clamp is needed.

Wrist Joint: The current wrist joint is stiffened by a clamp added after the initial assembly because the wrist was easily twisted as a result of cable forces and also by applying forces to the handle. Part of the problem is a weak connection to the elbow joint, which itself requires stiffening. However, with the alternate cable routing scheme, the wrist joint requires only one fixed pulley to clamp the two cables, so the joint could be made significantly smaller. This would also make the joint much less susceptible to bending from cable forces, and there would more options for the placement of stiffening elements. Finally, it would be beneficial to add a wrist-locking mechanism, which would allow the device to be easily transformed into a 2DOF system like KINARM.

Forearm: The forearm should include larger adjustment range for the trough than the $\sim$4 cm that is currently provided. In addition, the trough should be closer

to the wrist joint to better secure the limb. A possible solution would be to simply use a longer trough, but this might add unnecessary weight. Also, the telescopic slider adjustment needs to be improved for better durability. The current design runs the risk of binding because an aluminum piece slides along another aluminum piece. Finally, the current clamping system has too many thumbscrews. A fourth thumbscrew was added later on to provide a better stiffness at the wrist. Part of the problem stems from the fact that the wrist joint shaft is not clamped by the forearm. The wrist link itself is clamped to the shaft, and unfortunately, this configuration can easily lead to twisting of the forearm structure. The fourth thumbscrew reduced the twisting significantly, but not completely.

Handle: Currently, the handle is not located in a comfortable position for the user. The handle is attached vertically, which is awkward in some arm configurations (i.e. shoulder and elbow both near 0°). If the handle were angled so that the forearm is more pronated, it would be more comfortable. Other options instead of a handle include a trough or flat plate to rest the hand (no handle to grasp), so that the hand is flat (vertical, horizontal or somewhere in between). The particular task would likely dictate the best attachment, thus a choice of handles and troughs would be ideal.

Pulleys: There is always a desire to decrease the friction in the pulleys because there are so many of them in the system. Each one itself has a small amount of friction, but since each pulley has two bearings and there are many pulleys for each cable, the total pulley friction is significant. The pulleys could be changed to a single bearing system, as long as it does not allow the pulleys to wobble. Also, the pulley flanges should be widened to prevent thick cables from falling off the pulley. Pairs of guide pulleys before the last joint, or before a clamped joint can be replaced with a single pulley of slightly larger thickness (to accommodate two cables). This would reduce both mass and friction. Additionally, a way should be devised to keep the cables properly positioned on the pulleys in all cases. When the motors are off, the

brake keeps the cables on the pulleys, but there is enough slack to allow the cables to slide down to the bottom flange. Perhaps the pulleys could be machined with a grooved surface to encourage the cables to remain in place. During normal use, a parking clamp (manual or automatic) could be added to clamp the cables in place before the motors are turned off, so that there is no slack. This way, the system does not rely entirely on the motor brakes unless there is an emergency stop.

System Height: As already alluded to in previous suggestions, an important design upgrade would be to lower the entire profile of the system. This is easy to achieve with the alternate cable routing scheme since fewer cables and pulleys are needed at each joint, and thus the height of each joint can be reduced. Lowering the profile will reduce the strength requirements of the carriage, making smaller and fewer wheels more than sufficient. A low profile design would be stiffer and lighter.

Drive System: The drive system for Planar MEDARM need not be open-ended cable-drive. For example, the shoulder driving joint could be driven directly, and the elbow and wrist could be driven by an open-ended or closed-loop cable-drive system. This would increase the stiffness by decreasing dependence on the cables. This would also simplify the system, and would require fewer motors and pulleys, which would allow a large reduction in height of the system. In a 2DOF setup, several additional pulleys can be removed, further reducing the weight and size of the exoskeleton.

Transmission System: Currently, the motors are coupled to the gears using a timing belt with a gear ratio of 3, and then the ratio is decreased to 2 using the windup pulleys. This was not the original design because the arrangement was changed during assembly to accommodate larger pulleys and a new cable clamping design. Ideally, this setup should be redesigned to properly accommodate the new gear ratio, and new cable clamp system. This would reduce the inertia of the motor system because several components could be reduced in size. Another option is to have different gear ratios on different motors to offset the uneven force requirements

for the cables of the alternate cable routing scheme. Also, the idler pulleys used to tighten the timing belts are heavy and have relatively high friction, and should be replaced with lower-friction, lightweight alternatives.

Motor Assembly: The attachment of the motor mounts to the exoskeleton is a substantial source of compliance. Currently, the motor assembly is joined to the system by a single piece of aluminum extrusion. When the cables apply force, the motor assembly is pulled towards the driving joint, bending the extrusion. The result is visually obvious, and fortunately, this unwanted bending can easily be remedied by adding support brackets. Similarly, support should be added to prevent the motor assembly from twisting the extrusion. The cable length (and hence compliance) could be reduced by moving the motors as close as possible to the driving joint. Likely, this would mean that some motors would be placed underneath the track.

Secondary Encoder Mounting: The secondary encoders were added to the design after the initial design was completed, and as a result, the mounting fixtures are awkward to work with. Most importantly, they should be more easily adjustable. At the very least, they should be more accessible with more available adjustment. Also, the links should include a built-in channel to route the encoder cables back to the base. This will help to make sure that the cables do not influence joint motion. Finally, the shoulder tape scale is very exposed in the current prototype. Any fingerprints or scratches will disrupt the encoder readings. Therefore, a protective cover should be added to prevent damage from accidental bumps and grabs.

Shoulder Joint Alignment: Another welcome addition would be to add an external indicator of the location of the robot's shoulder joint axis. There is no equipment near the robot's shoulder joint axis, thus it is difficult to align the user's shoulder joint with the robot. A properly aligned bar fitted with a laser pointer could be added above the shoulder joint to indicate on the user's shoulder where the robot's joint centre is located. The bar would be hinged so that it can swing out of the way

when using the exoskeleton.

6.2 Cost Comparison

Another aspect of Planar MEDARM that can be compared with KINARM is cost. Table 6.1 compares estimates of the total parts cost for several possible variations of Planar MEDARM with KINARM. Planar MEDARM as a 3DOF device costs nearly twice as much as KINARM (only 2DOF). The majority of the cost difference comes from the motor system because Planar MEDARM requires four motors and drives whereas KINARM requires only two. Also, Planar MEDARM's optional secondary encoders add significant cost ($2,900). The mechanical components of Planar MEDARM are also more expensive because more parts are required to add the wrist joint. Moreover, the curved track and pulleys are expensive components. The cost difference is expected given the benefits that Planar MEDARM has over KINARM, including a wrist joint and under-the-arm mechanical design.

However, it is more fair to compare a 2DOF version of Planar MEDARM with KINARM. It is estimated that removing all components associated with the wrist joint while maintaining an open-ended cable transmission, will reduce the cost by approximately 20% (see Table 6.1). However, this is still not an ideal comparison. As suggested earlier, it would be more practical to operate a 2DOF version of Planar

Table 6.1: A comparison of the estimated parts costs for several variations of Planar MEDARM and KINARM.

Parts	**Planar MEDARM Cost**			**KINARM**
	3DOF	**2DOF***	**2DOF†**	**Cost**
Motion Control	$18,500	$14,200	$8,800	$8,800
Electrical	$1,950	$1,750	$1,500	$1,500
Mechanical	$6,650	$5,600	$4,500	$3,500
Total	**$27,100**	**$21,550**	**$14,800**	**$13,800**

* 2DOF, driven by open-ended cable drive, 3 motors.

† 2DOF, 2 motors, no secondary encoders, similar to KINARM.

MEDARM using a more direct approach. If the shoulder is driven directly, and the elbow is driven by a closed-loop cable, only two motors are required. In this case, Planar MEDARM and KINARM are of comparable cost because the motor and electronic systems are identical, and the only differences arise from the mechanical components. This 7% difference is a small cost difference given that this version of Planar MEDARM offers the advantage of placing all of the equipment underneath the user's arm.

6.3 Rehabilitation Applications

In addition to testing the performance of Planar MEDARM, some basic rehabilitation strategies were implemented. This section briefly introduces these strategies, and discusses in particular how Planar MEDARM functions using these strategies.

6.3.1 Resistive Exercise

In Section 2.2.2, it was mentioned that progressive-resistive exercise is an important aspect of the rehabilitation process. Virtual reality environments may also require the ability to apply resistive loads to the joints or end-point of the robot to simulate moving through materials of different viscosity. Thus, a rehabilitation robot should be able to apply a wide range of resistive loads. Resistive loads are simple loads that oppose motion with a magnitude proportional to the velocity of the motion. For example, a resistive torque, τ_i can be applied to joint i with the form:

$$\tau_i = -b_i\dot{\theta}_i \tag{6.1}$$

where $\dot{\theta}_i$ is the joint velocity, and b_i is the resistive load gain. The same idea can be applied to resistive end-point loads in which the resistive forces are applied in Cartesian space to the end-effector.

Robots tend to become unstable when resistive forces exceed a certain magnitude because the velocity signal used to calculate the resistive load is not perfectly

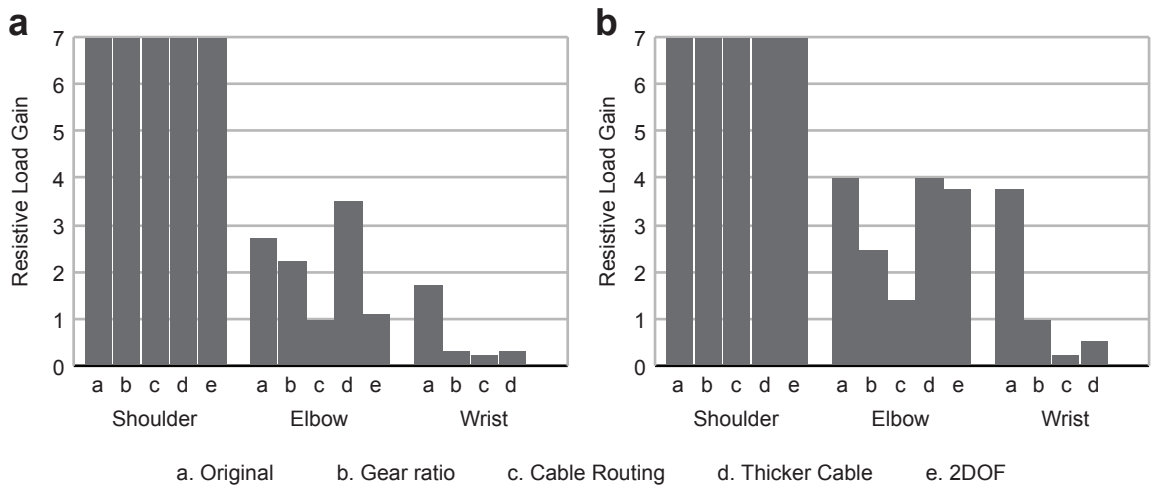

Figure 6.7: The maximum stable joint-based resistive load gains when using joint velocity as calculated from (a) motor encoders and (b) secondary encoders.

smooth. Flexibility in the system (in-plane or out-of-plane) also causes fluctuations in the velocity signal. Increasing the resistive load amplifies these issues, and ultimately can cause unstable oscillatory motion. In general friction in the system can help to dampen any oscillations. Therefore, robots with low friction such as Planar MEDARM and KINARM are usually limited in the amount of resistive loading that can be applied. With this in mind, some simple tests were performed to obtain an idea of the resistive loading capabilities of Planar MEDARM.

Joint-based resistive loading was tested first. The test involved applying a resistive load to each joint, one at a time, while moving the robot around the entire workspace using both smooth and abrupt movements. The highest resistive load gain that could be applied without causing any instability was recorded. Instability involved oscillatory motion of the motors, and would typically first manifest as tiny vibrations which could be felt at the robot's handle.

The results of this test are shown in Fig. 6.7. Tests were performed using velocity as measured by two different means: the motor encoders (Fig. 6.7a), and the secondary encoders (Fig. 6.7b). The tests were repeated for each variation of Planar MEDARM. Planar MEDARM was adjusted to its 50^{th} percentile length for all tests.

The first note to make is that using the secondary encoders allowed equal or higher resistive loading for all cases. This is expected because the high-resolution secondary encoders allow a smoother (less noisy) measure of velocity than the motor encoders. Another expected trend that is readily apparent is that the maximum resistive loading gain decreases for consecutive configurations changes: *systems a-c*. This coincides with the reduction in friction at the joints seen in Fig. 6.5a. This reduction in resistive loading capability is particularly noticeable at the wrist joint, because the wrist joint friction was reduced substantially. In addition, the shoulder joint exhibits enough friction that the maximum torque limits of the motors were reached before instability was apparent. A final note is that the maximum resistive load increased substantially for *system d*. The thicker cable increased the stiffness of the system, making it more difficult to excite oscillatory motion.

A similar test was performed for end-point resistive loads. Instead of applying joint torques proportional to joint velocity, end-point forces were applied to oppose end-point velocity. The same procedure was applied independently for x and y directions, as well as for the overall orientation of the end-effector (hand orientation). The results depend highly on the location of the end-point in the workspace, and it was easier to cause instability in some locations than others. This dependance on the end-point location relates back to the dynamic manipulability of the system as discussed in Section 5.4.3. As such, the recorded number reflects the highest resistive load gain that will not cause instability for the entire workspace. For certain positions, the maximum stable gain was substantially higher, but this level of loading caused instability in other locations. The test was performed only with *system d*.

Fig. 6.8 compares end-point resistive loads with and without velocity signal filtering. A second order Butterworth filter with a cutoff of 10Hz was applied to smooth out the velocity signals to see how much effect it had on the maximum resistive load gain. It is clear from Fig. 6.8a that without filtering, the secondary encoders out-

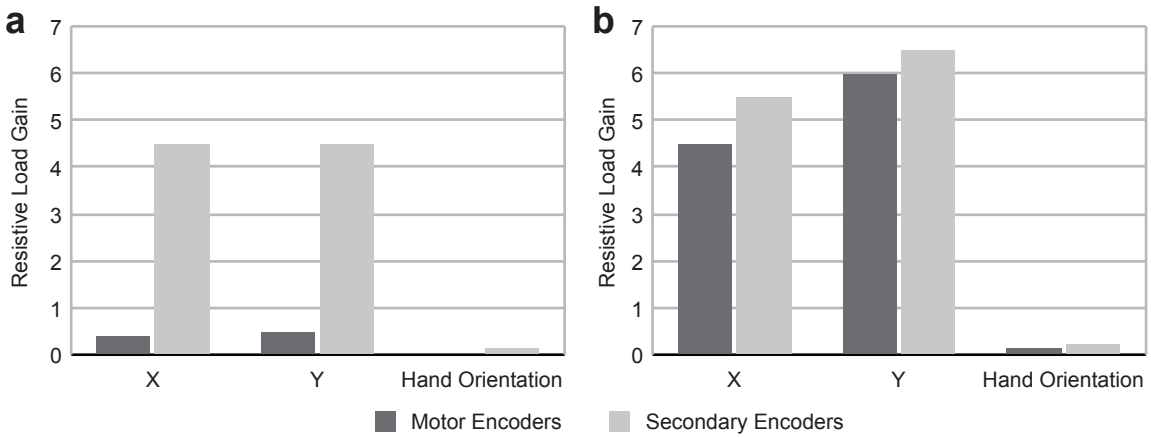

Figure 6.8: The maximum stable end-point based resistive load gains when using end-point velocity with filtering (a) disabled and (b) enabled. In (b), the velocity signals were filtered using a 2nd order Butterworth filter with a 10Hz cutoff.

perform the motor encoders. This is due to the resolution difference between the encoders. The difference between the two cases decreased with the addition of the filter (see Fig. 6.8b), although the secondary encoders still allowed a higher gain.

This testing has shown that the secondary encoders help to improve the ability to provide higher resistive loads. This capability will help to provide a broader range of virtual environments. It is clear from these results that it would be beneficial to stiffen the system. With a stiffer system, it would be more difficult to excite oscillatory motion and cause instability. However, the cost of these encoders is about $1,000 each, thus it is an expensive addition.

6.3.2 Assistive Trajectory Tracking

Another application for rehabilitation is to provide motion assistance. An assistive trajectory tracking algorithm based on previous work [45, 46], has been implemented without the need for force sensing. The basic algorithm discourages motion perpendicular to the desired trajectory. Forward movement can be unaffected or assisted by a force, while backward motion is discouraged. A channel is defined around the trajectory within which no forces are applied. This gives the user a chance to make

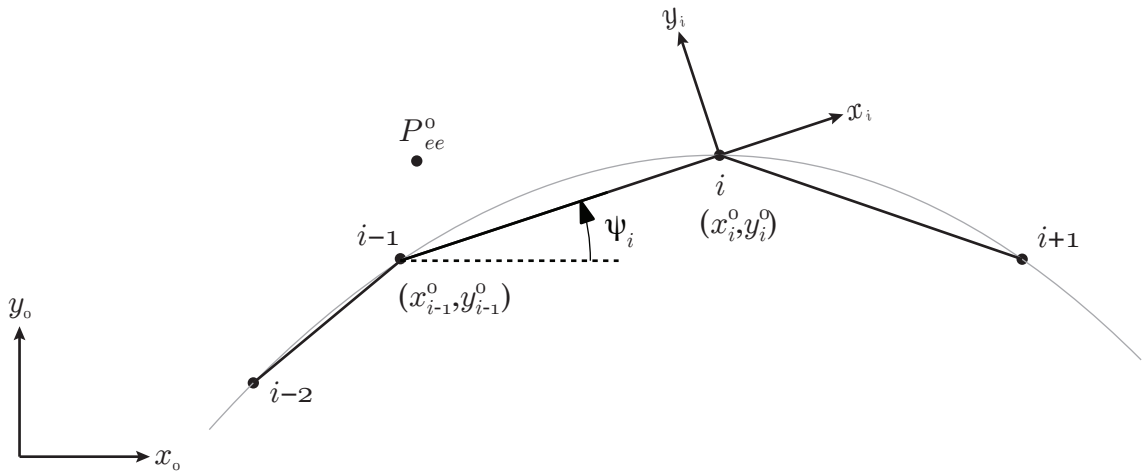

Figure 6.9: The assistive algorithm is designed to encourage the end-point of the robot, P^0_{ee}, along a trajectory. The trajectory is divided into a series of points joined by linear segments. The algorithm relates the end-point of the robot, P^0_{ee}, to one of these segments, and determines when to apply forces. Each segment has its own reference frame associated with it, which are related to the fixed reference frame 0 by a rotation and a distance.

the movement themselves without any interference from the robot.

The system operates based on creating linear movement channels between points along a trajectory. As a point is reached, the next point becomes the new frame of reference, and so on. As the points get closer together, approaching a continuous trajectory, the channel segments become shorter, and the channel itself effectively becomes continuous. The proposed algorithm was designed such that it will function the same way even when the points are separated by large distances. Assuming a linear trajectory between points, a force prevents movement backwards from the current position along the trajectory. The following provides the mathematical details of this algorithm. The proposed algorithm is described for the two-dimensional case, but it could be extended to work for a three-dimensional trajectory.

Consider a series of points along a trajectory as shown in Fig. 6.9. These points are defined in terms of the base reference frame 0. In Fig. 6.9, the end-point of the robot position, P^0_{ee}, has just passed in front of trajectory point $i-1$. The goal of the algorithm now is to assist the end-point of the robot towards trajectory point i.

The first step is to define all information in terms of the target trajectory point reference frame i. Point i is the origin of frame i, which has a position relative to the base frame given by x_i^0 and y_i^0. The current linear trajectory segment (joining points $i-1$ and i) defines the x_i axis where forward is positive, and the y_i axis is perpendicular to x_i as shown in Fig. 6.9. The current trajectory segment is rotated relative to the base frame by angle ψ:

$$\psi = \arctan\left(\frac{y_i^0 - y_{i-1}^0}{x_i^0 - x_{i-1}^0}\right) \tag{6.2}$$

The coordinates of P_{ee}^0 can be transformed to the new frame by a rotation:

$$P_{ee}^i = \begin{bmatrix} x_{ee}^i \\ y_{ee}^i \end{bmatrix} = \begin{bmatrix} \cos\psi_i & \sin\psi_i \\ -\sin\psi_i & \cos\psi_i \end{bmatrix} \begin{bmatrix} x_{ee}^0 - x_i^0 \\ y_{ee}^0 - y_i^0 \end{bmatrix} \tag{6.3}$$

Note that x_{ee}^i is always negative until it passes the trajectory point i. Also, note that y_{ee}^i is a direct measure of the distance the end-point of the robot is away from the desired trajectory. As soon as $x_{ee}^i > 0$, the trajectory point $i+1$ becomes the new target point, and thus the next segment becomes the current segment and the system must be redefined in terms of frame $i+1$. While $x_{ee}^i < 0$, it is possible to implement some virtual boundaries to discourage movement away from the desired trajectory.

Fig. 6.10 shows a close up view of the current segment. A channel is defined around the segment, as shown by the light gray shading. The end-point of the robot is free to move within this boundary. In the y_i direction, the channel has a fixed width of $2\epsilon_y$. If $y_{ee}^i > \epsilon_y$ or $y_{ee}^i < -\epsilon_y$, a force, f_y^i, will be applied to the robot in the y_i direction to push the end-point back into the channel.

The x_i direction boundary works in a similar way, but the boundary is not fixed. The boundary line is always a distance of ϵ_x behind the largest x_i distance reached by the end-point of the robot, x_{max}^i. As the end-point moves forward, x_{max}^i is updated to the current x_{ee}^i position. If the end-point moves backwards, x_{max}^i remains fixed. If the end-point moves more than ϵ_x behind x_{max}^i, a force, f_x^i, is applied to the robot in the x_i direction to push it back into the channel. Thus, the channel has constant

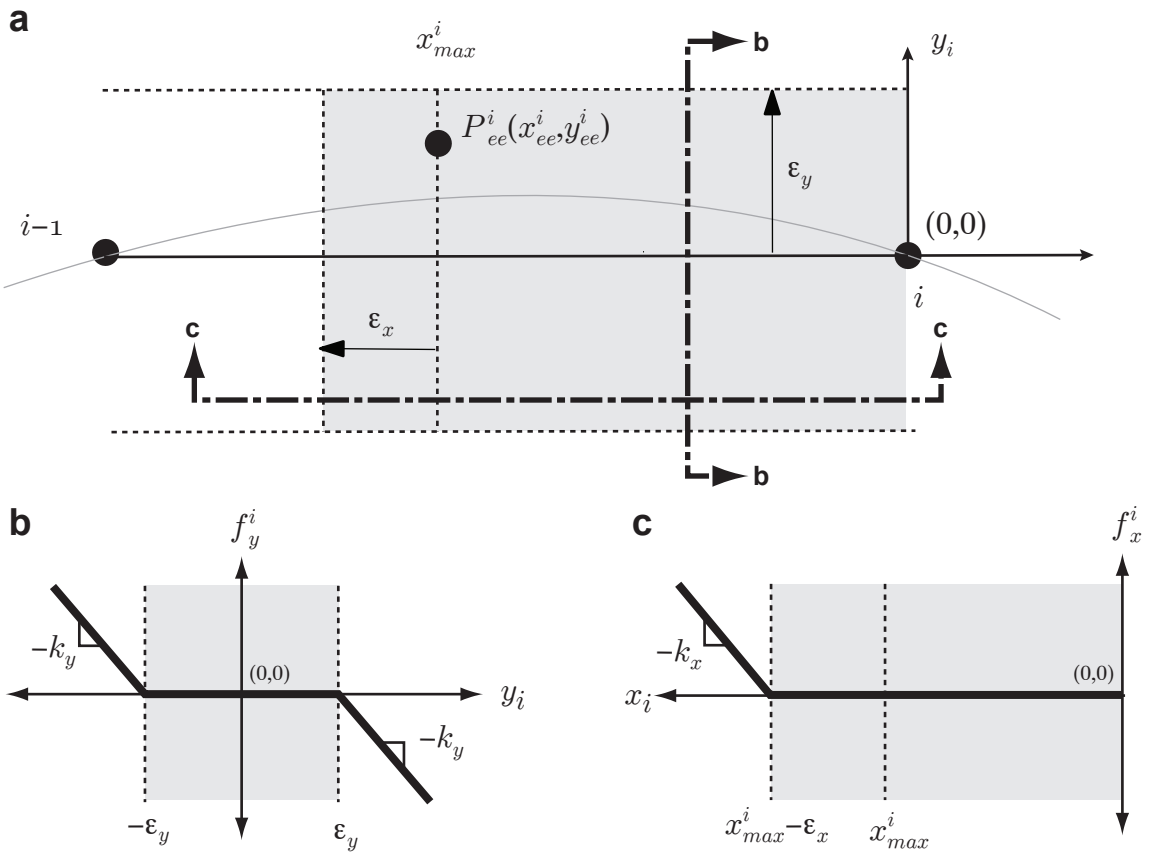

Figure 6.10: (a) A schematic diagram showing the notation for a single segment of the trajectory. All variables in this figure are defined in the i^{th} frame. The end-point of the robot, P^i_{ee}, is free to move within the channel (highlighted in light gray). The sides of the channel are fixed, while the back of the channel is continuously updated to match any movement made towards point i. (b) The force profile for motion in the y_i direction, as indicated by the section line "bb" in (a). (c) The force profile for motion in the x_i direction, as indicated by the section line "cc" in (a).

width, but shrinks in length as the user makes progress along the trajectory. Defining the channel in this manner gives the user a chance to stay in place without any forces.

The last step to the algorithm requires a transformation of the channels forces, f^i_x and f^i_y, to the base frame 0. The resulting forces, f^0_x and f^0_y, can then be applied to the robot. The transformation is simply the reverse of the rotation used in (6.3).

$$\begin{bmatrix} f^0_x \\ f^0_y \end{bmatrix} = \begin{bmatrix} \cos\psi_i & -\sin\psi_i \\ \sin\psi_i & \cos\psi_i \end{bmatrix} \begin{bmatrix} f^i_x \\ f^i_y \end{bmatrix} \tag{6.4}$$

There are many options for the channel forces, although a particularly simple and useful choice is spring force. This way, by changing the spring constant, the stiffness

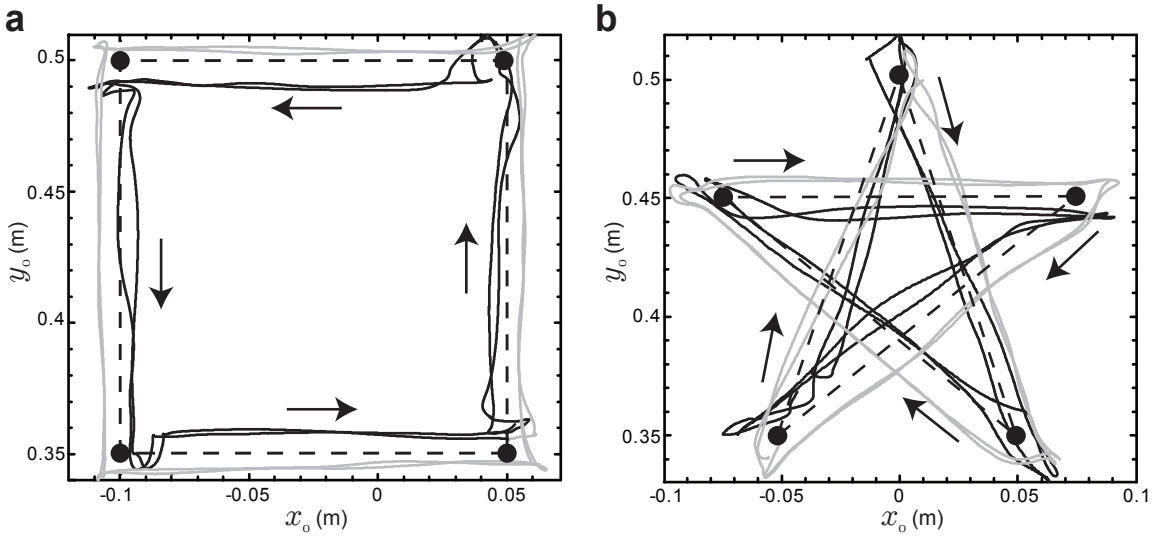

Figure 6.11: End-point position of Planar MEDARM as it moves through a channel defined by (a) four points of a square, and (b) five points of a star. The origin is defined as the shoulder joint centre. The channel width was defined to be $\epsilon_y = \epsilon_x = 0.01$m, and the spring constants of the wall were defined as $k_y = k_x = 400$N/m. The black and grey lines trace each of the channels walls as the end-point of Planar MEDARM was gently pressed up against the wall. The black circles indicate the trajectory points. The dashed line indicates the centre of the channel, and the arrow illustrate the direction of motion along each segment.

of the boundary can be changed. To apply a spring force when moving outside of the channel in the y_i direction, the applied force is:

$$f_y^i = \begin{cases} -k_y(y_{ee}^i - \epsilon_y), & y_{ee}^i > \epsilon_y \\ 0, & -\epsilon_y \leq y_{ee}^i \leq \epsilon \\ -k_y(y_{ee}^i + \epsilon_y), & y_{ee}^i < -\epsilon_y \end{cases} \tag{6.5}$$

Equation (6.5) is illustrated in Fig. 6.10b by a force profile in the y_i direction. Similarly, a spring force can be applied when moving backwards in the x_i direction:

$$f_x^i = \begin{cases} 0, & x_{ee}^i \geq (x_{max}^i - \epsilon_x) \\ -k_x(x_{ee}^i - x_{max}^i + \epsilon_x), & x_{ee}^i < (x_{max}^i - \epsilon_x) \end{cases} \tag{6.6}$$

Equation (6.6) is illustrated in Fig. 6.10b by a force profile in the x_i direction.

Additionally, a force may be applied in the x_i direction to assist the movement. In the simplest case, a constant force could be applied when $x_{ee}^i > (x_{max}^i - \epsilon_x)$. Another option would be to encourage the user to move within a velocity range along the track. If the end-point was moving too slowly, a force would be applied to speed the user up, and vice versa.

A sample recording of motion within two different channels is presented in Fig. 6.11. Fig. 6.11a shows a square trajectory defined by four points (black circles), and Fig. 6.11b shows a star trajectory defined by five points. The channel width was defined to be $\epsilon_y = \epsilon_x = 0.01$m, and the spring constants of the wall were defined as $k_y = k_x = 400$N/m. The centre of the channel is indicated by the dashed line, and the arrow illustrates the direction of motion.

The traces in Fig. 6.11 show the end-point of Planar MEDARM as the handle is gently pressed against the channel wall. The results show that the total channel width is approximately 0.02m as expected. As evident from the curved lines, it is quite a challenge to say outside the channel. It is difficult to maintain a constant force while moving in the correct direction, because the force constantly tries to push the end-point back into the channel. The fundamental goal of the algorithm is to prevent users from leaving the channel, therefore these results are an indication that the algorithm functions as desired.

Chapter 7: Conclusions and Future Work

7.1 Project Overview

This project began with the idea to design a rehabilitation robot that provides more complete control for the shoulder complex. The focus was to incorporate motion of the shoulder girdle because this part of the shoulder complex has been poorly addressed in previous devices. MEDARM was designed to overcome this shortcoming, providing independent control of the five major DOF of the shoulder. A key aspect of the design process was to find a way to couple the robotic exoskeleton to the sternoclavicular joint of the user without placing equipment in front or above the user's head. A novel mechanical design based on a curved track emerged from MEDARM's design process to solve this issue and enables the mechanism to drive a limb joint without requiring any equipment along the axis of rotation. Additionally, a method was developed to design a spherical joint for the glenohumeral joint so that singularities and collisions are avoided and manipulability is maximized. The technique provides a visually intuitive way to design the joint while ensuring that the design criteria are satisfied.

The curved track mechanism is actuated by a cable-drive transmission, and this combined system required testing in a more controlled way before implementing MEDARM's ambitious design. Therefore, a planar version of MEDARM called Planar MEDARM was designed to evaluate the performance of the new mechanism. Planar MEDARM was also designed to test out the feasibility of applying the new design to KINARM to remove the need to place equipment along the shoulder joint axis, and to provide a simple means of adding a wrist joint to the planar system. A complete prototype of Planar MEDARM was fully assembled, and its performance was analyzed and compared with KINARM.

The results of the performance evaluation indicate that Planar MEDARM performs as well as KINARM in most respects. Overall, the friction and inertia of Planar MEDARM closely match KINARM. While Planar MEDARM's shoulder joint currently exhibits notably higher friction and inertia, modifications to the curved track have been proposed to reduce friction and inertia to levels similar to KINARM. Measurements of joint compliance show that the structure of Planar MEDARM is the major source of compliance. The cable compliance is less than KINARM's compliance, thus there is potential to reduce compliance to comparable levels by stiffening the structure. Furthermore, the vertical compliance of Planar MEDARM is close to 3 times less than KINARM, which is a direct result of the additional support provided by the curved track.

A standard reaching experiment has shown that users can make reaching movements with Planar MEDARM without any significant adverse effects on the natural movements. The secondary encoders built into Planar MEDARM provide direct measurement of joint kinematics, and improve the ability to implement stable resistive exercise algorithms for both joint-based and end-point based movements. Additionally, the use of an assistive trajectory tracking algorithm has shown that Planar MEDARM is capable of providing motion assistance and guidance.

Planar MEDARM compares favourably with KINARM despite the added functionality and new mechanical design ideas. The new design allows all equipment to be placed underneath the user's arm, which is invaluable from a clinical perspective because it is more comfortable for patients and it provides better access to the limb by the clinician. Also, an actuated wrist joint has been included in the design. A wrist joint cannot be easily added to the current KINARM design without adversely affecting the robot's inertia. The Planar MEDARM prototype has successfully demonstrated the benefits of MEDARM's design, and has also shown its applicability to extending the functionality of KINARM.

7.2 Future Directions

As described in Section 6.1.4, the performance assessment of Planar MEDARM led to a number of suggestions for improvement for future prototypes. As a first step, these improvements should be implemented in a second prototype. However, before building the entire prototype, it would be useful to build just the curved track mechanism with the specific intent to reduce friction and inertia as much as possible. This process might require several iterations. Once it is confirmed that the friction can be reduced in a satisfactory manner, the rest of the second prototype should be assembled based on the list of suggestions. The results of the second prototype will determine whether or not KINARM should pursue this new design.

Planar MEDARM was only one aspect of this project - the ultimate goal is to build MEDARM. Therefore, as a second step, MEDARM's design should be iterated to incorporate the lessons learned from the Planar MEDARM project. Most of the suggestions from Section 6.1.4, are also relevant to MEDARM, and its design could certainly be improved by incorporating these ideas. Furthermore, the practical experience gained from the first and second prototypes will help to fine-tune MEDARM's design substantially before building the full device.

Several additional important thoughts should be kept in mind while iterating the MEDARM design, including the following:

- **Vertical Support Cable:** It would be beneficial to remove the need for the vertical cable supporting the curved track. To accomplish this, the weight of the track and carriage would have to be substantially reduced. Alternatively, the motor for joint 1 would have to be larger. Better counterbalancing about joint 1 axis could be used to offset the weight of the track, but this would increase inertia. One possible solution is the use of a passive spring-based system to achieve static equilibrium at MEDARM's zero configuration to counteract the gravitational load on the joint.

- **Link Sliders and Adjustment:** There is potential for simplification of the sliders used to position the cuffs along the exoskeleton. Currently, the design incorporates a T-channel in the main link, but this can be difficult to machine properly. Also, to avoid binding, the sliders should be modified to avoid aluminum pieces sliding over other aluminum pieces.
- **Joint Width:** It is important to reduce the overall size of the joints as much as possible to keep the device more streamlined and sturdy. With wide joints, the cable forces will be more likely to bend the joints, increasing compliance. Steps have been taken throughout the initial design phase to minimize this, but it is still likely to be a source of compliance. It is also important to make joint 5 as narrow and small as possible, as a large joint has the possibility of getting close to the head during motions involving full combined elevation and abduction.
- **Actuation System:** After implementing the design changes, there will be a need to optimize several components of the actuation system to account for these changes. Some aspects of the design which will have to be re-addressed include: motor sizes, gear ratios, pulley size (windup, guiding and driving), and cable size. The gear ratios, cable thicknesses, and pulley sizes need not be all equal for all joints/cables.

With all of these suggestions implemented in MEDARM's design, the third step should be to build a first prototype of MEDARM. As before, a full battery of tests should be carried out to evaluate the robot's performance.

In addition to improving the mechanical designs of the robots, there are a number of other aspects of this project that should be considered in the future. The first is dynamic modeling and control. In this thesis, a dynamic model based on estimates of dynamic parameters from CAD drawings was used to assist with several design choices. While sufficient for the design process, these estimates are not accurate enough to implement advanced model-based control algorithms. Therefore it will be

necessary to perform accurate dynamic calibration. However, the robots presented in this thesis are adjustable in many ways, and the calibration would be different for each subject. Thus it would be useful to develop a means of re-calibrating the system each time the exoskeleton is adjusted for a new subject.

Another way to widen the scope of this project is to perform field testing of the device. Pilot projects should be carried out to determine the effectiveness of the device from both patient and clinician perspectives. Potential patient groups for the initial phase of research should include stroke assessment and/or therapy. Another possible avenue for research might be basic sensorimotor research with healthy subjects. Once in use, there will undoubtedly be aspects of the system that could be improved, and this type of feedback is invaluable to the future of these robots.

7.3 Final Words

The Planar MEDARM prototype has already provided invaluable insight into the future development of KINARM, and it is clear that these results will have a significant influence on MEDARM's final design. The innovative designs and techniques developed during this project are important contributions to the robotic rehabilitation and assessment fields.

Although robotic technology should never replace a physiotherapist, advances in the technology will lead to an arsenal of new and powerful tools that enable therapists to provide patients with better care. The ultimate goal is to increase the quality of life of these patients, which in the end, is what matters most.

Bibliography

[1] Heart and Stroke Foundation of Canada. Stroke statistics, `http://www.heartandstroke.ca`, 2008.

[2] R. Teasell, N. Bayona, and J. Heitzner. Stroke rehabiliation evidence-based review: Clinical consequences of stroke. Monograph on the Internet, 2003.

[3] V. M. Zatsiorsky. *Kinematics of human motion*. Human Kinetics, Champaign, IL, 1st edition, 1998.

[4] M. C. Cirstea and M. F. Levin. Compensatory strategies for reaching in stroke. *Brain*, 123(5):940–953, 2000.

[5] S. H. Scott. Apparatus for measuring and perturbing shoulder and elbow joint positions and torques during reaching. *Journal of Neuroscience Methods*, 89(2):119–127, 1999.

[6] S. J. Ball, I. E. Brown, and S. H. Scott. Robotic exoskeleton for limb movement. Patent Application, 1 May 2007.

[7] P. W. McClure, L. A. Michener, B. J. Sennett, and A. R. Karduna. Direct 3-dimensional measurement of scapular kinematics during dynamic movements in vivo. *Journal of Shoulder and Elbow Surgery*, 10(3):269–277, 2001.

[8] M. A. Buckley, A. Yardley, G. R. Johnson, and D. A. Carus. Dynamics of the upper limb during performance of the tasks of everyday living–a review of the current knowledge base. *Proc. Institution of Mechanical Engineers Part H*, 210(4):241–247, 1996.

[9] J. Lenarcic, M. M. Stanisic, and V. Parenti-Castelli. Kinematic design of a humanoid robotic shoulder complex. In *Proc. IEEE International Conference on Robotics and Automation (ICRA'00)*, volume 1, pages 27–32, San Francisco, U.S.A., April 2000.

[10] S. G. Doody, L. Freedman, and J. C. Waterland. Shoulder movements during abduction in the scapular plane. *Archives of Physical Medicine and Rehabilitation*, 51(10):595–604, 1970.

[11] J. Rosen, J.C. Perry, N. Manning, S. Burns, and B. Hannaford. The human arm kinematics and dynamics during daily activities - toward a 7 DOF upper limb powered exoskeleton. In *Proc. 12th International Conference on Advanced Robotics (ICAR'05)*, pages 532–539, Seattle, U.S.A., July 2005.

[12] N. Klopcar and J. Lenarcic. Biomechanical considerations on the design of a humanoid shoulder girdle. In *Proc. IEEE/ASME International Conference on Advanced Intelligent Mechatronics (AIM'01)*, volume 1, pages 255–259, Corno, Italy, July 2001.

[13] V. H. Frankel and M. Nordin. *Basic biomechanics of the skeletal system*. Lea and Febiger, U.S.A., 1st edition, 1980.

[14] H. P. Van Cott and R. G. Kinkade. *Human Engineering Guide to Equipment Design*. McGraw-Hill, Washington D.C., U.S.A., revised edition, 1972.

[15] D. A. Winter. *Biomechanics and Motor Control of Human Movement*. John Wiley & Sons, Inc., New York, U.S.A, 2nd edition, 1990.

[16] C. Gowland, S. VanHullenaar, W. Torresin, J. Moreland, B. Vanspall, S. Barrecca, M. Ward, M. Huijbregts, P. Stratford, and R. Barclay-Goddard. *Chedoke-McMaster Stroke Assessment: Development, Validation and Administration Manual*. Chedoke-McMaster Hospitals, Hamilton, Ontario, Canada, 1995.

[17] D. J. Gladstone, C. J. Danells, and S. E. Black. The Fugl-Meyer assessment of motor recovery after stroke: a critical review of its measurement properties. *Neurorehabilitation and Neural Repair*, 16(3):232–240, 2002.

[18] M. Ferraro, J. H. Demaio, J. Krol, C. Trudell, K. Rannekleiv, L. Edelstein, P. Christos, M. Aisen, J. England, S. Fasoli, H. I. Krebs, N. Hogan, and B. T.

Volpe. Assessing the motor status score: a scale for the evaluation of upper limb motor outcomes in patients after stroke. *Neurorehabilitation and Neural Repair*, 16(3):283–289, 2002.

[19] P. S. Lum, C. G. Burgar, P. C. Shor, M. Majmundar, and H. F. Machiel Van der Loos. Robot-assisted movement training compared with conventional therapy techniques for the rehabilitation of upper-limb motor function after stroke. *Archives of Physical Medicine and Rehabilitation*, 83(7):952–959, 2002.

[20] S. Hesse, H. Schmidt, C. Werner, and A. Bardeleben. Upper and lower extremity robotic devices for rehabilitation and for studying motor control. *Current Opinion in Neurology*, 16(6):705–710, 2003.

[21] D. J. Reinkensmeyer, J. L. Emken, and S. C. Cramer. Robotics, motor learning, and neurologic recovery. *Annual Review of Biomedical Engineering*, 6:497–525, 2004.

[22] H. I. Krebs, B. T. Volpe, M. L. Aisen, and N. Hogan. Increasing productivity and quality of care: robot-aided neuro-rehabilitation. *Journal of Rehabilitation Research and Development*, 37(6):639–652, 2000.

[23] M. A. Smith, J. Brandt, and R. Shadmehr. Motor disorder in huntington's disease begins as a dysfunction in error feedback control. *Nature*, 403(6769):544–549, 2000.

[24] M. Demmer, W. S. Selbie, S. Bagg, and S. H. Scott. Quantitative assessment of arm movements in chronic stroke patients using KINARM. In *31st Annual Meeting of the Society for Neuroscience*, number 71.9, New Orleans, U.S.A., November 2003.

[25] S. Dukelow, K. D. Moore, J. S. Swaine, S. Bagg, K. Norman, and S. H. Scott. Robotic analysis of limb position sense following stroke. In *67th Annual Assembly of American Academy of Physical Medicine and Rehabilitation*, Honolulu, U.S.A., November 2006.

[26] R. Riener, T. Nef, and G. Colombo. Robot-aided neurorehabilitation of the upper extremities. *Medical and Biological Engineering and Computing*, 43(1):2–10, 2005.

[27] B. H. Dobkin. Strategies for stroke rehabilitation. *Lancet Neurology*, 3(9):528–536, 2004.

[28] S. E. Fasoli, H. I. Krebs, J. Stein, W. R. Frontera, and N. Hogan. Effects of robotic therapy on motor impairment and recovery in chronic stroke. *Archives of Physical Medicine and Rehabilitation*, 84(4):477–482, 2003.

[29] J. H. Cauraugh and J. J. Summers. Neural plasticity and bilateral movements: A rehabilitation approach for chronic stroke. *Progress in Neurobiology*, 75(5):309–320, 2005.

[30] S. M. Michaelsen, R. Dannenbaum, and M. F. Levin. Task-specific training with trunk restraint on arm recovery in stroke: randomized control trial. *Stroke*, 37(1):186–192, 2006.

[31] B. T. Volpe, H. I. Krebs, and N. Hogan. Is robot-aided sensorimotor training in stroke rehabilitation a realistic option? *Current Opinion in Neurology*, 14(6):745–752, 2001.

[32] R. Teasell, N. Foley, J. Jutai, T. Doherty, J. Bitensky, S. Bhogal, and M. Speechley. Stroke rehabiliation evidence-based review: Upper extremity interventions. Monograph on the Internet, 2003.

[33] B. T. Volpe, H. I. Krebs, N. Hogan, L. Edelsteinn, C. M. Diels, and M. L. Aisen. Robot training enhanced motor outcome in patients with stroke maintained over 3 years. *Neurology*, 53(8):1874–1876, 1999.

[34] H. Woldag, G. Waldmann, G. Heuschkel, and H. Hummelsheim. Is the repetitive training of complex hand and arm movements beneficial for motor recovery in stroke patients? *Clinical Rehabilitation*, 17(7):723–730, 2003.

[35] P. S. Lum, C. G. Burgar, and P. C. Shor. Use of the MIME robotic system to retrain multijoint reaching in post-stroke hemiparesis: why some movement patterns work better than others. In *Proc. IEEE International Conference on Engineering in Medicine and Biology Society (EMBC'03)*, volume 2, pages 1475–1478, Cancun, Mexico, September 2003.

[36] E. Taub, G. Uswatte, and R. Pidikiti. Constraint-induced movement therapy: a new family of techniques with broad application to physical rehabilitation–a clinical review. *Journal of Rehabilitation Research and Development*, 36(3):237–251, 1999.

[37] T. M. Sukal, M. D. Ellis, and J. P. A. Dewald. Dynamic characterization of upper limb discoordination following hemiparetic stroke. In *Proc. IEEE International Conference on Rehabilitation Robotics (ICORR'05)*, pages 519–521, Chicago, U.S.A., June 2005.

[38] M. P. Dijkers, P. C. deBear, R. F. Erlandson, K. Kristy, D. M. Geer, and A. Nichols. Patient and staff acceptance of robotic technology in occupational therapy: a pilot study. *Journal of Rehabilitation Research and Development*, 28(2):33–44, 1991.

[39] D. K. Rose and C. J. Winstein. The co-ordination of bimanual rapid aiming movements following stroke. *Clinical Rehabilitation*, 19(4):452–462, 2005.

[40] M. L. Harris-Love, W. S. McCombe, and J. Whitall. Exploiting interlimb coupling to improve paretic arm reaching performance in people with chronic stroke. *Archives of Physical Medicine and Rehabilitation*, 86(11):2131–2137, 2005.

[41] G. T. Thielman, C. M. Dean, and A. M. Gentile. Rehabilitation of reaching after stroke: task-related training versus progressive resistive exercise. *Archives of Physical Medicine and Rehabilitation*, 85(10):1613–1618, 2004.

[42] N. F. Taylor, K. J. Dodd, and D. L. Damiano. Progressive resistance exer-

cise in physical therapy: a summary of systematic reviews. *Physical Therapy*, 85(11):1208–1223, 2005.

[43] F. A. Mussa-Ivaldi and J.L. Patton. Robots can teach people how to move their arm. In *Proc. IEEE International Conference on Robotics and Automation (ICRA'00)*, volume 1, pages 300–305, San Francisco, U.S.A., April 2000.

[44] E. Taub, P. S. Lum, P. Hardin, V. W. Mark, and G. Uswatte. Autocite: automated delivery of ci therapy with reduced effort by therapists. *Stroke*, 36(6):1301–1304, 2005.

[45] R. Loureiro, F. Amirabdollahian, M. Topping, B. Driessen, and W. Harwin. Upper limb robot mediated stroke therapy - GENTLE/s approach. *Autonomous Robots*, 15(1):35–51, 2003.

[46] K. Koyanagi, J. Furusho, U. Ryu, and A. Inoue. Development of rehabilitation system for the upper limbs in a NEDO project. In *Proc. IEEE International Conference on Robotics and Automation (ICRA'03)*, volume 3, pages 4016–4022, Taipei, Taiwan, September 2003.

[47] D. Lynch, M. Ferraro, J. Krol, C. M. Trudell, P. Christos, and B. T. Volpe. Continuous passive motion improves shoulder joint integrity following stroke. *Clinical Rehabilitation*, 19(6):594–599, 2005.

[48] R. Colombo, F. Pisano, S. Micera, A. Mazzone, C. Delconte, M. C. Carrozza, P. Dario, and G. Minuco. Robotic techniques for upper limb evaluation and rehabilitation of stroke patients. *IEEE Transactions on Neural Systems and Rehabilitation Engineering*, 13(3):311–324, 2005.

[49] R. Riener, M. Frey, M. Bernhardt, T. Nef, and G. Colombo. Human-centred rehabilitation. In *Proc. IEEE International Conference on Rehabilitation Robotics (ICORR'05)*, pages 319–322, Chicago, U.S.A., June 2005.

[50] S. Jezernik, G. Colombo, and M. Morari. Automatic gait-pattern adaptation algorithms for rehabilitation with a 4-DOF robotic orthosis. *IEEE Transactions on Robotics and Automation*, 20(3):574–582, 2004.

[51] L. Dipietro, M. Ferraro, J. J. Palazzolo, H. I. Krebs, B. T. Volpe, and N. Hogan. Customized interactive robotic treatment for stroke: Emg-triggered therapy. *IEEE Transactions on Neural Systems and Rehabilitation Engineering*, 13(3):325–334, 2005.

[52] J. Rosen, M. Brand, M. B. Fuchs, and M. Arcan. A myosignal-based powered exoskeleton system. *IEEE Transactions on Systems, Man and Cybernetics [A]*, 31(3):210–222, 2001.

[53] K. Kiguchi, T. Tanaka, K. Watanabe, and T. Fukuda. Design and control of an exoskeleton system for human upper-limb motion assist. In *Proc. IEEE/ASME International Conference on Advanced Intelligent Mechatronics (AIM'03)*, volume 2, pages 926–931, Kobe, Japan, July 2003.

[54] B. Driessen, F. Liefhebber, T. T. Kate, and K. Van Woerden. Collaborative control of the manus manipulator. In *Proc. IEEE International Conference on Rehabilitation Robotics (ICORR'05)*, pages 247–251, Chicago, U.S.A., June 2005.

[55] J. Stein, H. I. Krebs, W. R. Frontera, S. E. Fasoli, R. Hughes, and N. Hogan. Comparison of two techniques of robot-aided upper limb exercise training after stroke. *American Journal of Physical Medicine and Rehabilitation*, 83(9):720–728, 2004.

[56] J. Tang, C. Carignan, and S. Gattewar. Virtual environment for robotic tele-rehabilitation. In *Proc. IEEE International Conference on Rehabilitation Robotics (ICORR'05)*, pages 365–370, Chicago, U.S.A., June 2005.

[57] J. Furusho, K. Koyanagi, Y. Imada, Y. Fujii, K. Nakanishi, K. Domen, K. Miyakoshi, U. Ryu, S. Takenaka, and A. Inoue. A 3-d rehabilitation system

for upper limbs developed in a 5-year nedo project and its clinical testing. In *Proc. IEEE International Conference on Rehabilitation Robotics (ICORR'05)*, pages 53–56, Chicago, U.S.A., June 2005.

[58] R. Sanchez, D. Reinkensmeyer, P. Shah, J. Liu, S. Rao, R. Smith, S. Cramer, T. Rahman, and J. Bobrow. Monitoring functional arm movement for home-based therapy after stroke. In *Proc. IEEE International Conference on Engineering in Medicine and Biology Society (EMBC'04)*, volume 2, pages 4787–4790, San Francisco, U.S.A., September 2004.

[59] M. McNeill, L. Pokluda, S. McDonough, and J. Crosbie. Immersive virtual reality for upper limb rehabilitation following stroke. In *Proc. IEEE International Conference on Systems, Man and Cybernetics (SMC'04)*, volume 3, pages 2783–2789, The Hague, Netherlands, October 2004.

[60] F. Amirabdollahian, G. T. Gomes, and G. R. Johnson. The peg-in-hole: a vr-based haptic assessment for quantifying upper limb performance and skills. In *Proc. IEEE International Conference on Rehabilitation Robotics (ICORR'05)*, pages 422–425, Chicago, U.S.A., June 2005.

[61] V. G. Popescu, G. C. Burdea, M. Bouzit, and V. R. Hentz. A virtual-reality-based telerehabilitation system with force feedback. *IEEE Transactions on Information Technology in Biomedicine*, 4(1):45–51, 2000.

[62] D. Jack, R. Boian, A. S. Merians, M. Tremaine, G. C. Burdea, S. V. Adamovich, M. Recce, and H. Poizner. Virtual reality-enhanced stroke rehabilitation. *IEEE Transactions on Neural Systems and Rehabilitation Engineering*, 9(3):308–318, 2001.

[63] T. Lee, Y. Takahashi, T. Miyoshi, T. Terada, K. Inoue, Y. Ito, K. Suzuki, and T. Komeda. Basic experiments of upper limb rehabilitation using haptic device system. In *Proc. IEEE International Conference on Rehabilitation Robotics (ICORR'05)*, pages 444–447, Chicago, U.S.A., June 2005.

[64] S. B. Ellenby. Safety issues concerning medical robotics. In *IEE Colloquium on Safety and Reliability of Complex Robotic Systems*, pages 3/1–3/4, 1994.

[65] N. Hogan, H. I. Krebs, J. Charnnarong, P. Srikrishna, and A. Sharon. MIT-MANUS: a workstation for manual therapy and training I. In *Proc. IEEE International Workshop on Robot and Human Communication*, pages 161–165, Tokyo, Japan, September 1992.

[66] H. I. Krebs, N. Hogan, M. L. Aisen, and B. T. Volpe. Robot-aided neurorehabilitation. *IEEE Transactions of Rehabilitation Engineering*, 6(1):75–87, 1998.

[67] H. I. Krebs, B. T. Volpe, D. Williams, J. Celestino, S. K. Charles, D. Lynch, and N. Hogan. Robot-aided neurorehabilitation: a robot for wrist rehabilitation. *IEEE Transactions on Neural Systems and Rehabilitation Engineering*, 15(3):327–335, 2007.

[68] C. G. Burgar, P. S. Lum, P. C. Shor, and H. F. Machiel Van der Loos. Development of robots for rehabilitation therapy: the Palo Alto VA/Stanford experience. *Journal of Rehabilitation Research and Development*, 37(6):663–673, 2000.

[69] K. Salisbury and W. T. Townsend. Compact cable transmission with cable differential. U.S. Patent 5207114, 1993.

[70] D. J. Reinkensmeyer, L. E. Kahn, M. Averbuch, A. McKenna-Cole, B. D. Schmit, and W. Z. Rymer. Understanding and treating arm movement impairment after chronic brain injury: progress with the arm guide. *Journal of Rehabilitation Research and Development*, 37(6):653–662, 2000.

[71] A. Toth, G. Fazekas, G. Arz, M. Jurak, and M. Horvath. Passive robotic movement therapy of the spastic hemiparetic arm with REHAROB: Report of the first clinical test and the followup system improvement. In *Proc. IEEE International Conference on Rehabilitation Robotics (ICORR'05)*, pages 127–130, Chicago, U.S.A., June 2005.

[72] P. Culmer, A. Jackson, R. Richardson, B. Bhakta, M. Levesley, and A. Cozens. Development of a dual robotic system for upper-limb stroke rehabilitation. In *Proc. IEEE International Conference on Rehabilitation Robotics (ICORR'05)*, pages 61–65, Chicago, U.S.A., June 2005.

[73] D. Mayhew, B. Bachrach, W. Z. Rymer, and R. F. Beer. Development of the MACARM - a novel cable robot for upper limb neurorehabilitation. In *Proc. IEEE International Conference on Rehabilitation Robotics (ICORR'05)*, pages 299–302, Chicago, U.S.A., June 2005.

[74] G. Rosati, P. Gallina, S. Masiero, and A. Rossi. Design of a new 5 d.o.f. wire-based robot for rehabilitation. In *Proc. IEEE International Conference on Rehabilitation Robotics (ICORR'05)*, pages 430–433, Chicago, U.S.A., June 2005.

[75] Y. Takahashi and T. Kobayashi. Upper limb motion assist robot. In *Proc. IEEE International Conference on Rehabilitation Robotics (ICORR'99)*, pages 216–226, Stanford, U.S.A., July 1999.

[76] G. R. Johnson, D. A. Carus, G. Parrini, Marchese S. Scattareggia, and R. Valeggi. The design of a five-degree-of-freedom powered orthosis for the upper limb. *Proc. Institution of Mechanical Engineers Part H*, 215(3):275–284, 2001.

[77] M. A. Buckley and G. R. Johnson. Computer simulation of the dynamics of a human arm and orthosis linkage mechanism. *Proc. Institution of Mechanical Engineers Part H*, 211(5):349–357, 1997.

[78] T. Rahman, W. Sample, R. Seliktar, M. Alexander, and M. Scavina. A body-powered functional upper limb orthosis. *Journal of Rehabilitation Research and Development*, 37(6):675–680, 2000.

[79] R. J. Sanchez, J. Liu, S. Rao, P. Shah, R. Smith, T. Rahman, S. C. Cramer, J. E. Bobrow, and D. J. Reinkensmeyer. Automating arm movement training following severe stroke: Functional exercises with quantitative feedback in a

gravity-reduced environment. *IEEE Transactions on Neural Systems and Rehabilitation Engineering*, 14(3):378–389, 2006.

[80] R. J. Sanchez, E. Wolbrecht, R. Smith, J. Liu, S. Rao, S. Cramer, T. Rahman, J. E. Bobrow, and D. J. Reinkensmeyer. A pneumatic robot for re-training arm movement after stroke: rationale and mechanical design. In *Proc. IEEE International Conference on Rehabilitation Robotics (ICORR'05)*, pages 500–504, Chicago, U.S.A., June 2005.

[81] M. Mistry, P. Mohajerian, and S. Schaal. Arm movement experiments with joint space force fields using an exoskeleton robot. In *Proc. IEEE International Conference on Rehabilitation Robotics (ICORR'05)*, pages 408–413, Chicago, U.S.A., June 2005.

[82] J. He, E. J. Koeneman, R. S. Schultz, H. Huang, J. Wanberg, D. E. Herring, T. Sugar, R. Herman, and J. B. Koeneman. Design of a robotic upper extremity repetitive therapy device. In *Proc. IEEE International Conference on Rehabilitation Robotics (ICORR'05)*, pages 95–98, Chicago, U.S.A., June 2005.

[83] N. G. Tsagarakis and D. G. Caldwell. Development and control of a 'soft-actuated' exoskeleton for use in physiotherapy and training. *Autonomous Robots*, 15(1):21–33, 2003.

[84] J. C. Perry and J. Rosen. Design of a 7 degree-of-freedom upper-limb powered exoskeleton. In *Proc. IEEE/RAS-EMBS International Conference on Biomedical Robots and Biomechatronics (BIOROB'06)*, Pisa, Italy, February 2006.

[85] C. Carignan, M. Liszka, and S. Roderick. Design of an arm exoskeleton with scapula motion for shoulder rehabilitation. In *Proc. 12th International Conference on Advanced Robotics (ICAR'05)*, pages 524–531, Seattle, U.S.A., July 2005.

[86] V. Zemlyakov and P. McDonough. Upper extremity exoskeleton structure and method. U.S. Patent 2003/0115954 A1, 26 June 2003.

[87] K. Nagai, I. Nakanishi, H. Hanafusa, S. Kawamura, M. Makikawa, and N. Tejima. Development of an 8 DOF robotic orthosis for assisting human upper limb motion. In *Proc. IEEE International Conference on Robotics and Automation (ICRA'98)*, volume 4, pages 3486–3491, Leuven, Belgium, May 1998.

[88] T. Nef and R. Riener. ARMin - design of a novel arm rehabilitation robot. In *Proc. IEEE International Conference on Rehabilitation Robotics (ICORR'05)*, pages 57–60, Chicago, U.S.A., June 2005.

[89] M. Mihelj, T. Nef, and R. Riener. ARMin - toward a six DoF upper limb rehabilitation robot. In *Proc. IEEE/RAS-EMBS International Conference on Biomedical Robots and Biomechatronics (BIOROB'06)*, pages 1154–1159, Pisa, Italy, February 2006.

[90] M. Mihelj, T. Nef, and R. Riener. ARMin II - 7 DoF rehabilitation robot: mechanics and kinematics. In *Proc. IEEE International Conference on Robotics and Automation (ICRA'07)*, pages 4120–4125, Rome, Italy, April 2007.

[91] D. W. Repperger, S. J. Remis, and G. Merrill. Performance measures of teleoperation using an exoskeleton device. In *Proc. IEEE International Conference on Robotics and Automation (ICRA'90)*, volume 1, pages 552–557, Cincinnati, U.S.A., May 1990.

[92] M. Bergamasco, B. Allotta, L. Bosio, L. Ferretti, G. Parrini, G. M. Prisco, F. Salsedo, and G. Sartini. An arm exoskeleton system for teleoperation and virtual environments applications. In *Proc. IEEE International Conference on Robotics and Automation (ICRA'94)*, volume 2, pages 1449–1454, San Diego, U.S.A., May 1994.

[93] F. Giuffrida, M. Piaggio, P. Morasso, and C. Guerrasio. G-exo, a modular exoskeleton as multi purpose multi media interface. In *Proc. IEEE International*

Workshop on Robot and Human Communication, pages 213–216, Tsukuba, Japan, November 1996.

[94] D.G. Caldwell, C. Favede, and N. Tsagarakis. Dextrous exploration of a virtual world for improved prototyping. In *Proc. IEEE International Conference on Robotics and Automation (ICRA'98)*, volume 1, pages 298–303 vol.1, Leuven, Belgium, May 1998.

[95] A. Nakai, T. Ohashi, and H. Hashimoto. 7 dof arm type haptic interface for teleoperation and virtual reality systems. In *Proc. IEEE/RSJ International Conference on Intelligent Robots and Systems*, volume 2, pages 1266–1271, Victoria, Canada, October 1998.

[96] S. Lee, J. Lee, M. Kim, and C.-W. Lee. A new master-arm for man-machine interface. In *Proc. IEEE International Conference on Systems, Man and Cybernetics (SMC'99)*, volume 4, pages 1038–1043, Tokyo, Japan, October 1999.

[97] Y. Jeong, Y. K. Kim, K. Kim, and J.-O. Park. Design and control of a wearable robot. In *Proc. IEEE International Workshop on Robot and Human Interactive Communication (RO-MAN'01)*, pages 636–641, Paris, France, September 2001.

[98] A. Schiele and G. Visentin. The esa human arm exoskeleton for space robotics telepresence. *European Space Agency, Automation and Robotics Section*, 2001.

[99] W. J. Poong and J. Seul. Teleoperated control of mobile robot using exoskeleton type motion capturing device through wireless communication. In *Proc. IEEE/ASME International Conference on Advanced Intelligent Mechatronics (AIM'03)*, volume 2, pages 1107–1112, Kobe, Japan, July 2003.

[100] T. Morizono, Y. Yamada, Y. Umetani, T. Yamamoto, T. Yoshida, and S. Aoki. Design of a new exoskeletal mechanism for a shoulder joint of wearable robots: the wearable hexa mechanism. In *Proc. IEEE International Conference on Robotics and Automation (ICRA'03)*, volume 2, pages 2323–2329, Taipei, Taiwan, May 2003.

[101] A. Frisoli, F. Rocchi, S. Marcheschi, A. Dettori, F. Salsedo, and M. Bergamasco. A new force-feedback arm exoskeleton for haptic interaction in virtual environments. In *Proc. of the First Joint Eurohaptics Conference and Symposium on Haptic Interfaces for Virtual Environments and Teleoperator Systems*, pages 195–201, Pisa, Italy, March 2005.

[102] J. J. Lee. *Tendon-Driven Manipulators: Analysis, Synthesis, and Control*. Ph.d. thesis, University of Maryland, 1991.

[103] L.-W. Tsai. *Robot Analysis: The Mechanics of Serial and Parallel Manipulators*. John Wiley & Sons, Inc., New York, U.S.A., 1999.

[104] L. Sciavicco and B. Siciliano. *Modelling and Control of Robot Manipulators*. Springer-Verlag, London, U.K., 2nd edition, 2000.

[105] K. H. Hunt. *Kinematic Geometry of Mechanisms*. Oxford University Press, New York, U.S.A., revised edition, 1990.

[106] J. J. Craig. *Introduction to Robotics: Mechanics and Control*. Pearson Prentice Hall, Upper Saddle River, New Jersey, U.S.A., 3rd edition, 2005.

[107] T. Yoshikawa. Manipulability of robotic mechanisms. *The International Journal of Robotics Research*, 4(2):3–9, 1985.

[108] P. I. Corke. A robotics toolbox for MATLAB. *IEEE Robotics & Automation Magazine*, 3(1):24–32, 1996.

[109] Compumotor. *Gemini GV Catalog 8000-4*. Parker Hannafin Corp, Rohnert Park, CA, U.S.A., 2008.

[110] G. F. Koshland, J. C. Galloway, and C. J. Nevoret-Bell. Control of the wrist in three-joint arm movements to multiple directions in the horizontal plane. *Journal of Neurophysiology*, 83(5):3188–3195, 2000.

[111] R. J. van Beers, P. Haggard, and D. M. Wolpert. The role of execution noise in movement variability. *Journal of Neurophysiology*, 91(2):1050–1063, 2004.